Synthesis and Analysis of Daptomycin Analogues

by

Robert Brill

A thesis

presented to the University of Waterloo

in fulfilment of the

thesis requirement for the degree of

Master of Science

in

Chemistry

Waterloo, Ontario, Canada, 2025

© Robert Brill 2025

Author's Declaration

I hereby declare that I am the sole author of this thesis. This is a true copy of the thesis, including any required final revisions, as accepted by my examiners.

I understand that my thesis may be made electronically available to the public.

Abstract

Daptomycin (Dap) is a naturally occurring, membrane-active, calcium-dependent cyclic lipodepsipeptide antibiotic (cLPA) which is used as a last-resort antibiotic to treat serious infections caused by Gram-positive (G+) bacteria including *Staphylococcus aureus* (*S. aureus*) and vancomycin-resistant enterococci (VRE). The appearance of Dap-resistant (Dap-R) bacteria with increasing frequency has motivated the search for Dap analogues that are active against Dap-R bacteria.

Recently, it has been shown that appending hydrophobic groups to tryptophan (Trp) or kynurenine (Kyn) yielded some Dap analogues with improved activity and were active against Dap-R bacteria. Chapter 2 of this thesis describes the synthesis and evaluation of Dap analogues with hydrophobic modifications to the side chain of the D-asparagine (Asn) residue at position 2 to determine if appending hydrophobic groups to D-Asn2 will also result in Dap analogs with improved activity. Eight Asn derivatives were synthesized containing alkyl or hydroxyl groups appended to the primary amide nitrogen of the D-Asn side chain. Dap analogues containing these D-Asn derivatives at position 2 were synthesized using Fmoc (9-fluorenylmethyloxycarbonyl) solid-phase peptide synthesis (SPPS). Dap analogs containing methyl (Me), ethyl (Et), n-propyl (Pr), n-butyl (Bu) and n-hexyl (Hex) on the D-Asn exhibited minimum inhibitory concentration (MIC) values that were 2–4-fold higher than Dap while the n-octyl (Oct) and piperidinyl (Pip) analogs had MIC values that were 8- and 32-fold greater than Dap, respectively. These results demonstrate that the activity of Dap cannot be improved by appending hydrophobic groups to D-Asn2 and suggest that D-Asn2 may not be closely associated with the cell membrane. These results also show that the primary amide of D-Asn2 is not essential for activity while the presence of at least one hydrogen on the nitrogen of the D-Asn2 side chain is very important to activity.

Membrane insertion studies using model membranes and fluorescence spectroscopy revealed that the hexyl and octyl analogues were able to insert into membranes even in the absence of Ca^{2+} consistent with their much-increased hydrophobicity compared to Dap.

In chapter 3, we wished to determine if it is possible to convert Dap into a Zn^{+2}-dependent antibiotic by substituting the two aspartate (Asp) residues in Dap's calcium-binding motif, Asp7 and Asp9, with Nγ-hydroxyasparagine (Asn(OH)), an amino acid that has a hydroxamic acid side chain. Hydroxamic acids, known for strong Zn^{2+} chelation, have been used in medicinal chemistry to improve metal-dependent interactions. The synthesis of an Asn(OH) building block with the hydroxamic acid side chain protected with a trityl (Trt) group (Fmoc-Asn(OTrt)-OH) was achieved following a multi-step route starting from Fmoc-Asp(tBu)-OH. Attempts to synthesize Dap analogues containing Asn(OH) at positions 7 or 9 using this building block via Fmoc SPPS failed. However, the synthesis of a Dap analogue containing Asn(OH) at position 2 was successful indicating that incorporation of this residue using this building block is sequence dependent. A new Asn(OH) building block containing a protecting group that is smaller than the Trt group, the dimethoxybenzyl (DMB) group (Fmoc-Asn(ODMB)-OH), was prepared. Attempts to prepare the target peptides using this new building block also failed as were attempts using an Asn(OH) building block with the hydroxamic acid side chain unprotected.

Acknowledgements

First, I would like to thank Prof. Scott Taylor for his inspiration and guidance throughout this project. The passion he brought to this project has driven me to learn and further investigate what has not yet been discovered. This mindset has taught me to think differently and will be applied to my future studies.

I would also extend thanks to all the members of the Taylor Lab for their comradery and support. Jeremy Goodyear has not only mentored me, but has taught me the value of perseverance, discipline and curiosity. My lab members, Gyeongsu Kim, Raphael Charette, Lindsey Shivers and Amr Elagamy, have all supported me along my academic journey in unique ways and I could not have done it without them. A thank you to Ryan Scott for being there, whenever the time.

I thank my advisory committee members, Prof. Eric Fillion and Prof. Elizabeth Meiering for their advice along the way.

Finally, I would like to thank my family Renee, Jeff, Zachary, Jake and Jersey for their encouragement and love.

Table of Contents

Author's Declaration ..... **ii**
Abstract ..... **iii**
Acknowledgements ..... **v**
List of Figures ..... **viii**
List of Tables ..... **x**
List of Schemes ..... **xi**
List of Abbreviations ..... **xii**
Chapter 1- General Introduction **1**
1.1 The problem of multidrug resistant bacteria (MDR) 1
1.2 The ESKAPE pathogens 2
1.3 Daptomycin (Dap) 4
1.4 Dap's mechanism of action (MoA) 5
1.4.1 Fundamentals of Dap's MoA 5
1.4.2 The membrane depolarization mechanism 8
1.4.3 The membrane reorganization mechanism 12
1.5. Dap Resistance Mechanisms 13
1.5.1 Lysyl-PG (LPG) and MprF 13
1.5.2 Cardiolipin Synthase (CL-S) 14
1.5.3 PG synthase 15
1.5.4 LiaFSR 16
1.6 Chemical synthesis of Dap 16
1.6.1 Fmoc Solid Phase Peptide Synthesis (SPPS) 17
1.6.2 Moreira and Taylor's Synthesis of Dap 21
1.7 Dap Structure Activity Relationships (SAR) 22
1.8 Thesis Objectives 27
1.8.1 Objective # 1 27
1.8.2 Objective # 2 28
Chapter 2- Modification of Asn2 on Daptomycin **31**

2.1 Objectives ... 31
2.2 Results and Discussion ... 31
2.2.1 Amino Acid Synthesis ... 31
2.2.2 Synthesis of Dap Analogues ... 33
2.2.3 MIC Determinations ... 36
2.2.4 Membrane Insertion Studies ... 37
2.3 Concluding remarks ... 39
Chapter 3- Modification of DXDG Motif in Dap ... **41**
3.1 Objectives ... 41
3.2 Results and Discussion ... 41
3.2.1 Amino Acid Synthesis ... 41
3.2.2 Synthesis of Dap Analogues ... 42
3.2.3 Biological Studies ... 49
3.3 Future Directions ... 51
Chapter 4- Experimental Section ... **52**
4.1 General Experimental Method ... 52
4.2 Experimental Section for Chapter 2 ... 54
4.3 Experimental Section for Chapter 3 ... 60
Letter of Copyright Permission ... **65**
References ... **67**
Appendices: Spectral Data of New Compounds ... **78**
Appendix A: Chapter 2 ... 79
Appendix B: Chapter 3 ... 103

List of Figures

Figure 1. The structures of the cell membranes of G+ and G- bacteria 2
Figure 2. The structure of daptomycin 5
Figure 3. The structure of PG and lipid II 6
Figure 4. CD traces of Dap under the several conditions 7
Figure 5. Fluorescence of Dap increases as Ca^{2+} is added in increments to a solution of Dap in the presence of PC/PG liposomes. 8
Figure 6. Structure of perylene-Dap 10
Figure 7. Excimer Fluorescence of Perylene-Dap. 11
Figure 8. The synthesis and translocation of LPG by MprF. 14
Figure 9. The conversion of PG to CL by cardiolipin synthase. 15
Figure 10. The general structure of an Fmoc-protected amin acid used for Fmoc SPPS. 19
Figure 11. The structure of the 2'-chlorotritylchloride (CTC) linker. 20
Figure 12. Examples of common coupling agents. 21
Figure 13. Summary of the results of Dap SAR studies. 23
Figure 14. Three of the Dap analogues prepared by Elshahawi and coworkers using a prenyltransferase. 25
F**igure 15**. Structure of Kynomycin 26
Figure 16. The structure of hexokynomycin. 26
Figure 17. The general structure of alkylated Asn analogues to be studies in this thesis. 28
Figure 18. Tthe general structure of hydroxamic acids and the general structure of hydroxamic acids bound to Zn^{2+} and the structure of N^{g}-hydroxyasparagine. 29
Figure 19. The structure of bacitracin. 29
Figure 20. Comparison of successive esterification coupling conditions by their HPLC traces for Dap-D-Asn(Hex)2 35
Figure 21. The structure of Fmoc/DMB-protected glycine. 36
Figure 22. Membrane insertion curves for Dap analogues with amino acids containing hydroxamic acid substitutions at position 2. 38
Figure 23. Membrane binding curves measuring Kyn13 flourescence for Dap and Dap-D-Asn(OH)2 at 439 nm. 50
Figure A. 1. HPLC chromatogram of crude Dap-D-Asn(Me)2 after cleavage. 79
Figure A. 2. HPLC chromatogram of pure synthetic Dap-D-Asn(Me)2.. 79
Figure A. 3. ESI+HRMS of pure Dap-D-Asn(Me)2. 80
Figure A. 4. ESI+HRMS of pure Fmoc-D-Asn(Et)-OH. 81
Figure A. 5. HPLC chromatogram of crude Dap-D-Asn(Et)2 after cleavage. 82
Figure A. 6. HPLC chromatogram of pure synthetic Dap-D-Asn(Et)2.. 82
Figure A. 7. ESI+HRMS of pure Dap-D-Asn(Et)2 83
Figure A. 8. ESI+HRMS of pure Fmoc-D-Asn(Pr)-OH. 84
Figure A. 9. HPLC chromatogram of crude Dap-D-Asn(Pr)2 after cleavage. 84
Figure A. 10. HPLC chromatogram of pure synthetic Dap-D-Asn(Pr)2.. 85

Figure A. 11. ESI+HRMS of pure Dap-D-Asn(Pr)2. 86
Figure A. 12. ESI+HRMS of pure Fmoc-D-Asn(Bu)-OH. 87
Figure A. 13. HPLC chromatogram of crude Dap-D-Asn(Bu)2 after cleavage. 88
Figure A. 14. HPLC chromatogram of pure synthetic Dap-D-Asn(Bu)2. 88
Figure A. 15. ESI+HRMS of pure Dap-D-Asn(Bu)2. 89
Figure A. 16. ESI+HRMS of pure Fmoc-D-Asn(Hex)-OH. 90
Figure A. 17. HPLC chromatogram of crude Dap-D-Asn(Hex)2 after cleavage..... 90
Figure A. 18. HPLC chromatogram of pure synthetic Dap-D-Asn(Hex)2 after cleavage.. 91
Figure A. 19. ESI+HRMS of pure Dap-D-Asn(Hex)2..... 92
Figure A. 20. ESI+HRMS of pure Dap-D-Asn(Oct)2. 93
Figure A. 21. HPLC chromatogram of crude Dap-D-Asn(Oct)2 after cleavage. 93
Figure A. 22. HPLC chromatogram of pure synthetic Dap-D-Asn(Oct)2. 94
Figure A. 23. ESI+HRMS of pure Dap-D-Asn(Oct)2. 95
Figure A. 25. HPLC chromatogram of pure synthetic Dap-D-Asn(Pip)2. 96
Figure A. 26. ESI+HRMS of pure Dap-D-Asn(Pip)2. 97
Figure A. 27. ^{1}H-NMR spectrum of Fmoc-Asn(Et)-OH (300 MHz, DMSO-d_6) at 298 K..... 98
Figure A. 28. ^{13}C-NMR spectrum of Fmoc-Asn(Et)-OH (75 MHz, DMSO-d_6) at 298 K..... 98
Figure A. 29 ^{1}H-NMR spectrum of Fmoc-Asn(Pr)-OH (300 MHz, DMSO-d_6) at 298 K..... 99
Figure A. 30. ^{13}C-NMR spectrum of Fmoc-Asn(Pr)-OH (75 MHz, DMSO-d_6) at 298 K..... 99
Figure A. 31 ^{1}H-NMR spectrum of Fmoc-Asn(Bu)-OH (300 MHz, DMSO-d_6) at 298 K..... 100
Figure A. 32. ^{13}C-NMR spectrum of Fmoc-Asn(Bu)-OH (75 MHz, DMSO-d_6) at 298 K..... 100
Figure A. 33. ^{1}H-NMR spectrum of Fmoc-Asn(Hex)-OH (300 MHz, DMSO-d_6) at 298 K.... 101
Figure A. 34. ^{13}C-NMR spectrum of Fmoc-Asn(Hex)-OH (75 MHz, DMSO-d_6) at 298 K..... 101
Figure A. 35. ^{1}H-NMR spectrum of Fmoc-Asn(Oct)-OH (300 MHz, DMSO-d_6) at 298 K..... 102
Figure A. 36. ^{13}C-NMR spectrum of Fmoc-Asn(Oct)-OH (75 MHz, DMSO-d_6) at 298 K 102
Figure B. 1. HPLC chromatogram of crude Dap-D-Asn(OH)2 after cleavage. 103
Figure B. 2 HPLC chromatogram of pure synthetic Dap-D-Asn(OH)2. 103
Figure B. 3. ESI+HRMS of pure Dap-D-Asn(OH)2. 104
Figure B. 4. ^{1}H-NMR spectrum of Fmoc-Asn(OH)-OH (300 MHz, DMSO-d_6) at 298 K..... 99
Figure B. 5. ^{13}C-NMR spectrum of Fmoc-Asn(DMB)-OH (75 MHz, DMSO-d_6) at 298 K 105
Figure B. 6. ESI+HRMS of pure Fmoc-Asn(DMB)-OH……..... 100
Figure B. 7. ^{1}H-NMR spectrum of Fmoc-Asn(OH)-OH (300 MHz, DMSO-d_6) at 298 K..... 107
Figure B. 8. ^{13}C-NMR spectrum of Fmoc-Asn(OH)-OH (75 MHz, DMSO-d_6) at 298 K 107

List of Tables

Table 1. Reaction conditions for the coupling reaction of amino acids **8-14**. 32
Table 2. Coupling conditions examined for the synthesis of Fmoc-D-Asn(Bu)-OH. 33
Table 3. Yields of Dap analogues..... 36
Table 4. MIC values of Dap and Dap analogues against B. subtilis ATCC 6051. 37

List of Schemes

Scheme 1. An overview of solid phase peptide synthesis (SPPS)……..……18
Scheme 2. An overview of Fmoc solid phase peptide synthesis (Fmoc SPPS)……...……..…19
Scheme 3. The mechanism for peptide bond formation using a carbodiimide and HOAt in solution…….…….……21
Scheme 4. Taylor and Moreira's synthesis of Dap……. ….……22
Scheme 5. Synthesis of Fmoc-D-Asn(alkyl)-OH derivatives....……...…….32
Scheme 6. Synthesis of Dap-D-Asn(R)2 analogues…….…….34
Scheme 7. Synthesis of Fmoc-D-Asn(O-Trt)-OH…….…...…….……41
Scheme 8. Coupling attempts of Fmoc-Asn(OTrt)-OH on Dap-L-Asn(OH)7 and Dap-L-Asn(OH)9……...……43
Scheme 9. Synthesis of Dap-D-Asn(OH)2…….……44
Scheme 10. Synthesis of Fmoc-Asn(ODMB)-OH…….……45
Scheme 11. Alternative synthetic routes to prepare Fmoc-Asn(OH)-OH…….....…….46
Scheme 12. Possible activation and subsequent coupling of **34** to the peptide sequence……...….46
Scheme 13. Synthetic routes for Dap-Asn(OH)9 and Dap-Asn(OH)7……...…..….47
Scheme 14. Proposed mechanism of Lossen rearrangement…….….48
Scheme 15. Proposed mechanism of aspartimide formation on O^{t}Bu-protected Asp…….....….49
Scheme 16. Proposed mechanism of aspartimide formation on hydroxamate amino acids…....49
Scheme 17. Synthesis of peptide **41** using tetrapeptide **39** as a building block……..…51

List of Abbreviations

2-MP	2-methylpiperidine
4-MP	4-methylpiperidine
Å	Angstrom
Ala	alanine
Arg	arginine
Asn	asparagine
Asn(OH)	N^{γ}-hydroxyasparagine
Asp	aspartate
Boc	tert-butyloxycarbonyl
Bu	butyl
CD	circular dichroism
CL	cardiolipin
cLPA	calcium-dependent cyclic lipodepsipeptide antibiotic
CL-S	Cardiolipin Synthase
CTC	2'-chlorotritylchloride
Dap	daptomycin
Dap-R	Dap-resistant
DCC	*N,N'*-dicyclohexylcarbodiimide
DCM	dichloromethane
DIAD	diisopropyl azodicarboxylate
DIC	*N,N'*-diisopropylcarbodiimide
DIPEA	diisopropylethylamine
DM	dimyrsitoyl
DMAP	dimethylaminopyridine
DMB	dimethoxybenzyl
DMF	dimethylformamide
DMSO	dimethyl sulfoxide
DO	dioleoyl
DSC	Differential scanning calorimetry
DVB	1,4-divinybenzene
EDC	1-Ethyl-3-(3-dimethyl aminopropyl)carbodiimide
Et	ethyl
EtOH	ethanol
Fmoc	9-fluorenylmethyl oxycarbonyl
FRET	Förster Resonance Energy Transfer
G-	Gram-negative
G+	Gram-positive
GFP	green fluorescent protein
GI	gastrointestinal
Glu	glutamate
Gly	glycine
HA	Hydroxamic acid
HAI	hospital-acquired infections
HATU	hexafluorophosphate azabenzotriazole tetramethyl uronium
HCTU	hexafluorophosphate 6-chlorobenzotriazole tetramethyl uronium
Hex	hexyl
HOAt	hydroxy-7-azabenzotriazole
HOBt	hydroxybenzotriazole
HPLC	high performance liquid chromatography
HS-AFM	highspeed atomic force microscopy
ICBF	isobutylchloroformate
Kyn	Kynurenine
LPG	Lysyl-PG
LPS	lipopolysaccharides
LTA	lipoteichoic acids
LUV	Large unilamellar vesicle
Lys	lysine
MDR	multidrug resistant bacteria
Me	methyl
MeCN	acetonitrile
MeGlu	(2S,3R)-2-methylglutamate
MIC	Minimum inhibitory concentration
MoA	mechanism of action
MprF	multiple resistance factor
MRSA	Methicillin-resistant *Staphylococcus aureus*
MS	mass spectroscopy
MSSA	methicillin-susceptible *Staphylococcus aureus*
NMM	*N*-methylmorpholine.
NMP	*N*-methyl pyrrolidinone
NMR	nuclear magnetic resonance
NRPS	non-ribosomal peptide synthetases
^{o}C	degrees Celsius
Oct	octyl

OD600	optical density at 600 nm
Orn	ornithine
PC	phosphatidylcholine
PG	phosphatidylglycerol
PGN	peptidoglycan
PGP	protecting group
Pip	piperidinyl
PO	palmitoyl-oleoyl
Pr	propyl
PS	polystyrene
PyAOP	7-azabenzotriazol-1-yloxy) tripyrrolidinophosphonium hexafluorophosphate
PyBOP	(Benzotriazol-1-yloxy) tripyrrolidinophosphonium hexafluorophosphate
RIF	region of increased fluidity
SAR	Structure Activity Relationships
Ser	serine
SPPS	solid-phase peptide synthesis
^{t}Bu	*tert*-butyl
TFA	trifluoroacetic acid
THF	tetrahydrofuran
Thr	threonine
TIPS	triisopropylsilane
Trp	Tryptophan
Trt	trityl
VISA	vancomycin intermediate *S. aureus*
VRE	vancomycin resistance enterococci
WHO	World Health Organization

Chapter 1- General Introduction

1.1 The problem of multidrug resistant bacteria (MDR)

Natural products have been used to treat infectious diseases throughout history. Reports suggest that its earliest use comes from a region in modern-day Sudan, where residents reportedly drank fermented beverages containing tetracycline-producing Streptomyces.[1] However, it was Sir Alexander Fleming's discovery of the antibiotic penicillin in 1928 that inspired extensive investigations into natural product antibiotics by companies and academics around the world.[2] Unfortunately, widespread overprescription and misuse of antibiotics induced uncontrolled spread of antibiotic-resistant bacteria. Additionally, novel antibiotic research reached its peak in the middle of the 20th century, dubbed the 'Golden Age of Antibiotics' but has since declined. The primary driver of this decline is the short dosing period for antibiotics compared to drugs used to control chronic diseases, meaning comparably less income for drug producers.[3] As fewer novel antibiotics are developed there is greater prevalence of bacteria becoming resistant to treatment as well as multiple drugs therapies. Thus, bacteria that are resistant to many commonly used antibiotics, called multidrug resistant bacteria (MDR), have become a major health issue. The World Health Organization (WHO) classifies MDR one of the greatest potential threats to global health.[4] It is predicted that if no action is taken, MDR bacteria could directly cause ten million deaths each year by the year 2050.[4] Hence, the WHO has called for more research into novel therapies to combat the growing threat of MDR bacteria.

1.2 The ESKAPE pathogens

In general, bacteria are classified into two different categories: Gram-positive (G+) and Gram-negative (G-) depending on how they respond to the Gram stain. The Gram stain consists of treating the bacteria with a dye (crystal violet) which is retained by the peptidoglycan (PGN) layer (Figure 1).[5] The stain is treated with ethanol which removes the stain from the thin peptidoglycan layer found in G- bacteria but does not remove the stain from the thicker layer of peptidoglycan in G+ bacteria. The bacteria are then treated with safranin, a counter stain. The G+ bacteria are stained violet while G-bacteria are counter stained.[5] In addition to possessing a thinner layer of peptidoglycan, G- bacteria also differ from G+ bacteria by possessing an outer membrane which contains lipopolysaccharides (LPS). G+ bacteria do not possess an outer membrane, however, their thicker layer of peptidoglycan is decorated with lipoteichoic acids (LTAs).

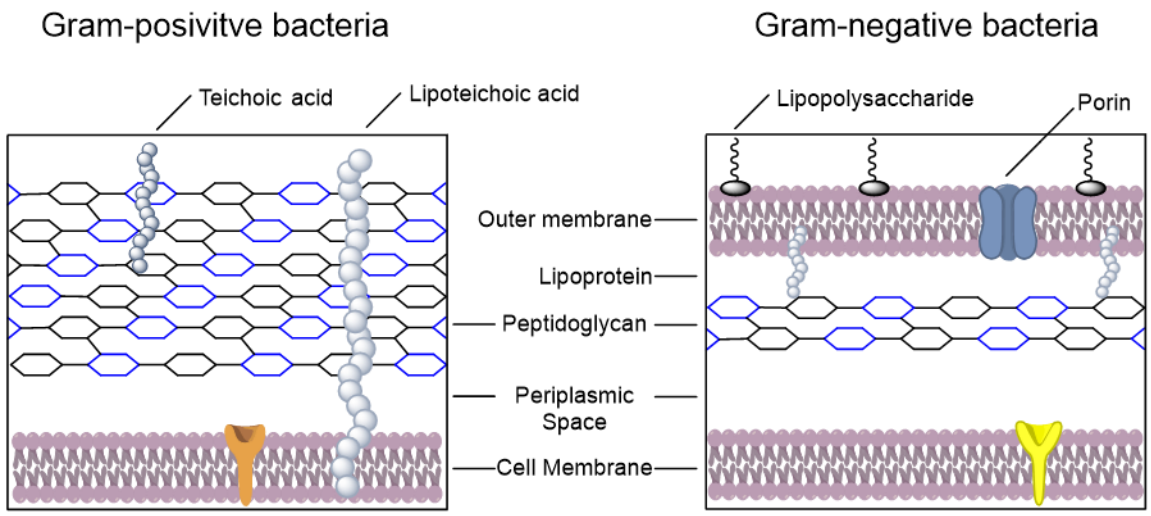


Figure 1. The structures of the cell membranes of G+ and G- bacteria

Although there are many bacterial infections that can lead to serious health consequences, the bacterial infections of particular interest today are caused by the so-called ESKAPE pathogens

which consists of the G+ bacteria *Enterococcus faecium (E. faecium), Staphylococcus aureus (S. aureus),* and the G- *bacteria Klebsiella pneumoniae, Acinetobacter baumannii, Pseudomonas aeruginosa,* and *Enterobacter* species.[6] These bacteria often cause of many of the life-threatening infections seen in the clinical setting today.[7] This thesis is mainly concerned with infections caused by G+ bacteria.

Among the G+ bacteria, *S. aureus* has resulted in the greatest public health concerns as methicillin-resistant *S. aureus* (MRSA) contributes to more deaths in America than HIV/AIDS, homicide, emphysema, and Parkinson's disease combined.[6] Since its first clinical appearance only sixty years ago, MRSA has now spread worldwide in both developed and developing countries. Although MRSA is resistant to many treatments including several traditional beta-lactam antibiotics, it is still susceptible to certain antibiotics such as the glycopeptide antibiotic vancomycin, the cyclic lipopeptide antibiotic Dap, and has now been observed to struggle under exposure to new generation beta-lactam like ceftaroline.[8]

Infections from Enterococci species cause a variety of diseases including urinary tract infections and bacteremia. In the 1980's enterococci that are resistant to vancomycin, one of the main lines of defense against enterococci, aptly named, vancomycin resistance enterococci (VRE) infections emerged. Interestingly, certain pneumonia cases have been attributed to VRE infections but also commonly found as natural colonisers in the gastrointestinal (GI) tract.[9] Consequently, most infections from VRE are endogenously acquired but hospital-acquired infections (HAI) reported are detrimental to patients including immunocompromised individuals.[9] Most concern comes from *Enterococcus faecium* because they show diverse mutagenesis between lab isolates. The main variants of VRE differ in their tendencies to populate in either hospitals or communities but both variants weakly respond to beta-lactam antibiotics as treatment options.[10] VRE remains a

threat to the critically ill and is commonly associated with nosocomial infection, which puts pressures on the health care and economic systems and demands novel antibiotic research.

Other G+ bacteria that pose a major threat are *Streptococcus pneumoniae* and *Mycobacterium tuberculosis*, both of which cause respiratory complications, have quick routes of transmission, and easily infect new targets.[11]

1.3 Daptomycin (Dap)

Dap (Figure 2) is a Ca^{2+}-dependent, cyclic lipopeptide antibiotic (cLPA) in the A21978C family, which is produced by the soil bacterium *Streptomyces roseosporus* (*S. roseosporus*) via non-ribosomal peptide synthetases (NRPS).[12] Dap was discovered by researchers at Eli Lilly in the early 1980s. It consists of a 10-amino acid macrocycle closed by a depsi (ester) bond between the side chain OH of threonine (Thr4) and the α-COOH of kynurenine (Kyn13). A linear tripeptide is attached to the Thr residue and decanoic acid is appended to the *N*-terminus. In addition to Kyn, Dap contains five other non-proteinogenic residues: D-asparagine (Asn2), ornithine (Orn6), D-alanine (Ala8), D-serine (Ser11), and (2S,3R)-2-methylglutamate-12 (MeGlu12). Dap contains a DXDG sequence in its macrocycle (Asp7-D-Ala8-Asp9-Gly10), a Ca^{2+}-binding motif that is found in other Ca^{2+} binding antibiotics and is a section of the EF-hand motif, a larger sequence found in many Ca^{2+}-binding proteins like calmodulin.[13] Dap exhibits maximal activity at 1-1.25 mM Ca^{2+}, which is approximately the physiological level of Ca^{2+} in humans.[14]

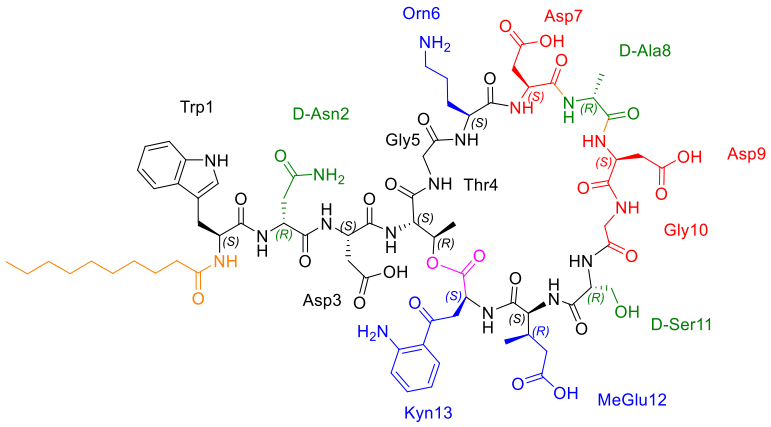


Figure 2. The structure of daptomycin (Dap). The uncommon amino acids are shown in blue. The D-amino acids are shown in green. The ester bond is shown in pink. The Ca^{2+}-binding DXDG motif is shown in red apart from D-Ala8. The lipid tail is shown in orange.

Although many cLPAs have been discovered, Dap is one of only two cLPAs approved for clinical use, the other being polymyxin/colistin. Dap was approved for clinical use in 2003 for treatment of complex skin infections caused by G+ pathogens, including methicillin-resistant *Staphylococcus aureus* (MSRA) and vancomycin-resistant enterococci (VRE).[14] In 2006, Dap was granted approval to treat bacteremia and right-sided endocarditis caused by MRSA and methicillin-susceptible *Staphylococcus aureus* (MSSA).[15] It is an important last-resort antibiotic used to treat serious G+ infections that do not respond to many of the other commonly used antibiotics. However, it is inactive against G- bacteria.

1.4 Dap's mechanism of action (MoA)

1.4.1 Fundamentals of Dap's MoA

There is still debate regarding the MoA of Dap. It is known to exert its effect in the cell membrane and does not enter the cytoplasm.[16] The presence of Ca^{2+} and the fatty acyl tail of Dap are requirements for activity.[17] Dap has also been shown to bind phosphatidylglycerol (PG, Figure 3) a phospholipid found in the cell membrane of G+ bacteria. It is not active against bacteria that

do not have or have only small quantities of PG in their cell membrane such as G- bacteria.[18,19,20] It is highly active against *Streptococcus pneumoniae in vitro* but not *in vivo*. This has been attributed to its sequestration by lung surfactant which contains large quantities of PG.[21] Data has recently been provided which suggests that Dap forms a tripartite complex with PG and lipid II.[22] Lipid II is a plasma-membrane-anchored precursor consisting of a single peptide glycan subunit attached to a polyisoprenoid pyrophosphate moiety (C55PP) (Figure 3). During PGN biosynthesis, enzymes transfer a PGN subunit from lipid II and incorporate it into the growing PGN network. This process generates C55 polyisoprenoid monophosphate (C55P) which is regenerated into lipid II completing the lipid II cycle. Some limited data also suggests that Dap can also form a complex with PG and C55P or C55PP.[22]

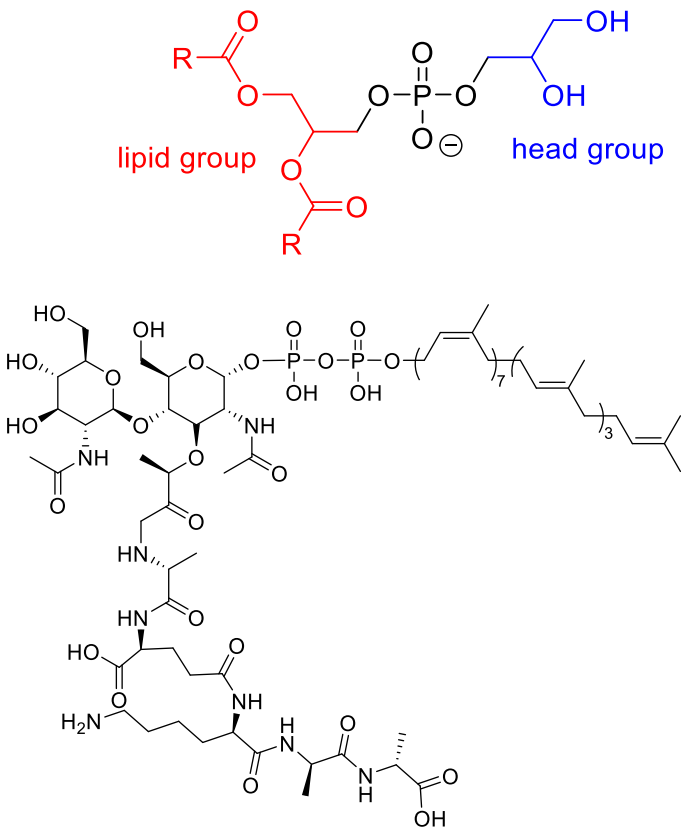


Figure 3. The structure of PG (top) and lipid II (bottom).

Circular dichroism (CD) studies have shown that Dap undergoes a structural change when bound to Ca^{2+} and PG.[18] All three components must be present for this structural change to occur (Figure 4). It is not known what this structural change consists of as direct investigation of the Dap-Ca^{+2}-PG complex by NMR or x-ray crystallography has been prevented by the tendency of this complex to precipitate out of solution at concentrations required for structural studies.[23]

A: Daptomycin

B: Daptomycin and Ca^{2+}

C: Daptomycin and PC/PG liposome

D: Daptomycin and Ca^{2+} and PC/PG liposome

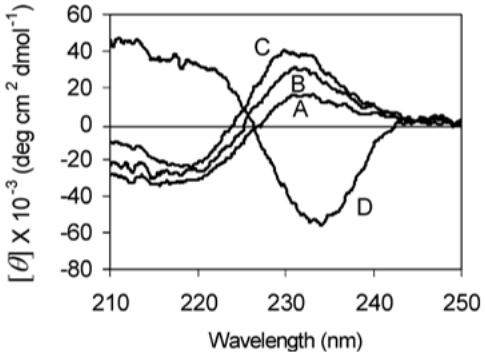


Figure 4. CD traces of Dap under the following conditions: (A) Dap (6 μM) in 20 mM HEPES (B) Dap in the presence of 5 mMCa^{2+}, (C) Dap in the presence of PC (phosphatidylcholine)/PG liposomes (180 μM) (D) Dap in the presence of 5 mM Ca^{2+} and PC/PG liposomes. Figure reproduced from Chem. Biol., 2004, **11**, 949–957 with permission.[18]

Trp1 and Kyn13 are natural fluorophores. However, Kyn's absorption spectrum overlaps with Trp's emission spectrum. Hence, with Dap, FRET occurs between Trp and Kyn upon excitation of Trp and only Kyn fluorescence is observed.[23] Kyn is a solvatochromic fluorophore meaning its fluorescence intensity depends on the polarity of the solvent: the fluorescence of the Kyn residue increases as the environment becomes less polar. This property of Kyn has been exploited for mechanism of action (MoA) studies. For example, the insertion of Dap into model membranes can be followed by monitoring changes in the fluorescence spectrum of the Kyn residue (λ_{Ex}=365 nm, λ_{Em}=442 nm) as a function of Ca^{2+} concentration. As shown in Figure 5, in the absence of Ca^{2+}, Dap does not interact with the model membranes and the fluorescence signal

is very low. However, upon the addition of Ca^{2+}, Dap binds to the Ca^{2+} which neutralizes some of the negative charges on Dap allowing it to insert into the membrane and the fluorescence of the Kyn residue increases as it is transferred into the apolar medium of the membrane. Both Ca^{2+} and PG must be present for Dap to insert into the membrane. The fluorescence at 442 nm can be plotted as a function of Ca^{2+} concentration to obtain membrane insertion curve (Figure 5). The fluorescence increases up to about 1 mM Ca^{2+} which is consistent with Dap exhibiting maximal biological activity at this Ca^{2+} concentration.

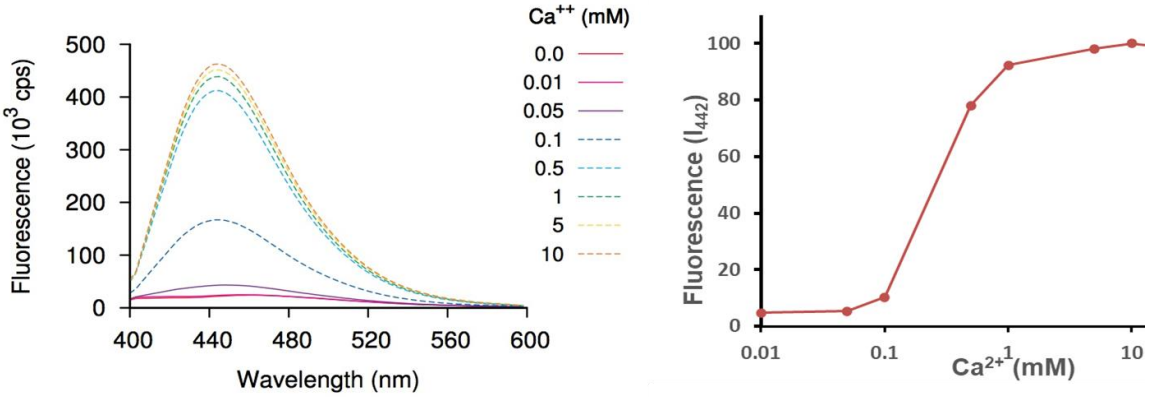


Figure 5. The graph on the left shows how the fluorescence of Dap increases as Ca^{2+} is added in increments to a solution of Dap in the presence of PC/PG liposomes. In the graph on the right, the fluorescence at 442 nm from the graph on the left is plotted as a function of Ca^{2+} concentration to give a membrane insertion curve. Figure reproduced from BBA-Biomembranes, 2016, **9**, 1999-2005 with permission.[24]

1.4.2 The membrane depolarization mechanism

Some studies on bacteria using K^+-selective electrodes and membrane potential-sensitive and K^+-sensitive fluorescent probes, have suggested that Dap exerts its activity by forming cation-selective pores.[25,26] This results in membrane depolarization and cell death. However, these studies were conducted at Dap concentrations that were greater than its MIC concentrations which Dap is known to cause cell lysis. Nevertheless, several studies using model membranes suggest that Dap

is indeed capable of forming pores. Using a fluorescence assay that is based on the pH-sensitive indicator pyranine, Zhang et al., showed that Dap can form cation-selective permeable pores in PC/PG liposomes. Permeabilities were highest for Na^+ and K^+.[27] More recently, Seydlova et al., performed conductance measurements using planar lipid membranes and found that Dap formed discrete pores of various sizes.[28] The frequency of pore formation was voltage dependent. Using the voltage-sensitive dyes they showed that *B. subtilis* cells with high initial membrane potential were rapidly permeabilized by Dap while low initial membrane potential hindered Dap pore formation. However, they used membranes consisting of pure 1,2-diphytanoyl-sn-glycero-3-phospho-(1'-rac-glycerol) which is not a good model of a bacterial membrane as native bacteria have a more diverse membrane lipid composition. Moreover, the concentration of Dap used in the *B. subtilis* studies was well above the MIC. Data that further supports the pore-forming mechanism has recently been provided by Zuttion et al. Using highspeed atomic force microscopy (HS-AFM) they showed that Dap formed toroidal pores on a supported lipid bilayer consisting of pure PG.[29] However, the membranes were not potentiated, and the timescale of pore formation did not match what is observed for cell death *in vivo*.[23,30]

The membrane depolarization mechanism requires the formation of pores which suggests that Dap must oligomerize in the cell membrane. In 2011, Muraih et al., observed FRET between native Dap and fluorescently-labelled Dap on PC/PG liposomes suggesting that Dap may be oligomerizing upon insertion into membranes.[23] No oligomerization was evident on liposomes that did not contain PG. Muraih et al., also provided further evidence of Dap oligomerization using an active Dap derivative containing a perylene butanoic acid tail (Figure 6).[31] Perylene is a fluorophore capable of forming excimers. It was reasoned that if perylene-Dap oligomerized on membranes, then the perylene residues would come into close contact with one another and form

excimers which would be evident by a shift in the fluorescence spectrum (460 nm for perylene monomer fluorescence to 520 nm for perylene excimer fluorescence). Little to no excimer fluorescence was detected using liposomes that contained only PC or lacked Ca^{2+}, however a large amount of excimer fluorescence was detected using liposomes containing PG in the presence of Ca^{2+} (Figure 7). The same result was obtained using isolated bacterial membranes. They also titrated perylene-Dap into a solution of liposomes containing PG in the presence of Ca^{2+} and measured conversion of monomers to excimers using fluorescence. As the excimer formation approached its maximum, the stoichiometry of PG to perylene-Dap reached a 1:1 ratio.[31] Therefore, it was suggested that a single molecule of PG allows Dap to assume a conformation which is favourable for oligomers to form.

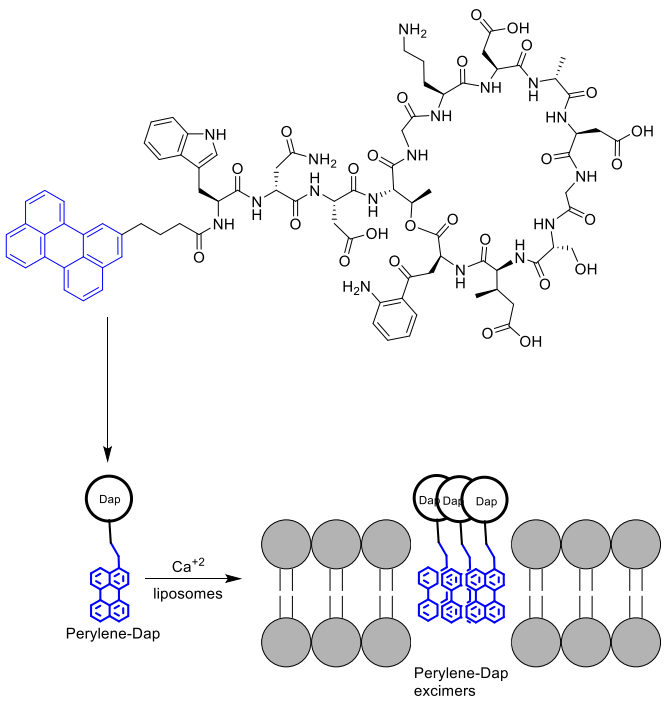


Figure 6. Structure of perylene-Dap. If perylene-Dap oligomerized on membranes, then the perylene residues should come into close contact with one another and form excimers.

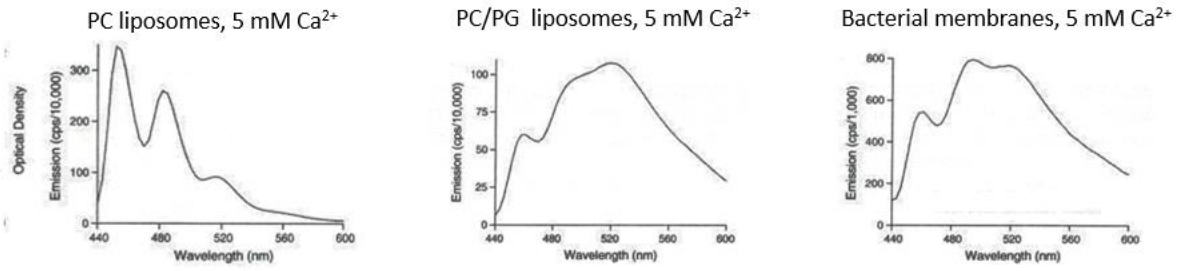


Figure 7. Excimer Fluorescence of Perylene-Dap. Fluorescence studies on excimers formed when overlap occurs between two fluorophores. Perylene monomer emission at 455 nm. Perylene excimer emission at 520 nm. Figure reproduced from BBA-Biomembranes, 2012, **3**, 673-678 with permission.[31]

If Dap is capable of forming pores, then it must also be able to span or translocate across the cell membrane. Palmer and coworkers showed that Dap evenly distributes across the inner and outer leaflet using fluorescently-labelled Dap and the reducing agent dithionite which selectively reacts with the fluorophore on DM (dimyrsitoyl)PC/DMPG liposomes. However, on PO (palmitoyl-oleoyl) PC/POPG or DO (dioleoyl) PC/DOPG membranes only 25% of Dap translocated to the inner leaflet.[32] Using fluorescence confocal microscopy Kreutzberger et al., reported that Dap does not translocate to the inner vesicles of POPC/POPG giant multilamellar vesicles.[33] Thus, it appears that the ability of Dap to translocate in model membranes depends upon the composition of the model membrane.

The validity of the membrane depolarization mechanism has been questioned mainly because membrane depolarization is not temporal with cell death and membrane depolarization occurs very slowly at Dap's MIC compared to the rate of membrane depolarization caused by well-established pore formers such as gramicidin.[33,34]

1.4.3 The membrane reorganization mechanism

Using *B. subtilis* expressing GFP (green fluorescent protein)-labelled proteins that have critical roles in cell wall/membrane maintenance, Mueller and coworkers found that upon exposure to Dap at its MIC, MurG and PlsX, dissociate from the *B. subtilis* cell membrane.[35] These two proteins are essential for cell wall synthesis (MurG) and phospholipid synthesis (PlsX) and are associated with the cytosolic side of the cell membrane. They are especially important in cell division where new membrane synthesis occurs. This area of the cell membrane must be dynamic to enable efficient cell synthesis and is referred to as a region of increased fluidity (RIF). Fluorescently-labelled Dap was found to colocalize with a dye that is known to accumulate in RIFs, like the division septum where new membrane synthesis occurs. It was suggested that Dap preferentially binds to RIFs and rigidifies/reorganizes the membrane.[35] This results in dissociation of MurG and PlsX from the cell membrane and cessation of cell wall synthesis and hence cell division. Studies on model membranes support the proposal that Dap prefers to interact with RIFs and alters membrane fluidity. Differential scanning calorimetry (DSC) performed on liposomes containing PG using have shown that reduced fluid lipid domains form upon Dap insertion.[36] An increase in cholesterol content in the liposomes, which rigidifies membranes, reduces Dap binding.[37] Fluorescence studies have shown that Dap inserts more readily into liposomes containing unsaturated phospholipids (which makes the membrane more fluid) compared to liposomes consisting of less fluid saturated phospholipids.[32]

It has been proposed that Dap, in the presence of Ca^{2+}, binds to PG at RIFs, where PG and the biosynthesis protein machinery congregate such as the division septum.[38] Dap and PG aggregate and/or oligomerize which leads to reorganization of the RIFs. This causes delocalization or dissociation of RIF-dependent proteins (such as MurG and PlsX) which leads to cessation of

cell wall synthesis, and impaired cell growth and division which slowly leads to membrane depolarization as a secondary effect. These events were proposed to occur within the 15 min of exposure. Long-term effects (30-60 min) involve further rigidification of the RIFs and increased membrane depolarization. If Dap does indeed form a complex with PG and lipid II then another facet of Dap's MoA would involve the Dap-PG oligomer sequestering lipid II which further contributes to the cessation of cell wall synthesis and possibly the delocalisation of the cell wall biosynthetic machinery.[22]

1.5. Dap Resistance Mechanisms

Most mutations that have been found in the genomes of Dap-resistant (Dap-R) *S. aureus* and Enterococci effect the functionality of the cell membrane; however, resistance mechanisms differ between species, and few are comprehensively described and understood.[39,40] Four of the more dominant Dap-resistance mechanisms are discussed briefly below.

1.5.1 Lysyl-PG (LPG) and MprF

Lysyl-PG is a naturally found cell component in G+ bacteria. It is formed by the lysination of PG which is catalyzed by the membrane protein MprF (multiple resistance factor) and transferred from the inner to outer leaflet of the membrane (Figure 8). Isolates of Dap-R *S. aureus* and *E. faecalis* have increased levels of LPG and decreased levels of PG in their membrane. This indicates that the resistance mutations in *mprF* are gain of function mutations.[41,42]

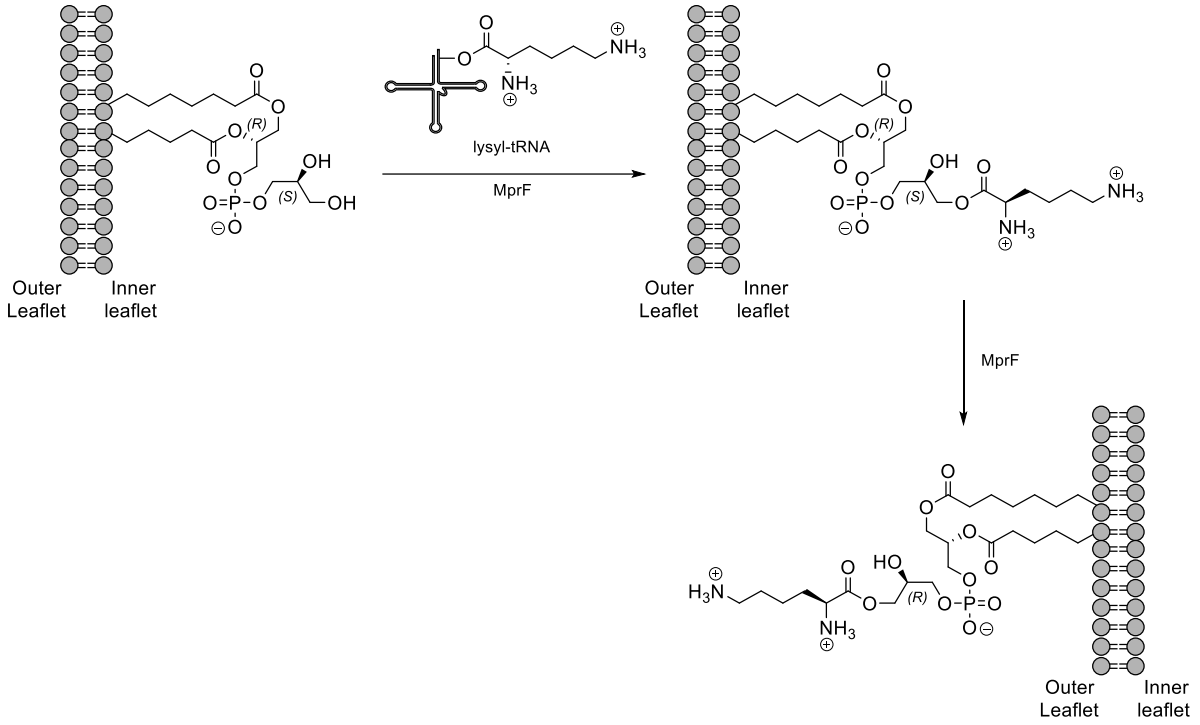


Figure 8. The synthesis and translocation of LPG by MprF.

A definitive explanation for how increased LPG content in the membrane confers Dap resistance has yet to be provided. Increasing LPG content would result in a reduced amount of PG in the membrane which would obviously hinder Dap's affinity to bacterial membranes. It has been proposed that LPG confers resistance to Dap by electrostatically repelling Dap from the bacterial membrane.[43] However, a strong correlation between Dap activity and membrane charge in bacteria was not found.[41,44]

1.5.2 Cardiolipin Synthase (CL-S)

Cardiolipin synthase (CL-S) catalyzes the final step in the conversion of PG into the phospholipid cardiolipin (CL) (Figure 9). CL is a naturally occurring cell component in G+ bacteria. Mutations in the *cls* gene have been reported in Dap-R *S. aureus* and Enterrococci.[45,46,47]

The *cls* mutations in Dap-R *S. aureus* were shown to lead to decreased levels of PG.[48] Mutants of *cls* isolated from Dap-R *E. faecalis* and *E. faecium* showed increased CL synthase activity.[49] Since CL is produced from PG, it is possible that an increase of CL results in less PG and hence decrease binding of PG to the membrane. However, isothermal calorimetry has been used in model membranes containing 10% CL to show Dap binding is still favourable. Zhang et al., showed that the translocation and oligomerization of Dap is inhibited by the presence of CL in liposomes. CL-rich membranes in *S. aureus* have been shown to have increased thickness.[50] It was suggested that this increase in thickness imparts Dap resistance by decreasing Dap's ability to penetrate the membrane and aggregate.

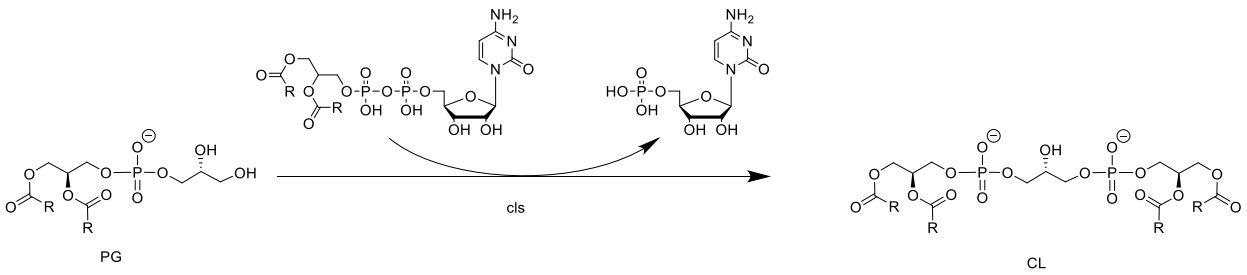


Figure 9. The conversion of PG to CL by cardiolipin synthase.

1.5.3 PG synthase

PG synthase catalyzes the synthesis of PG by dephosphorylating its immediate precursor, phosphatidylglycerol phosphate. Not surprisingly, mutations in PG synthase that lead to a reduction of PG content in the cell membranes are often less susceptible to Dap.[51,52,53] Notably, mutations in the *pgsA* gene have recently been described to be linked to reduced susceptibility to Dap in *B. subtilis.*

1.5.4 LiaFSR

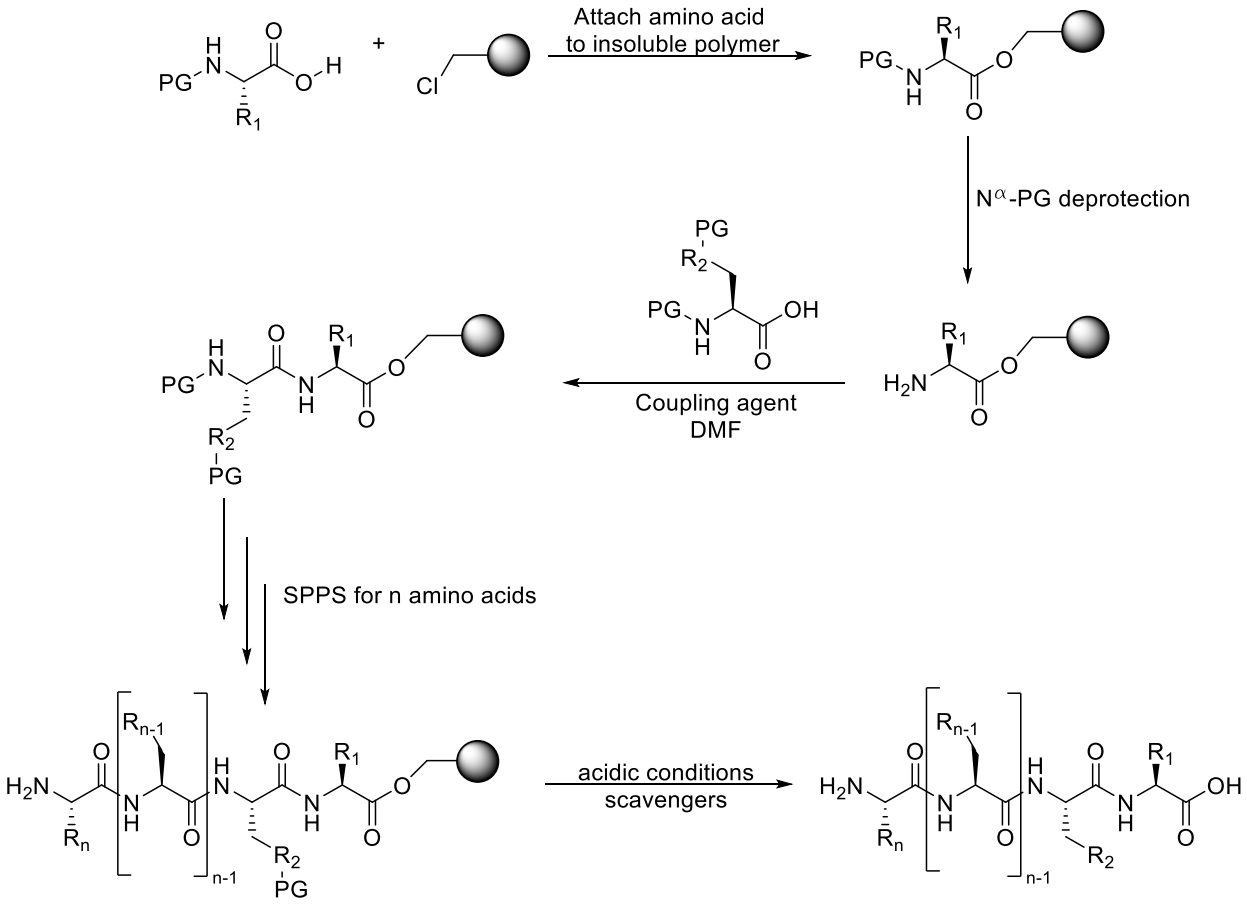
The LiaFSR system is a regulator of cell envelope stress and been shown to control several genes involving membrane and protein synthesis, key enzymes and transcription factors.[54,55] It is a three-component system consisting of LiaS, a histidine kinase/phosphatase that binds to LiaR, and a response regulator which are both inhibited by LiaF. The complex is active when stress occurs, and a signal cascade produces proteins that respond to cell stress factors. *S. aureus* and Enterococcal species that are highly resistant to Dap often have mutations in the liaFSR regulation system.[56] Mutations in *liaFSR* lead to upregulation of the LiaFSR system. LiaR knockout mutants of clinical isolates of Dap-R *E. faecalis* demonstrated extreme sensitivity to Dap.[57] When bacteria are subjected to Dap the LiaFSR system is activated and anionic phospholipids move away from the division septum and become reorganized in the cell membrane.[58,59] The now reorganized membrane exhibits additional thickness and odd septa formation. This reorganization confers Dap resistance.

1.6 Chemical synthesis of Dap

Five chemical syntheses of Dap have been reported in the literature.[62,63,61] A summary of all five routes will not be presented here, instead, the most recent synthesis will be discussed as it is the most efficient and is highly relevant to the work described in this thesis.[62] For an in-depth analysis of these five syntheses the reader is directed to the review by Taylor and Moreira (*Prog. Mol. Biol. Transl. Sci.,* 2025, **212**, 163-234). However, before we discuss the synthesis of Dap, a brief discussion on Fmoc-based solid phase peptide synthesis (SPPS) is presented below as this is the strategy that has been employed in this thesis.

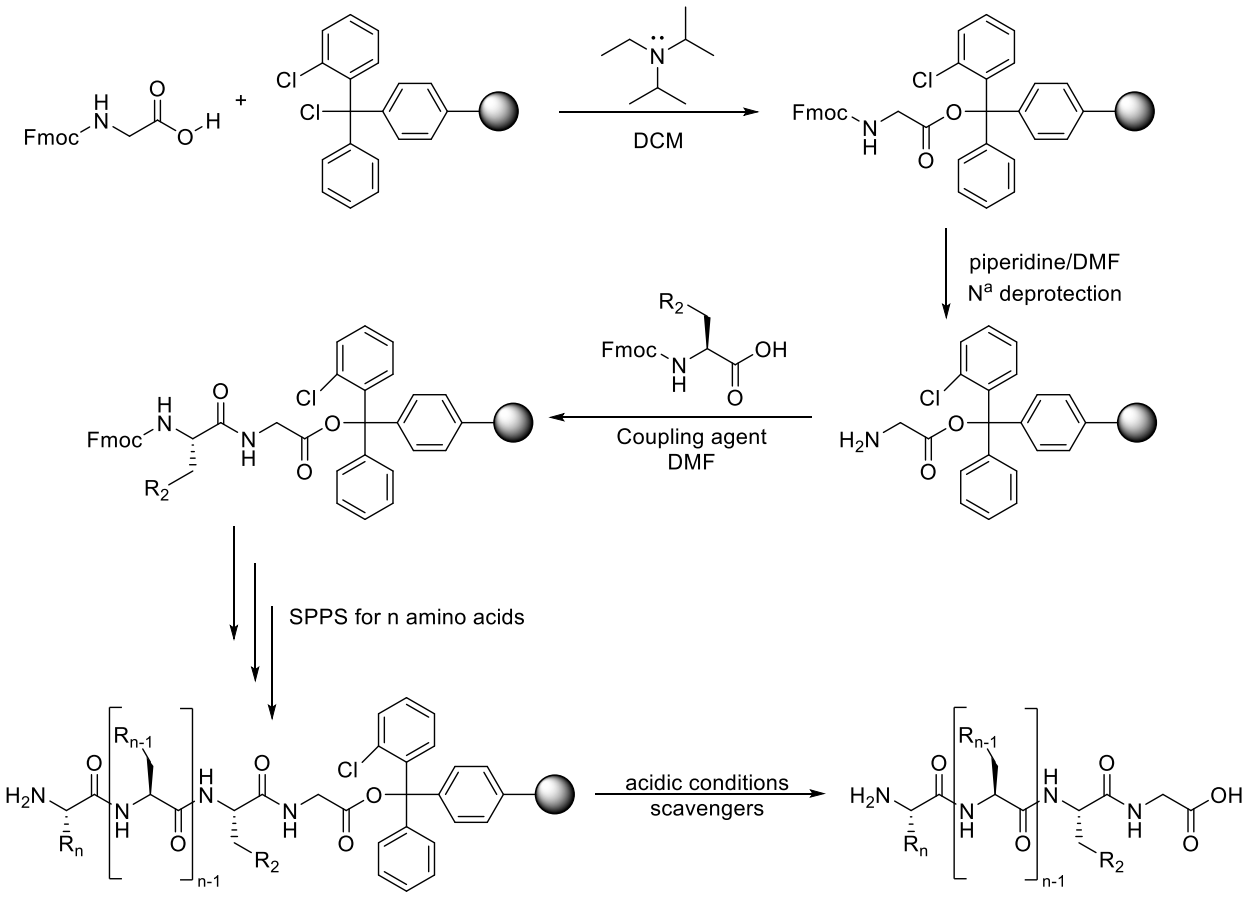
1.6.1 Fmoc Solid Phase Peptide Synthesis (SPPS)

In the 1960's Bruce Merrifield (Nobel Prize, 1984) invented SPPS which revolutionized peptide synthesis.[63] The idea is simple and is outlined in Scheme 1. The chemistry is performed on an insoluble polystyrene resin (such as polystyrene crosslinked with 1,4-divinylbenzene (PS-DVB)). The first amino acid, with its α-amino group and side chain protected (if necessary), is attached to the resin via its α-carboxyl group. The protecting group (PGP) on the α-amino group is then removed. A coupling reagent is then used to attach the next protected amino acid to the first resin-linked amino acid and then its α-amino group is deprotected. This process is repeated until all amino acids have been added. The peptide is then removed from the resin, globally deprotected (all side chain PGP's removed) and then purified by HPLC (high-performance liquid chromatography). The key features of SPPS are: (1) the reactions are driven to completion using excess reagents/amino acids; (2) purification after each step is accomplished by removing the excess reagents/amino acids through filtration and rinsing; (3) the resin acts as a PGP for the C-terminus.



Scheme 1. An overview of solid phase peptide synthesis (SPPS).

In Fmoc SPPS (Scheme 2), the α-amino group of each amino acid is protected with a base-labile Fmoc PGP (Figure 10), the peptide is attached to the resin via an acid-labile linker and the side chain PGPs are also designed to be labile to acid. A commonly used highly acid-labile linker in Fmoc SPPS is the 2'-chlorotritylchloride (CTC) linker (Figure 11). After each amino acid is coupled on, the Fmoc group is removed usually with 20% piperidine in DMF (dimethylformamide). At the end of the synthesis, the peptide is cleaved from the resin and globally deprotected with acid, usually with trifluoroacetic acid (TFA) with added cation scavengers (since the side chains are protected with PGPs that produce reactive cations upon removal with acid) such as small amounts of water and triisopropylsilane (TIPS).



Scheme 2. An overview of Fmoc solid phase peptide synthesis (Fmoc SPPS).

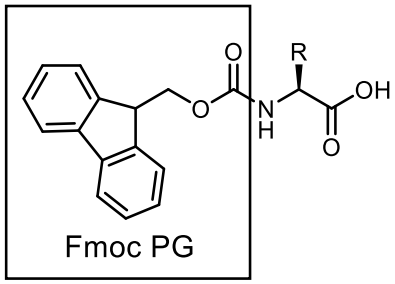


Figure 10. The general structure of an Fmoc-protected amino acid used for Fmoc SPPS.

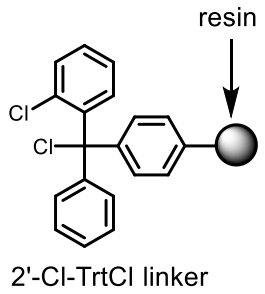


Figure 11. The structure of the 2'-chlorotritylchloride (CTC) linker.

There are many reagents that are used for the coupling reaction (Figure 12) and they all act by activating the carboxylic acid group. Carbodiimides are among the most widely used coupling agents. The most common carbodiimide coupling agent was *N,N'*-dicyclohexylcarbodiimide (DCC) but has since been replaced with *N,N'*-diisopropylcarbodiimide (DIC) due to toxicity concerns.[64] Carbodiimides readily react with and activate the carboxyl group on amino acids. An additive such as 1-hydroxy-7-azabenzotriazole (HOAt) and hydroxybenzotriazole (HOBt), is usually included to form a less reactive intermediate which reduces epimerization (Scheme 3). Other coupling strategies use uronium salts like hexafluorophosphate azabenzotriazole tetramethyl uronium (HATU) and hexafluorophosphate 6-chlorobenzotriazole tetramethyl uronium (HCTU) which require a hindered base like *N*-methylmorpholine. A third class of coupling agents are phosphonium salts which include (7-azabenzotriazol-1-yloxy)tripyrrolidinophosphonium hexafluorophosphate (PyAOP) and (Benzotriazol-1-yloxy)tripyrrolidinophosphonium hexafluorophosphate (PyBOP). These couplings agents are highly stable in solution.

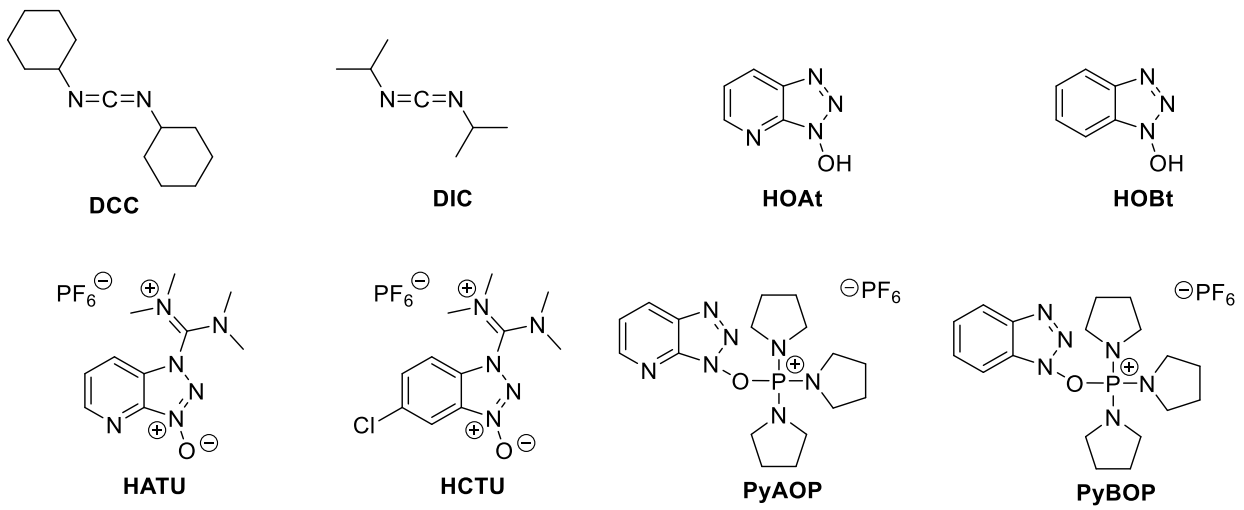
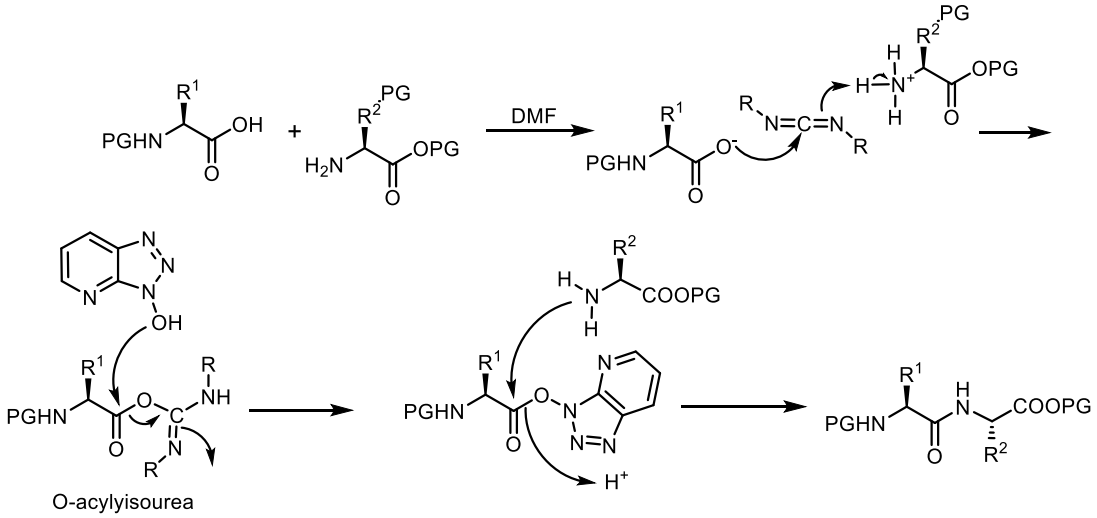


Figure 12. Examples of common coupling agents.

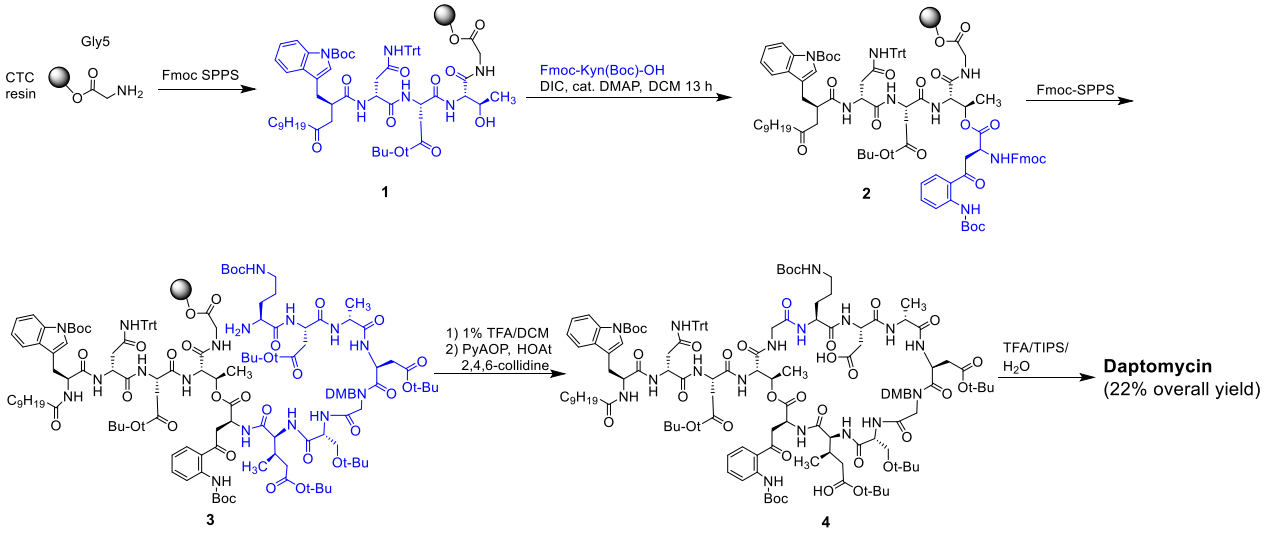


Scheme 3. The mechanism for peptide bond formation using a carbodiimide and HOAt in solution.

1.6.2 Moreira and Taylor's Synthesis of Dap

The highest yielding and most efficient synthesis of Dap has recently been reported by the Taylor group (Scheme 4).[62] Beginning with glycine (Gly5) loaded on to CTC-linked polystyrene resin, the next four amino acids were coupled in sequence using DIC/HOBt and the *N*-terminus of the resulting pentapeptide was lipidated to give peptide **1**. The ester bond formation between the

α-COOH of the Fmoc-Kyn building block and the side chain OH of Thr4 was accomplished using Steglich esterification conditions (catalytic amount of dimethylaminopyridine (DMAP) in anhydrous DCM) yielding the branched peptide **2**. The rest of the amino acids were installed to give peptide **3**. Peptide **3** was cleaved from the resin with 1% trifluoroacetic acid (TFA) in DCM (these conditions do not remove the less acid-labile PGs on the side chains) and was cyclized with PyAOP, HOAt and 2,4,6-collidine to give peptide **4**. Finally, the global deprotection was done with a TFA/water/TIPS solution (95/2.5/2.5), providing Dap in a 22% overall yield.



Scheme 4. Taylor and Moreira's synthesis of Dap.

1.7 Dap Structure Activity Relationships (SAR)

A host of Dap analogues have been made by semi-synthesis, combinatorial biosynthesis, chemoenzymatic synthesis, and total synthesis. Although semi-synthetic routes have yielded many analogues they only allow for modification of the side chains of Orn6 or Kyn13, the lipid tail, and replacement/modification of Trp1. Theoretically, combinatorial biosynthesis and chemoenzymatic

synthesis allow for individual substitutions at almost all positions, but only a handful of analogues have been prepared using these methods. Regarding methods for preparing Dap analogues that allow for amino acid substitutions at all positions, total synthesis has proven to be the most powerful and has provided the greatest number of Dap analogues by far. Indeed, it was the development of the total synthesis routes that enabled a highly detailed SAR of Dap to be established. A summary of the results of SAR studies on Dap is shown in Figure 13. Although it is not practical to discuss all the results from SAR studies in detail, some of the SAR studies that are very pertinent to this thesis are discussed below. For a more detailed summary of the SAR studies the reader is referred to (*Prog. Mol. Biol. Transl. Sci.,* 2025, **212**, 163-234).

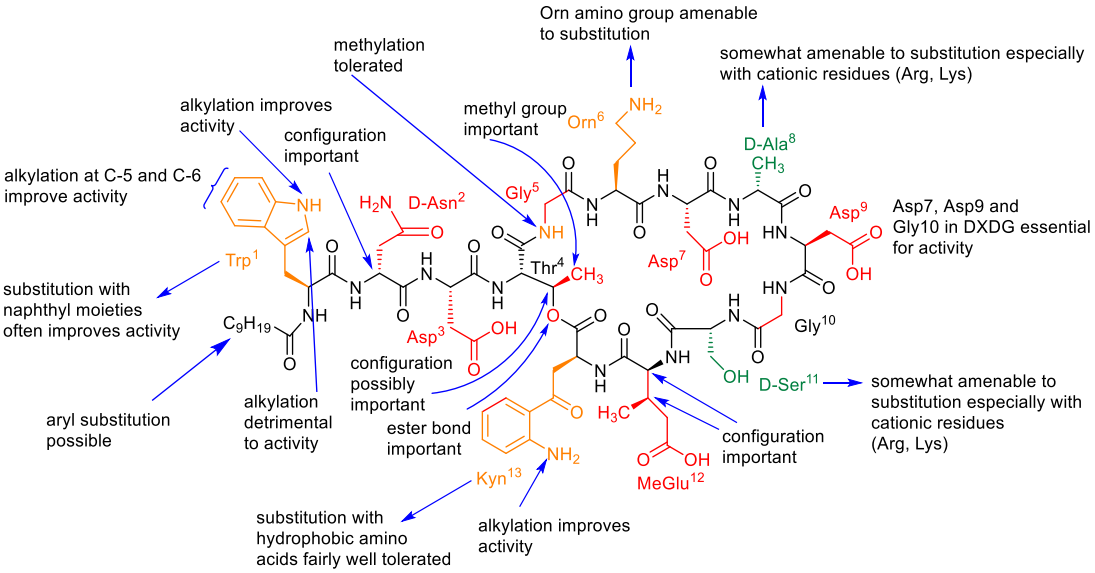


Figure 13. Summary of the results of Dap SAR studies. Residues shown in green were found to be somewhat amenable to substitution with Ala while the residues in red were not amenable to substitution with L-Ala or D-Ala.

One of the most important parts of Dap's structure is its DXDG motif (Asp7-D-Ala8-Asp9-Gly10). Analogs containing Ala or Asn at position 7 were completely devoid of activity and unable

to insert into membranes even at very high concentrations of Ca^{2+}.[65] Replacement of Asp9 residue in Dap or a Dap analog with Ala, Asn, D-Asp, Glu, or MeGlu results in complete loss of activity.[63,66] These results suggest that Asp7 and Asp9 are directly involved in binding Ca^{2+}. The Gly residue in this motif is also very important to activity as substitution with Ala or sarcosine (*N*-methylglycine) results in a large loss of activity.[60] Interestingly, D-Ala8 can be substituted with cationic residues (D-Orn, D-Lys and D-Arg, D-2-aminobutyric acid) with only moderate to little loss of activity.[66] It was suggested that the cationic residues enhance membrane binding to the negatively charged phosphate groups of membrane phospholipids via electrostatic interactions. Additionally, the stereochemical configuration of D-Ala8 is important since substitution with L-Ala led to a very large loss of activity.[60]

One of the more salient results of the SAR studies was the finding that appending hydrophobic groups to certain residues often resulted in analogues that were more potent than Dap. This increase in potency is probably due to the hydrophobic appendage increasing the overall hydrophobicity of the peptide which helps promote its interaction with the cell membrane. Examples of this are discussed below.

The Singh group reported the synthesis of Dap analogues with improved activities via modification of the Trp residue using an indole prenyltransferase.[67,71] Of particular note are analogs **5-7** (Figure 14) which were 1.5 to 20-fold more potent than Dap against several strains of Dap-susceptible (Dap-S) *E. faecalis, S. aureus*, *E. faecium*, *Micrococcus luteus*, *B. subtilis*, *Mycobacterium aurum*, and *Mycobacterium smegmatis* and were 9 to 10-fold more potent than Dap against several Dap-R strains of *S. aureus, E. faecalis,* and *E. faecium*. They also reported that the activity of analogues **5-7** exhibited little to no Ca^{2+}-dependence. This suggests that these analogues might exert their antibacterial activity via a mechanism different than that of Dap.

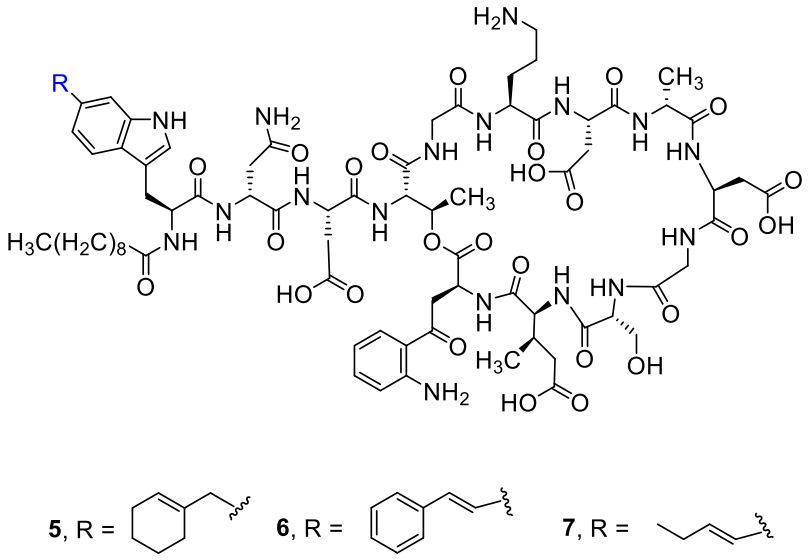


Figure 14. Three of the Dap analogues prepared by Elshahawi and coworkers using a prenyltransferase.

Chow et al., created several dozen analogues of Dap by total synthesis and tested them on several strains of MSSA, MRSA, *Streptococcus faecalis* and Enterococci.[60] Of these analogues, the one containing *N*-methylated Kyn (called Kynomycin, Figure 15) was found to be the most promising in that it exhibited 2 to 4-fold greater activity than Dap against these bacteria. Kynomycin was chosen for further study. Against 101 *S. aureus* strains and 72 Enterococcus spp., Kynomycin exhibited MICs that were 1.76-fold and 2.68-fold lower than the MIC of Dap, respectively.[69] It also exhibited a lower frequency of inducing resistance mechanisms in *S. aureus* while maintaining lower toxicity when compared to Dap. It was active against Dap-R strains and showed better efficacy than Dap in mouse infection models of *S. aureus* and *E. faecalis*.

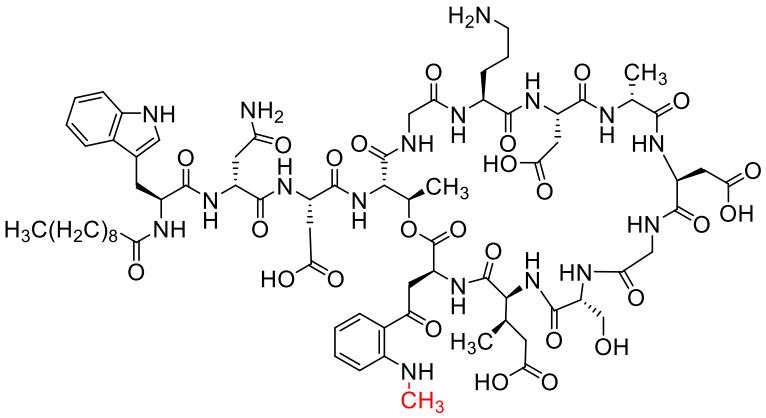


Figure 15. Structure of Kynomycin

Guan et al prepared a series of Dap analogues containing alkyl groups attached to the side chain amino group of Kyn13 via semi-synthesis. The analogue with a hexyl group, called hexakynomycin (Figure 16), proved to have the best overall activity with a 4 to 128-fold reduction in MIC compared to Dap against strains of MRSA, MSSA, vancomycin intermediate *S. aureus* (VISA) and VRE.[70] Hexakynomycin exhibited a lower clearance rate and an increased half-life in mice compared to Dap. Unfortunately, hexakynomycin did not exhibit improved efficacy compared to Dap in a mouse infection model due to high plasma protein binding.

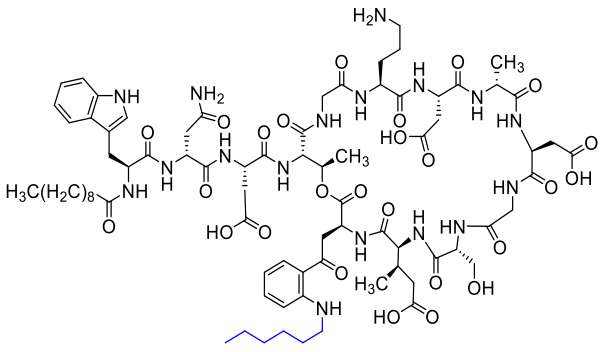


Figure 16. The structure of hexokynomycin.

1.8 Thesis Objectives

1.8.1 Objective # 1

Although Dap has been in clinical use for over two decades, reports of Dap-resistance are still quite rare. Nevertheless, reports of Dap resistance have been appearing with increasing frequency over the last decade.[71] One reason for this might be due to an increase in Dap use as Dap came off patent in 2015 and is now available as a generic drug. This increase in Dap-R bacteria is causing considerable concern in the medical community as Dap is usually successful against serious G+ infections that do not respond to many other commonly used antibiotics. Indeed, it is the increasing appearance of Dap-R bacteria that has been the main driving force behind the SAR studies mentioned in Section 1.7 and the search for Dap analogues with improved activity such as analogues that are active against Dap-R bacteria.

One residue in Dap that has not been interrogated to any significant extent is Asn-2. Replacing D-Asn with D-Ala in Dap resulted in a significant reduction in activity indicating that the side chain amide of this residue is important for activity.[60] As mentioned in Section 1.7, one strategy that has been used for increasing the potency of Dap and for generating Dap analogs that are active against Dap-R bacteria is to append hydrophobic groups to certain residues. Since Asn2 is close to the lipophilic tail and possibly close to the cell membrane when Dap is inserted in the cell membrane, we propose that adding alkyl groups to the side chain of Asn2 might increase membrane permeability and therefore potency. Hence, one of the objectives of this thesis is to synthesize a series of D-Asn derivatives bearing alkyl groups on the side chain (Figure 17), incorporate these D-Asn analogues into Dap at position 2 using Fmoc SPPS and then evaluate the resulting peptides for their antibacterial activity.

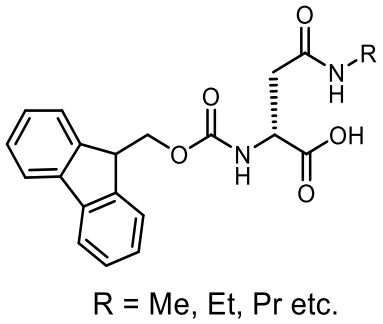


Figure 17. The general structure of alkylated D-Asn analogues to be studies in this thesis.

1.8.2 Objective # 2

Hydroxamic acids (HAs, Figure 18) are weak acids ($pK_a \approx 8.5$). Nevertheless, they chelate very strongly with certain metal ions, especially Fe^{+3} and Zn^{2+} (Figure 18).[72] A good example of how strong metal binding affinity of hydroxamic acids for Zn^{+2} have been used in medicinal chemistry is the development of a potent inhibitor of the Zn-dependent matrix metalloprotease, MM2 by Maola et al.[73] These workers identified a peptide, ACQGPTFKCDAIWRECG, from a peptide library that was a good inhibitor of MM2 (K_i = 3.4 μM). The x-ray crystal structure of the inhibitor bound to MM2 revealed that the Asp residue in the inhibitor chelated with the Zn^{2+} ion in the active site. Given that hydroxamates bind more tightly to zinc ions than carboxyl groups, they reasoned that replacing the Asp residue with N^{γ}-hydroxyasparagine (Asn(OH), Figure 18) should result in a more potent inhibitor. This indeed turned out to be the case with the new inhibitor having a K_i = 116 nM (30-fold increase in potency).

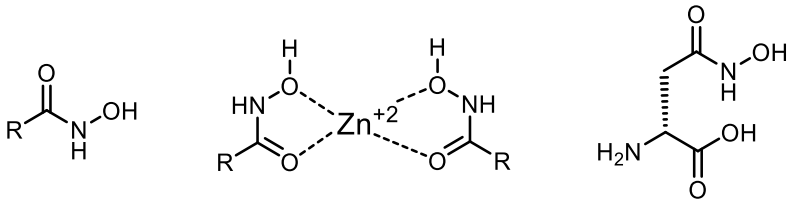


Figure 18. Left: the general structure of hydroxamic acids. Center: the general structure of hydroxamic acids bound to Zn^{2+}. Right: the structure of N^{γ}-hydroxyasparagine (Asn(OH)).

It is worth noting that there is a Zn^{+2}-dependent cyclic peptide antibiotic called bacitracin (Figure 19) which is produced by NRPS in *Bacillus licheniformis* and *Bacillus subtilis*. It was first discovered in 1943 and is still widely used today for its activity against G+ bacteria. In combination with neomycin and polymyxin B, bacitracin is used as a topical ointment, called Neosporin, for treating minor cuts and burns. Bacitracin is not administered systemically as its degradation product is nephrotoxic.[74] However, since systemic absorption of orally administered bacitracin is limited, it is safe when taken orally. Bacitracin has thus been used for the treatment of gastrointestinal infections such as those associated with VRE and *Clostridium difficile*. It functions by binding to C55PP. The Zn^{+2} coordinates the pyrophosphate head group of C55PP and the carboxylate of the Glu residue and sulfur atom of the aminothiazoline moiety in bacitracin.

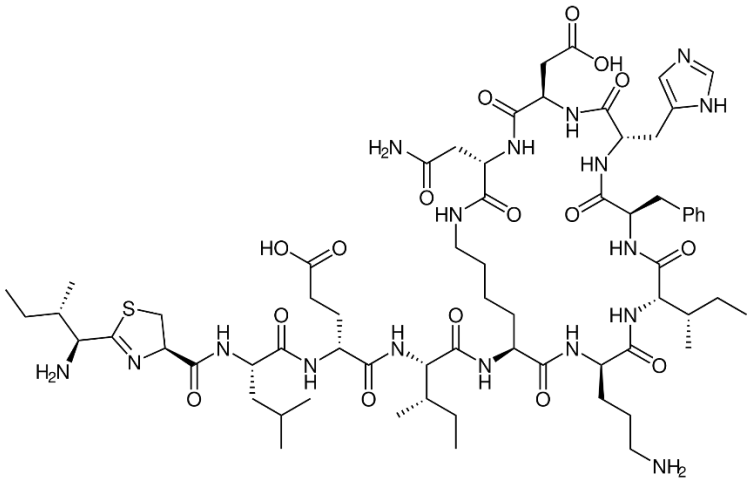


Figure 19. The structure of bacitracin.

As mentioned previously, Dap requires approximately 1 mM Ca^{2+} for full activity and the two Asp residues in the DXDG motif play a key role in binding to the Ca^{2+} ion. Dap is almost completely inactive in the presence of 1 mM of other cations such as Na^{+}, K^{+}, Ba^{2+}, Mg^{2+}, Ni^{2+} and Cu^{2+}.[75],78 However, this is not the case with Zn^{2+} where, in the presence of 1 mM Zn^{+2}, Dap exhibits an MIC that is about 16-fold greater than the MIC in the presence of 1 mM Ca^{2+}. We wish to determine if it is possible to create a Dap analogue that is as active in the presence of Zn^{2+} as Dap in the presence of Ca^{2+}. Given hydroxamic acids strong affinity for Zn^{+2} and zinc ions strong affinity for phosphates, another objective of this thesis is to determine if either or both of the Asp residues in the DXDG motif of Dap can be substituted with Asn(OH) using Fmoc SPPS and if the resulting Dap analogues exhibit good activity in the presence of Zn^{2+}.[77]

Chapter 2- Modification of Asn2 on Daptomycin

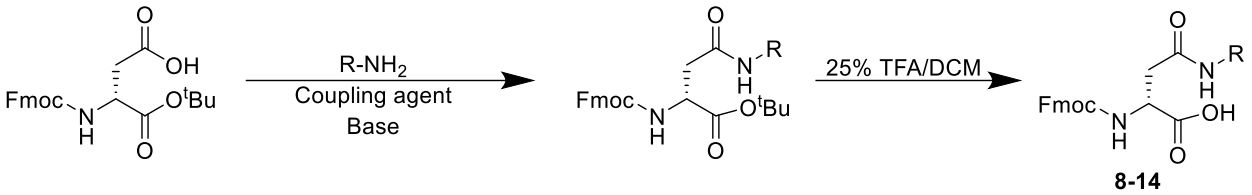
2.1 Objectives

The literature is lacking examples of side chain modifications to D-Asn2 in Dap. As mentioned in Section 1.8, since D-Asn2 is close to the lipophilic tail and possibly close to the cell membrane when Dap is inserted in the cell membrane, adding alkyl groups to the side chain of Asn2 might increase membrane permeability and therefore potency. The objectives of the work in this chapter are to prepare D-Asn derivatives bearing alkyl groups on the side chain (Figure 17), incorporate these D-Asn analogues into Dap at position 2 using Fmoc SPPS and then evaluate the resulting peptides for their antibacterial activity.

2.2 Results and Discussion

2.2.1 Amino Acid Synthesis

The modified D-Asn derivatives outlined in Figure 17 are not commercially available and must be synthesized. Fortunately, these amino acids are very straightforward to synthesize using the procedure of Zhong and Anslyn which was optimized for each amino acid derivative (Scheme 5).[78] The side chain of commercially available Fmoc-D-Asp-O^{t}Bu was coupled to an amine using a coupling agent and the product was precipitated from solution, filtered and dried. This crude material was subjected to 25% TFA/DCM and the final product purified by silica gel chromatography. The results are summarized in Table 1.



Scheme 5. Synthesis of Fmoc-D-Asn(alkyl)-OH derivatives. R group is an alkyl group.

Table 1. Reaction conditions for the coupling reaction and yield (2 steps) of amino acids **8-14**.

Entry	Amine	Coupling agent	Base	Solvent	Time/ Temp	Product	Yield
1	Methylamine	IBCF	NMM	THF	0ºC-rt/18h	**8**	84%
2	Methylamine	HCTU	NMM	DMF	rt, 10 min	**8**	90%
3	Ethylamine	HCTU	NMM	DMF	rt/30 min	**9**	88%
4	Propylamine	HCTU	NMM	DMF	rt /2 h	**10**	76%
5	Butylamine	HCTU	NMM	DMF	rt /1 h	**11**	42%
6	Hexylamine	BOP	DIPEA	DCM	rt /1 h	**12**	62%
7	Octylamine	BOP	DIPEA	DCM	rt /1 h	**13**	55%
8	Piperidine	HCTU	NMM	DMF	rt /30 min	**14**	51%

We started by making the methyl derivative (entry 1) using the original procedure of Zhong and Anslyn which used isobutylchloroformate (ICBF)/*N*-methylmorpholine (NMM) in tetrahydrofuran (THF). Although this worked well, the reaction was slow and took 18 h to complete. However, using HCTU as coupling agent we were able to obtain the product in comparable yield but in just 10 min (entry 2). HCTU was kept as a coupling agent for the ethyl, propyl, butyl (entries 3-5) and piperidine (entry 8) derivatives though the yields decreased as the alkyl chain on the amine increased (ethyl to propyl to butyl, entries 3-5). Attempts to improve the

yield of the butyl derivative using IBCF/NMM, EDC/DIPEA and DIC/HOBt were unsuccessful (Table 2) with the exception when using BOP/DIPEA (diisopropylethylamine) as coupling agent and on a small scale. Nevertheless, BOP/DIPEA worked reasonably well for hexyl (**12**, entry 6) and octyl (**13** entry 7) derivatives.

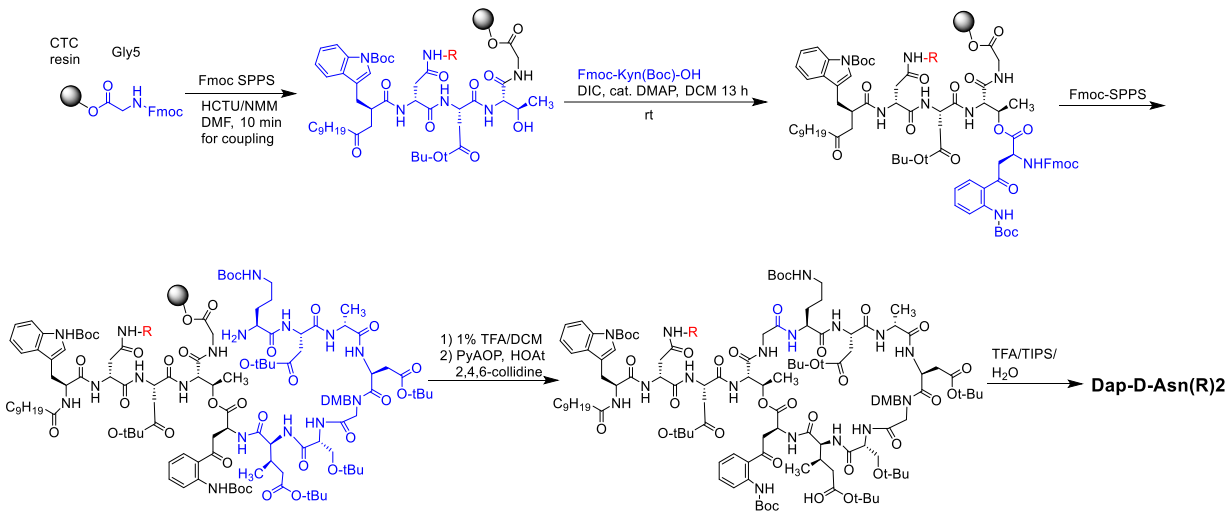
Table 2 Coupling conditions examined for the synthesis of Fmoc-D-Asn(Bu)-OH. Yields refer to the amino acid building block after t-Bu deprotection (2 steps).

Entry	Coupling agent	Base	Solvent	Equiv Butylamine	Yield
1	IBCF	NMM	THF	3	Fmoc removed
2	IBCF	NMM	THF	1.1	Trace
3	EDC	DIPEA	DMF	1.1	Trace
4	DIC/HOBt	N/A	DMF	1.1	NR
5	BOP	DIPEA	DCM	1.1	75%[a]
6	BOP	DIPEA	DCM	1.1	37%[b]

[a]Reaction conducted using 50 mg amino acid. [b]Reaction conducted using 500 mg amino acid.

2.2.2 Synthesis of Dap Analogues

Dap analogues containing amino acids **8-14**, collectively **Dap-D-Asn(R)2**, were prepared using the route developed by Moreira and Taylor with one notable difference (Scheme 6).[62] In the original procedure, 4 equiv of amino acid and DIC/HOBt were use as coupling agents and each coupling reaction lasted 3 h. Fmoc deprotections were accomplished using two 5 min treatments with 4-methylpiperidine (4-MP). Hood et al. reported that couplings could be achieved much faster (in 10 min) using 3 equiv of amino acid, 5 equiv of HCTU, and 10 equiv of NMM in DMF.[79] These coupling conditions were adopted for the synthesis of the Dap analogues.



Scheme 6. Synthesis of Dap-D-Asn(R)2 analogues.

The esterification step using the Steglich conditions reported by Moreira and Taylor (10 equiv of Fmoc-L-Kyn(Boc)-OH, DIC, cat. DMAP, 18 hours) worked well for all the analogues apart from the analogue containing the hexyl Asn derivative (Dap-D-Asn(Hex)2) where the reaction only went to about 30% completion (Figure 20, top chromatogram). The ester procedure was modified to include equal parts of dry DCM, dry DMF and NMP (*N*-methyl pyrrolidinone) with 1% Triton X-100 and a catalytic amount of DMAP. In this procedure, Triton X-100 is a surfactant used to prevent aggregation of peptide in solution which has been previously described by Hojo et al.[80] With the lipid tail and hexyl chain in sequence before the ester bond is formed, it is possible that aggregation was limiting the availability of the Thr OH side chain. The use of 1% Triton X-100 increased the conversion to the ester but was less than 50% complete (Figure 20, bottom chromatogram). Each esterification reaction attempt uses 10 equivalents of the Kyn building block, which is quite valuable, therefore, it was decided that we would continue the synthesis since it is known that the hydroxy group on Thr is unreactive under the subsequent coupling conditions (3 equiv of amino acid, 5 equiv of HCTU, and 10 equiv of NMM in DMF).

The final peptide was obtained in only a 2.6% yield, amounting to 4 mg, which was sufficient for subsequent studies.

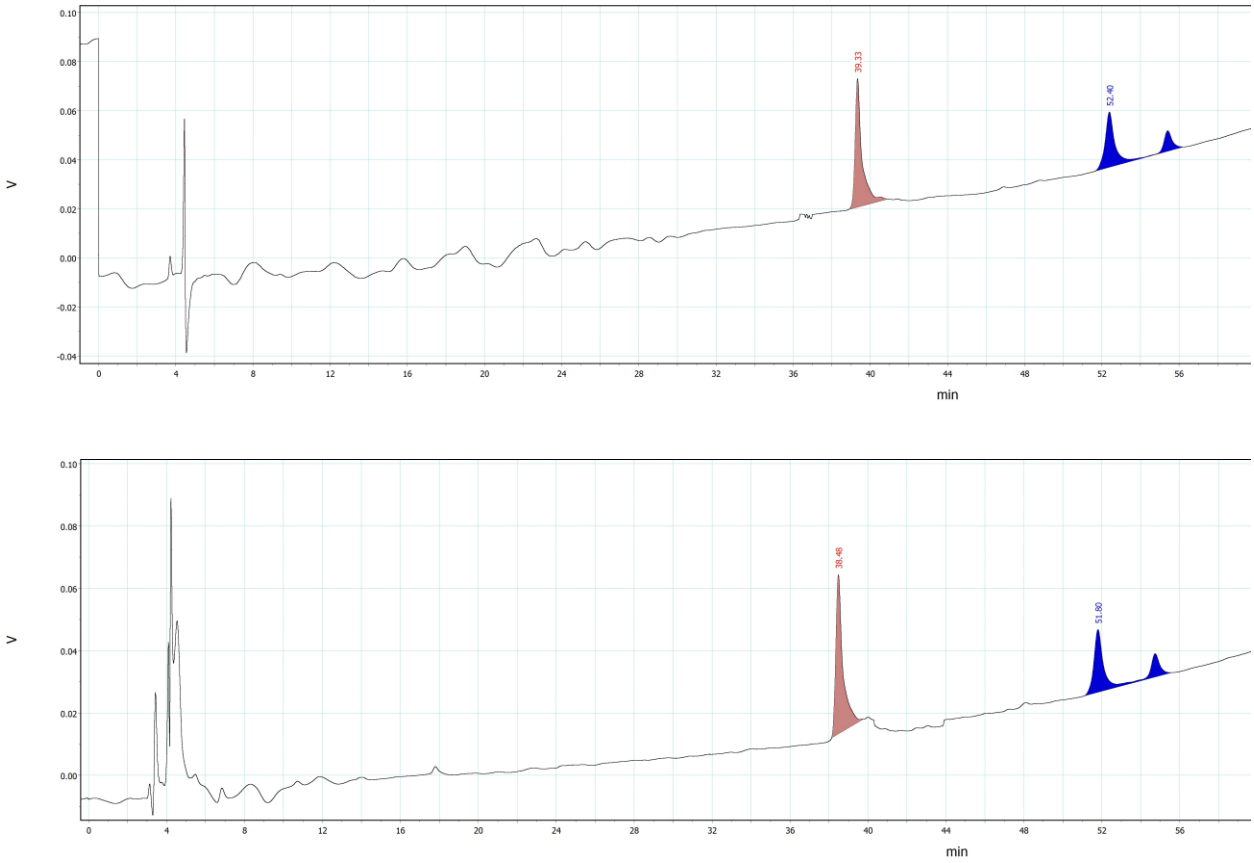
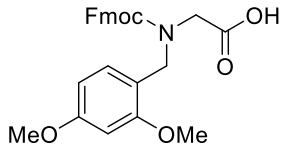


Figure 20. Comparison of successive esterification coupling conditions by their HPLC traces for Dap-D-Asn(Hex)2 at λ=220 nm. Top: Steglich conditions. Bottom: 1% Triton X-100 conditions.Red peak: Uncoupled starting material. Blue peaks: Coupled ester product and associated CO_2 adduct.

The glycine residue at position 10 was incorporated using Fmoc-(DMB)-Gly-OH as a building block (Figure 21). The role of the DMB (dimethoxybenzyl) protecting group is to prevent aspartamide formation after the Asp9 residue is added. Once Fmoc-(DMB)-Gly-OH is installed into the growing peptide chain the *N*-terminus of the resulting peptide is a tertiary amine. It was found that deprotection of the Fmoc moiety on this peptide required more time due to steric hindrance. Moreover, once the Fmoc group has been removed from this residue, the resulting *N*-

terminus is a secondary amine which are known to couple slower than primary amines. At the end of the synthesis of some of the analogues, some truncated peptides were isolated and identified by MS (mass spectroscopy). This was probably due to incomplete formation of the peptide bond between Gly10 and Asp 9. It is possible that the new 10 min coupling time used for peptide bond formation was insufficient to allow for complete bond formation between Gly10 and Asp 9 and this may account for some of the overall low yields of some of the peptides (Table 2.3).



15

Figure 21. The structure of Fmoc/DMB-protected glycine (**15**).

Table 3. Yields of Dap analogues

Analogue	Yield
Dap-D-Asn(Me)2	4%
Dap-D-Asn(Et)2	7%
Dap-D-Asn(^{n}Pr)2	3%
Dap-D-Asn(^{n}Bu)2	4%
Dap-D-Asn(Hex)2	3%
Dap-D-Asn(Oct)2	10%
Dap-D-Asn(Pip)2	8%

2.2.3 MIC Determinations

The MIC value of Dap and each analogue against *B. subtilis* ATCC 6051 were determined using a broth microdilution assay. The results are summarized in Table 4. All the analogues exhibited MIC values that were higher than Dap. Analogues bearing a Me, Et, n-Pr, n-Bu and n-

hexyl group exhibited MIC values that were 2-4 times higher than Dap while the octyl and piperidine analogues were 8 and 32-fold greater respectively.

Table 4. MIC values of Dap and Dap analogues against B. subtilis ATCC 6051.

Dap or Dap Analogue	MIC (μg/mL)
Dap	1
Dap-D-Asn(Me)2	2
Dap-D-Asn(Et)2	4
Dap-D-Asn(^{n}Pr)2	2
Dap-D-Asn(^{n}Bu)2	4
Dap-D-Asn(Hex)2	4
Dap-D-Asn(Oct)2	8
Dap-D-Asn(Pip)2	32

2.2.4 Membrane Insertion Studies

Membrane insertion curves (see Section 1.4.1) were obtained for each analogue using 1:1 DOPG/DOPC liposomes (Figures 22). The hexyl and octyl derivative exhibit a higher fluorescence value than Dap in the absence of Ca^{2+} suggesting that they can insert into the membrane to some extent without Ca^{2+}. This is probably due to their much greater hydrophobicity compared to Dap and they do not require Ca^{2+} to neutralize some of the negative charges on Dap to partially insert into the membrane. The octyl derivative shows only a small increase in fluorescence as the concentration of Ca^{2+} is increased (Figure 22) suggesting that its antibacterial activity may be independent of Ca^{2+} concentration. The Elshahawi group has reported that certain highly hydrophobic appendages on Trp 1 result in loss of Ca^{2+} dependence on activity (see section 1.7), however, these Trp analogues were more potent than Dap.[68,81]

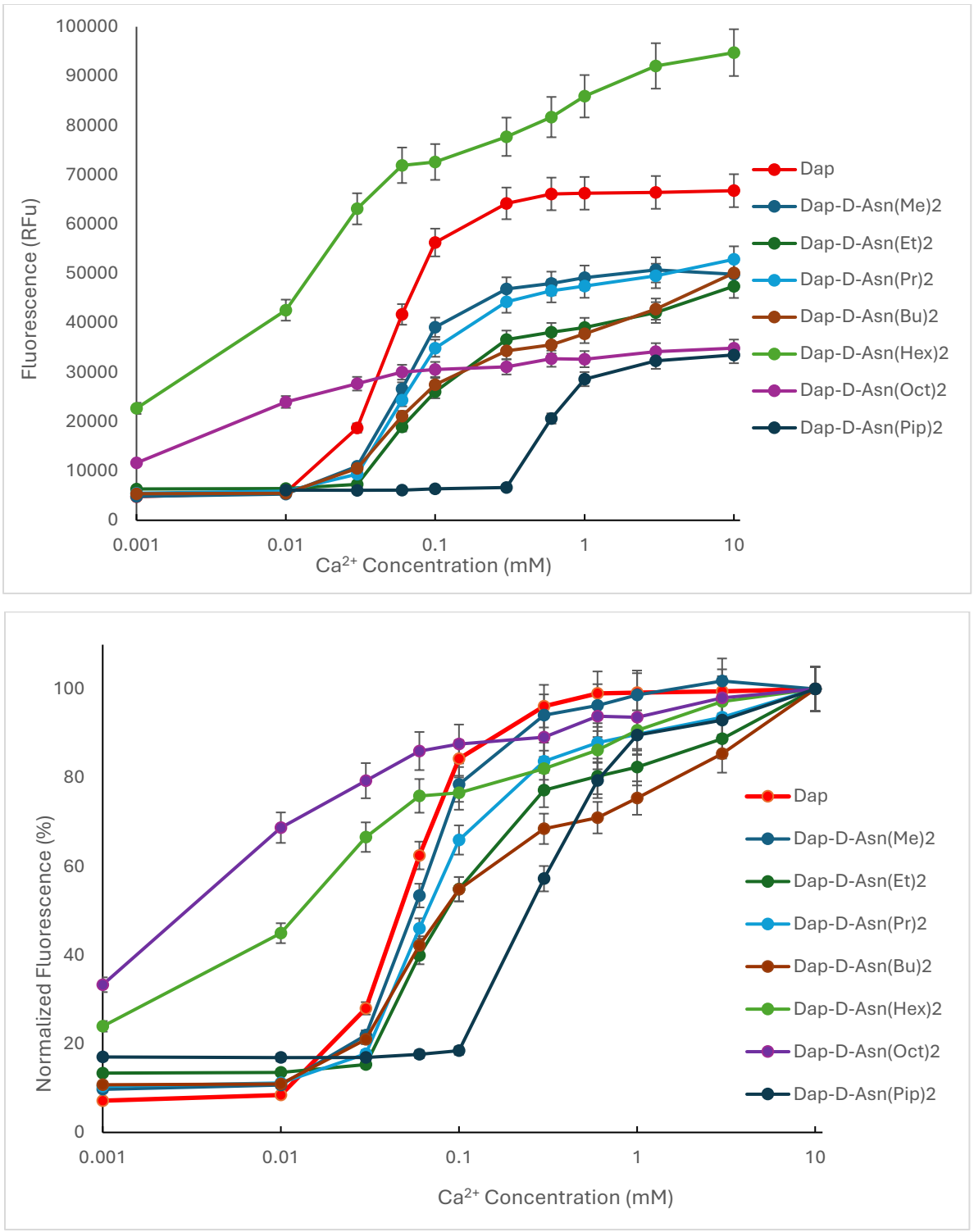


Figure 22. Membrane insertion curves for Dap analogues with amino acids containing alkyl substitutions at position 2. Upper panel: data not normalized to 100%. Lower panel: data not normalized to 100%. Dap membrane insertion curve for Dap bolded red for emphasis. Data plotted at 0.001 mM Ca^{2+} contains 0 mM Ca^{2+}.

The hexyl analogue shows some Ca^{2+} dependence for activity and its fluorescence at 10 mM Ca^{2+} is considerably greater than that of Dap suggesting that the Kyn residue in the hexyl analogue is inserted deeply into the membrane; however, the hexyl analogue is 4-fold less active than Dap suggesting that its orientation in the membrane is not optimal for activity.

Apart from the hexyl derivative, none of the other analogues exhibited a maximal fluorescence value as great as that as Dap even at 10 mM Ca^{2+} (Figure 22). This suggests that the Kyn residue in these Asn analogues does not insert as deeply into the membrane compared to the Kyn residue in Dap even though these analogues should be more hydrophobic than Dap.

From the normalized data in Figure 22 it can be seen that, with the exception of the methyl analogue, the membrane insertion curves of the Et, Pr, Bu and Pip analogs are shifted to the right of the Dap insertion curve meaning that these analogues require more Ca^{2+} than Dap to achieve maximal membrane insertion. The piperidyl analogue, which is much less active than Dap, exhibits a membrane insertion curve that is shifted far to the right compared to Dap and requires a much higher concentration of Ca^{2+} to reach maximal insertion compared to Dap. This phenomenon, where analogues that are less active than Dap require a higher concentration of Ca^{2+} to reach maximal activity or membrane insertion has been reported by Barnawi et al with other Dap analogues.[82]

2.3 Concluding remarks

NMR structures of Dap in the absence of PG but in the presence or absence of Ca^{2+} have been reported by several groups.[18,83,84] Each group obtained their spectra under different conditions (pH etc.) and so obtained somewhat different structures. Nevertheless, some conformational similarities amongst the structures highlight Dap's amphipathic nature. The macrocycle adopts a

hairpin structure with the hydrophobic side chains Kyn13, Trp1 and the fatty acid forming a hydrophobic face at one end of the hairpin while the side chains of the four acidic residues and Orn6 form a hydrophilic face at the other end. There were no major differences between the structures in the presence and absence of Ca^{2+} and no Ca^{2+} binding site was obvious in any of the structures. NOEs between the protons of the fatty acid and the aromatic rings of Trp1, Kyn13, and D-Asn2 indicate spatial proximity and suggest that these three residues may be involved in interactions with the cell membrane since the fatty acid is almost certainly involved in hydrophobic interactions with the cell membrane.[85] This hypothesis is consistent with the increase in activity found for Dap analogues bearing hydrophobic groups on Trp1 and Kyn13 (see Section 1.7) but is not consistent with our results on Asn2 which clearly show that appending hydrophobic groups to the side chain of D-Asn2 leads to a decrease in activity. However, it is important to keep in mind the NMR structures of Dap are not a very good guide for predicting how Dap will respond to modifications since it is known that Dap undergoes a large conformation change when bound to Ca^{2+} and PG (see section 4.1.1) and the structure of the Dap/Ca^{2+}/PG complex is not known.

Our finding that the methyl, ethyl, propyl and butyl analogues were only 2 to 4-fold less active than Dap suggests that the primary amide of the D-Asn2 side chain is not crucial for activity. However, the least active of all the D-Asn2 analogues studied here by far was the piperidinyl analogue which has a tertiary amide side chain. This removes any hydrogens on the side chain amide nitrogen. It could be that at least one of N-H hydrogens on the side chain of D-Asn2 is important for activity and may be involved in hydrogen bonding with a membrane target such as PG.

Chapter 3- Modification of DXDG Motif in Dap

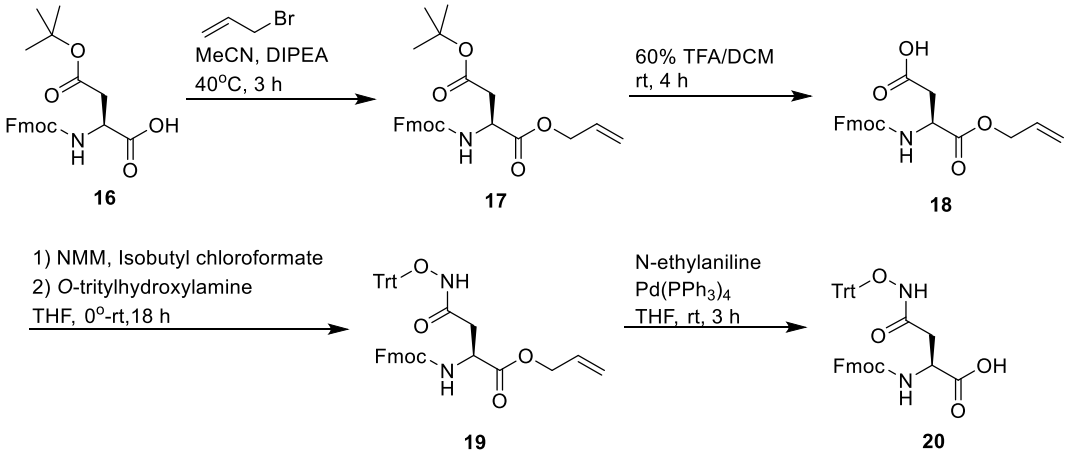
3.1 Objectives

As discussed in Section 1.8.2, Dap exhibits very modest activity in the presence of 1 mM Zn^{2+}. Armed with the knowledge that hydroxamic acids have a very high affinity for Zn^{2+}, the objectives of the work described in this chapter is to determine if it is possible to synthesize Dap analogs in which hydroxamic acid substitution occurs at either or both of the Asp residues in the DXDG motif. Residues 7 and 9 in Dap (DXDG motif) are believed to be involved in Ca^{2+} chelation, so we propose that substitution with Asn(OH), will result in novel Dap analogues that exhibit good activity in the presence of Zn^{2+}.[77]

3.2 Results and Discussion

3.2.1 Amino Acid Synthesis

For the synthesis of the Dap analogues, we needed to prepare Fmoc-L-Asn(OTrt)-OH. The synthesis of Fmoc-L-Asn(OTrt)-OH is more involved than the alkyl analogues but is still quite straightforward using the route used by Xia et al. (Scheme 7).[86]

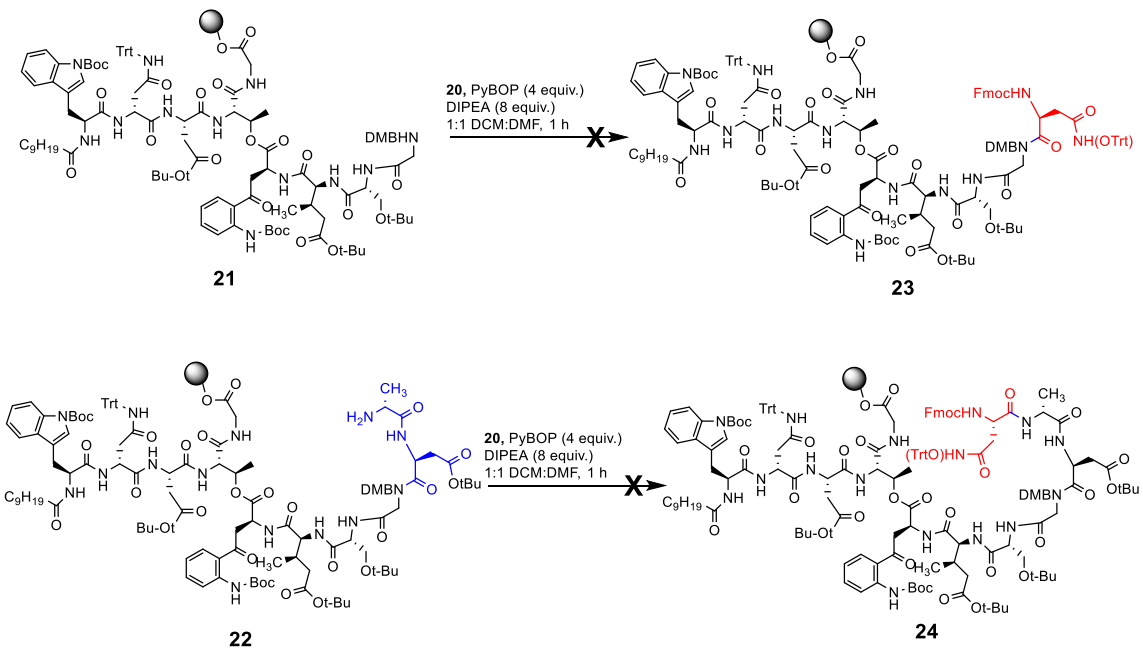


Scheme 7. Synthesis of Fmoc-Asn(O-Trt)-OH

Beginning with Fmoc-Asp(^{t}Bu)-OH (**16**), the terminal carboxyl group was protected using excess allyl bromide, in the presence of DIPEA in acetonitrile to give compound **17** in a 90% yield. The *ter*t-butyl moiety in **17** was removed with 60% TFA/DCM yielding compound **18**. After removal of the TFA by rotary evaporation, crude compound **18** was treated with isobutyl chloroformate (IBCF) and NMM followed by *O*-tritylhydroxylamine which gave compound **19** in a 75% yield over 2 steps. Removal of the allyl group in **19** using *N*-ethyl aniline and a catalytic amount of $Pd(Ph_3)_4$ provided Fmoc-L-Asn(OTrt)-OH (**20**) in a 77% yield. The overall yield was 52%.

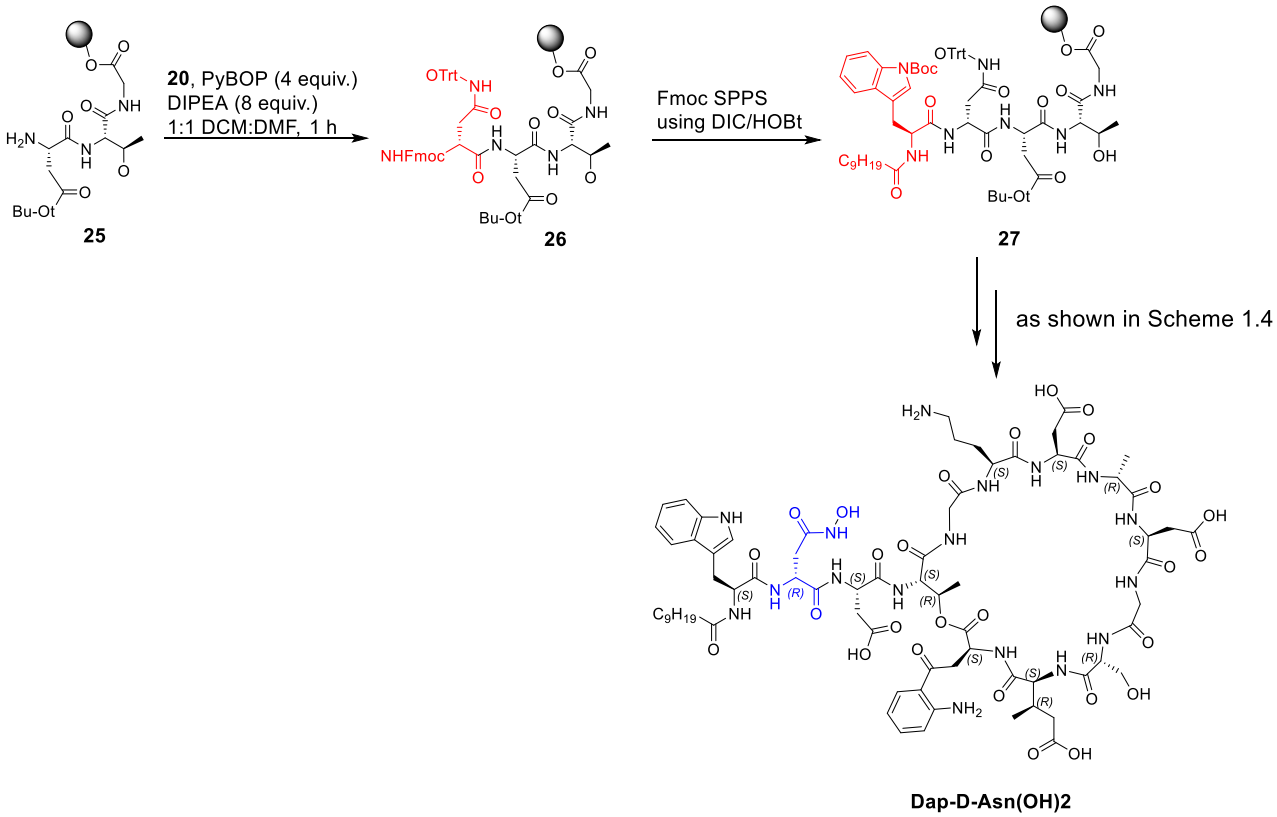
3.2.2 Synthesis of Dap Analogues

Although our ultimate target was a Dap analogue with both Asp7 and Asp 9 substituted with Asn(OH), we first attempted to prepare the monosubstituted analogs, Dap-Asn(OH)7 and Dap-Asn(OH)9, using the conditions employed by Xia et al. (PyBOP, DIPEA in DMF/DCM, 1 h) for installing Fmoc-Asn(OTrt)-OH into peptides (Scheme 8). Peptides **21** and **22** were prepared by Fmoc SPPS and then this peptide was subjected to Fmoc-Asn(OTrt)-OH (**20**, 4 equiv) under the above-mentioned conditions. Unfortunately, none of the desired peptides, **23** or **24**, were obtained as the ninhydrin test for amines still showed the presence of a free amine. This was confirmed by cleaving the peptide from the support and examining the crude mixture by MS which showed only the uncoupled starting peptides. We also tried extending the reaction conditions to 24 h but still none of peptides **23** and **24** were formed. We also tried using DIC/HOBt as coupling agents, but these conditions were also unsuccessful.



Scheme 8. Coupling attempts of Fmoc-Asn(OTrt)-OH on Dap-L-Asn(OH)7 linear sequence (**22**) and Dap-L-Asn(OH)9 linear sequence (**21**)

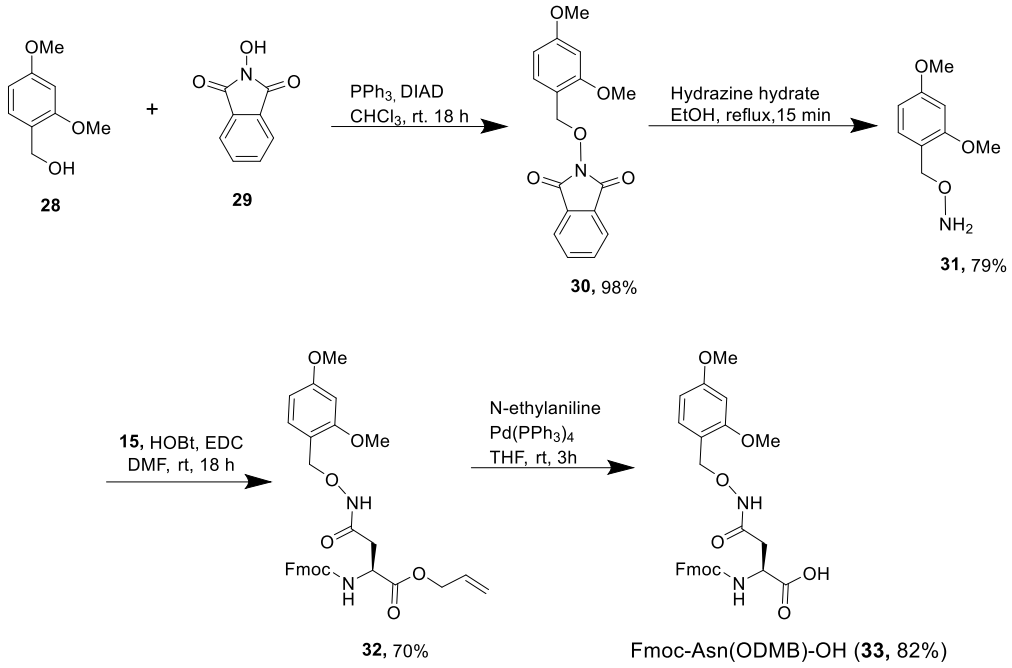
Our inability to prepare peptides **23** and **24** was surprising. To determine if the installation of Fmoc-Asn(OTrt)-OH is dependent upon the amino acid sequence, we decided to see if we could prepare a Dap analogue containing Asn(OH) at position 2 (replacing Asn2 with Asn(OH) to give Dap-D-Asn(OH)2). Peptide **25** was prepared using Fmoc SPPS. Using the conditions of Xia et al. Fmoc-D-Asn(OTrt)-OH was installed with out difficulty within 1 h, yielding peptide **26.** Trp1 and the acyl tail was installed to give peptide **27** and then our usual Fmoc SPPS route/conditions were used to complete the desired peptide Dap-D-Asn(OH)2 (Scheme 9). These results indicate that the installation of Fmoc-Asn(OTrt)-OH is sequence dependent.



Scheme 9. Synthesis of Dap-D-Asn(OH)2

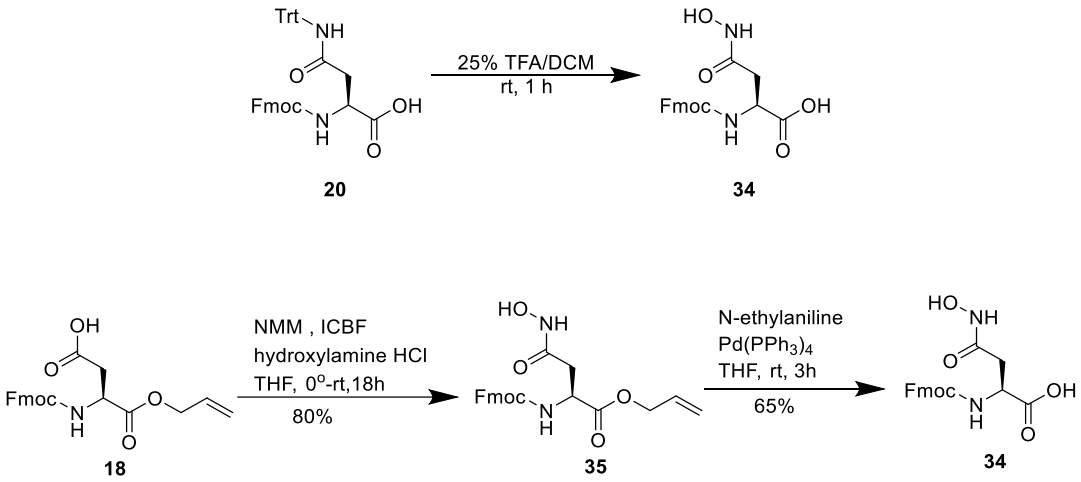
We reasoned that the steric bulk of the Trt protecting group might be preventing the coupling from taking place at positions 7 and 9. Therefore, we decided to prepare a new building block in which the side chain of Asn(OH) was protected with a smaller dimethoxybenzyl group. This building block was prepared using the route originally devised by Barlaam and coworkers shown in Scheme 10.[87] Dimethoxybenzylalcohol (**28**) and *N*-hydroxyphthalimide (**29**) were coupled using a Mitsunobu reaction to give compound **30** in a 98% yield. Treating **30** with hydrazine hydrate provided O-DMB-hydroxylamine (**31**) in a 79% yield. Compound **31** was coupled to amino acid **18** using EDC/HOBt to give fully protected amino acid **32** in a 70% yield. The allyl group in compound **32** was removed using our previous conditions to give Fmoc-

Asn(ODMB)-OH (**33**) in an 82% yield (Scheme 10). Unfortunately, attempts to install amino acid **33** into peptide **21** using both PyBOP/DIPEA or DIC/HOBt were also unsuccessful.



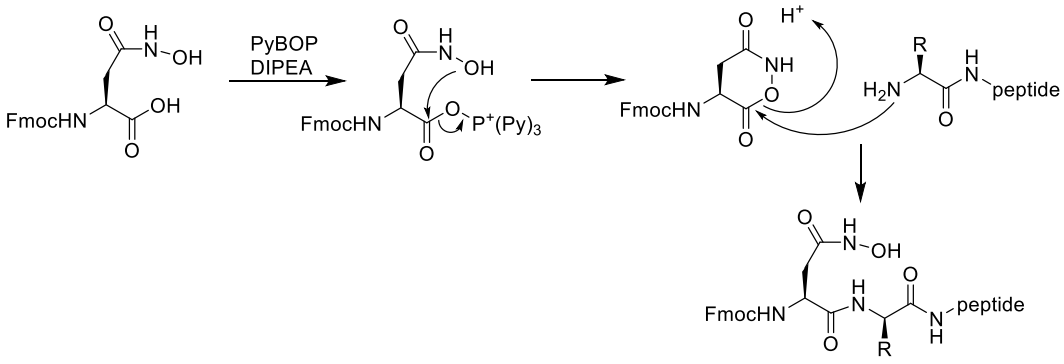
Scheme 10. Synthesis of Fmoc-Asn(ODMB)-OH

Our next tactic was to try and install the Asn(OH) using no PGP on the side chain. The Trt group in amino acid **20** was removed using 25% TFA in DCM for one hour to give amino acid **34** (Scheme 3.5) in an 89% yield. We also found that amino acid **34** could be prepared by reacting amino acid **18** with NMM/ICBF and hydroxylamine hydrochloride to give amino acid **35**, which upon allyl group removal provided amino acid **34** (Scheme 11).



Scheme 11. Alternative synthetic routes to prepare Fmoc-Asn(OH)-OH

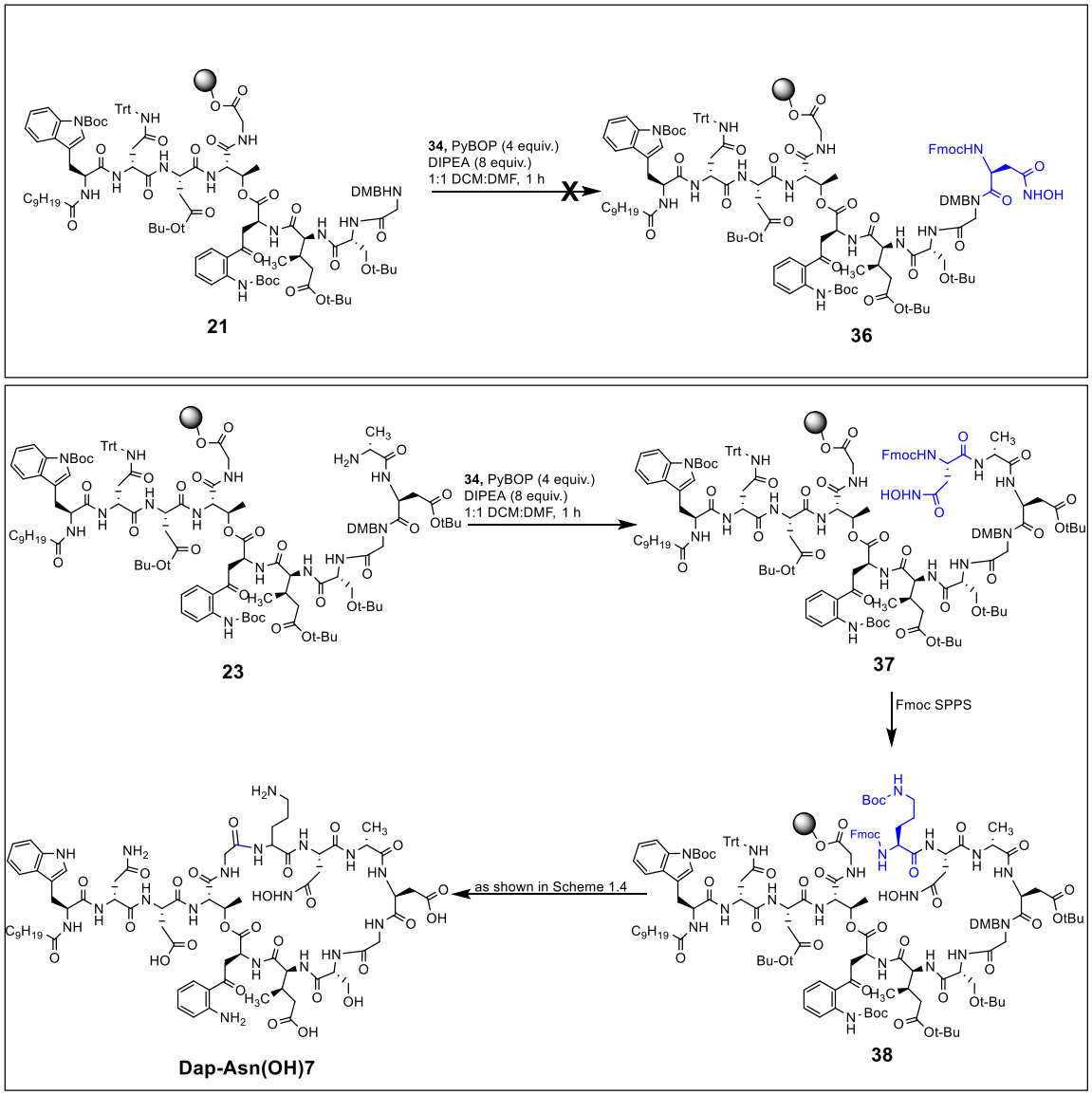
It is possible that building block **34** could cyclize upon activation and that this cyclic compound could react with the *N*-terminus of the peptide and form the desired product (Scheme 12).



Scheme 12. Possible activation and subsequent coupling of **34** to the peptide sequence.

Peptides **21** and **22** were subjected to building block **34** and the conditions of Xia et al. The reaction involving peptide **21** resulted in a very complex mixture and no coupled product **36** as determined by MS and HPLC. The reaction involving peptide **22** yielded a complex mixture by HPLC; however, MS analysis showed that some of the desired peptide (**37**) was formed. Although

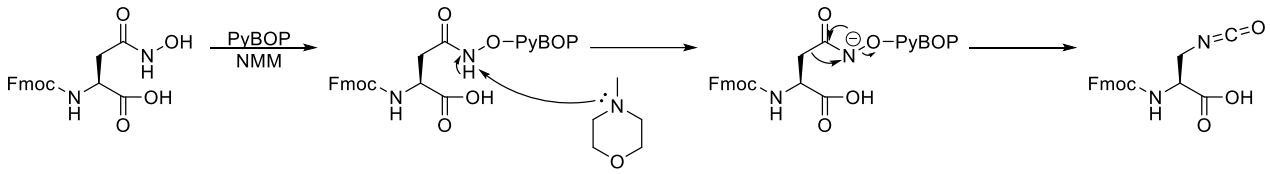
many byproducts were present, we decided to proceed with peptide **37**. Therefore, Orn6 was installed (**38**), the peptide was cleaved from the support, cyclized and then globally deprotected (Scheme 13). MS analysis of the crude mixture showed that the desired peptide was formed; however, after attempting to purify it by HPLC, only trace amounts of product were obtained.



Scheme 13. Synthetic routes for Dap-Asn(OH)9 (Top) and Dap-Asn(OH)7 (Bottom).

Our finding that using building block **34** yielded complex mixtures was not entirely unexpected. It is entirely possible that PyBOP could react with both the α-COOH and

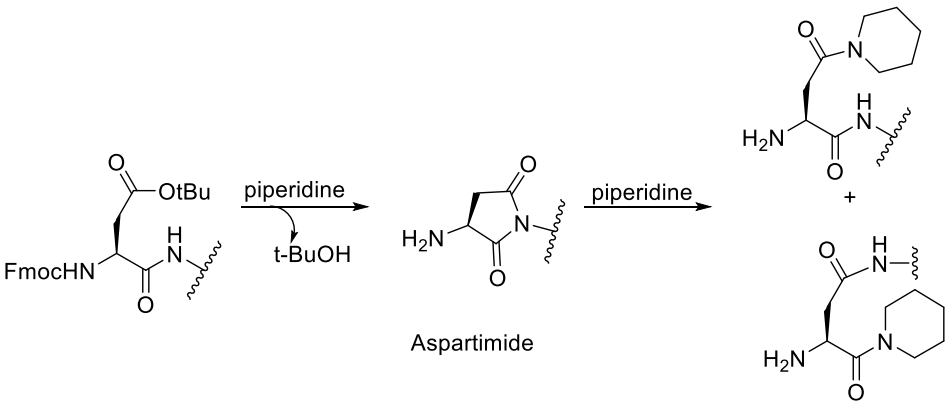
hydroxylamine groups. If it reacted with the side chain, then it is possible that it could undergo a Lossen rearrangement, as outlined in Scheme 14. The Lossen rearrangement shares similarities with the Curtius and Hofmann rearrangements which result in the formation of isocyanates which are good electrophiles.[88] It is understood the reaction begins with the activation of the hydroxamic acid in the presence of base and involves a carbon migration, however studies have shown little evidence proving the exact mechanism. Recently, researchers have proposed a self-propagative mechanism which needed a source of initiation. In summary, the initiation comes from a base in the environment which causes a homo-condensation event. This later undergoes a Lossen rearrangement, producing an isocyanate.[88] However, the Lossen rearrangement usually requires elevated temperatures (about 90 ºC). This condition, along with the fact that MS analysis of the crude reaction mixture did not detect a peptide having a mass that was 16 amu less than the desired product suggests that the Lossen rearrangement probably did not occur.



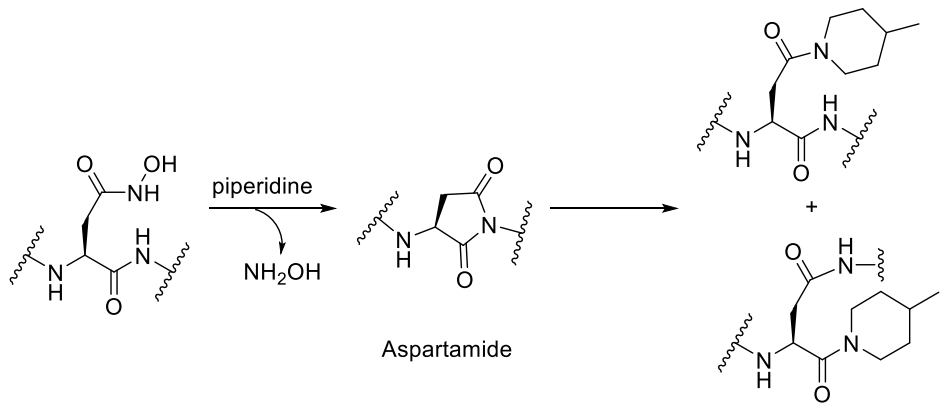
Scheme 14. Proposed mechanism of Lossen rearrangement

Another possibility is the formation of an aspartimide during peptide synthesis. This is a commonly encountered side reaction in peptide synthesis where amino acids can cyclize on the protected side chains of Asp, Asn, Glu and Gln (though the reaction is by far more prevalent on Asp) during Fmoc deprotection (Scheme 15). This reaction can occur whenever the peptide is subjected to piperidine. This reaction almost always occurs when there is an Asp-Gly sequence in the peptide. It can be prevented by using a DMB protecting group on the Gly a-amino group. This is why a DMB PG on Gly10 was used during the syntheses of Dap and its analogues. It is possible that aspartimide formation could also occur when using building block **34** as shown in Scheme 16.

Since we had a DMB-protected Gly at position 10, then this reaction could not have occurred when we tried to install Asn(OH) at position 9, but it could occur if Asn(OH) was installed at position 7. MS of the crude products after deprotection and extension of peptide **37** showed peaks that were 66 amu greater than the expected mass indicating that aspartimide formation had occurred.



Scheme 15. Proposed mechanism of aspartimide formation on O^{t}Bu-protected Asp.



Scheme 16. Proposed mechanism of aspartimide formation on hydroxamate amino acids

3.2.3 Biological Studies

Since we had Dap-D-Asn(OH)2 we tested it for biological activity against *B. subtilis* ATCC 6051 and found that it had an MIC of 2 mg/mL, which is only 2-fold greater than that of Dap. Its membrane insertion curve was very similar to that of Dap (Figure 23). However, this analogue requires slightly more calcium to reach maximum fluorescence.

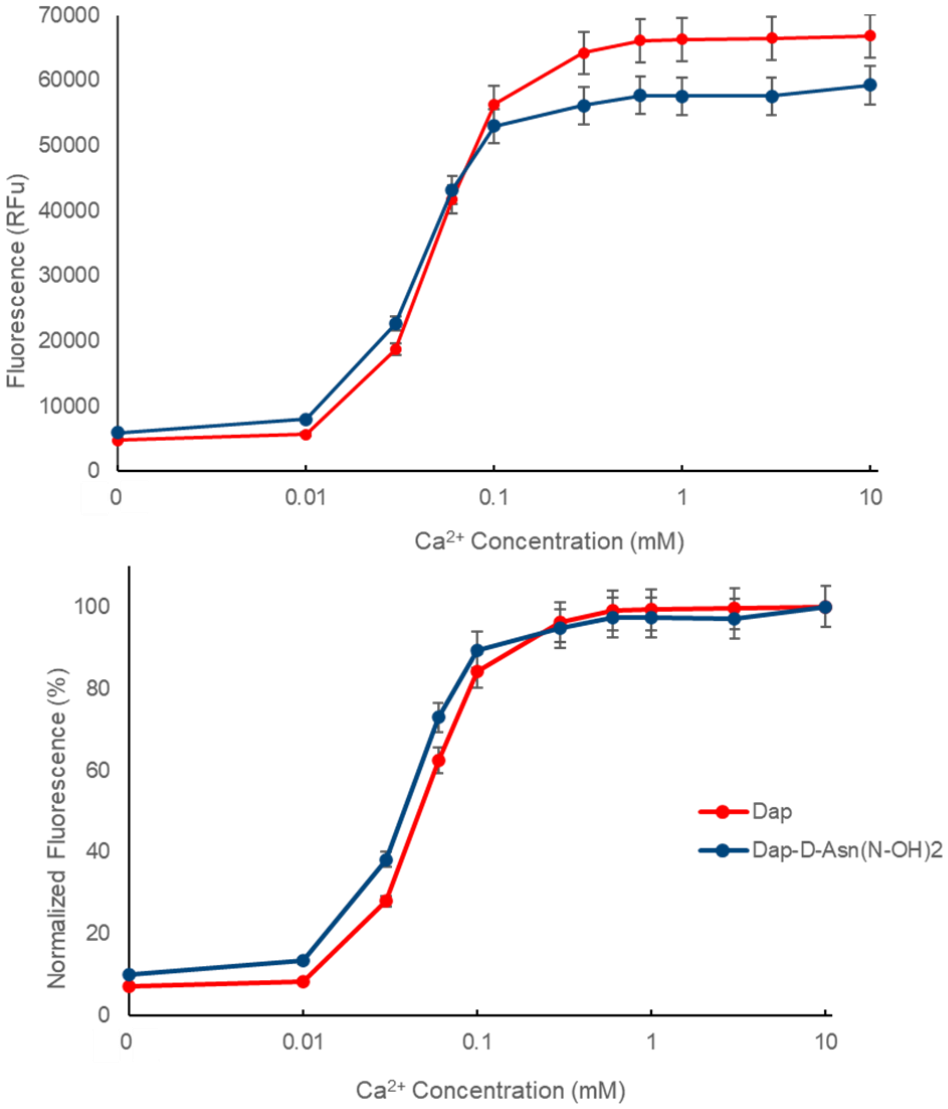
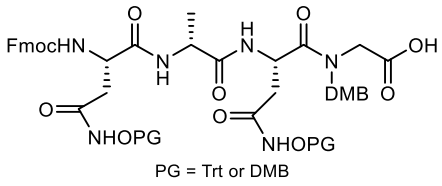


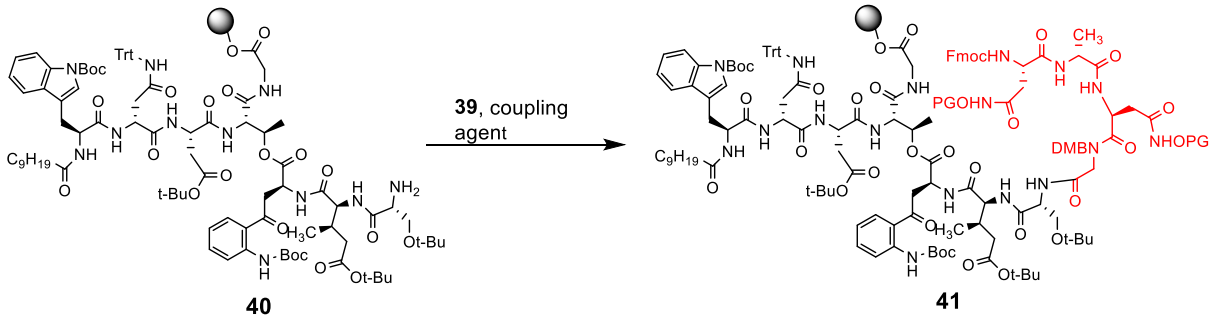
Figure 23. Membrane binding curves measuring Kyn13 fluorescence for Dap and Dap-D-Asn(OH)2 at 439 nm. Red: Dap. Blue: Dap-D-Asn(OH)2. Top panel: Data not normalized. Bottom panel: Data is normalized.

3.3 Future Directions

The synthesis of Dap analogues having Asn(OH) at positions 7 or 9 has proven to be more challenging than anticipated. The fact that we could install Asn(OH) at position 2 without difficulty suggests that the peptides **21** and **22** adopt a conformation that is not amenable to coupling using building blocks **20** and **33**. Perhaps the side chain protecting groups on these building blocks are too large and sterically hinder the coupling reaction. One possible solution to this problem is to prepare tetrapeptide **39** in solution and then couple it to peptide **40** to give peptide **41** as outlined in Scheme 17. Peptide **44** would be converted into the desired target analogue using our usual Dap synthesis protocols.



39



40 **41**

Scheme 17. Synthesis of peptide **41** using tetrapeptide **39** as a building block.

Chapter 4- Experimental Section

4.1 General Experimental Method

All reagents used for peptide synthesis were obtained from commercial sources including coupling reagents, resins and Fmoc amino acids. Unless stated otherwise ACS grade N-dimethylformamide (DMF), 4-methylpiperidine (4-MP), N-methyl-pyrrolidinone (NMP), trifluoroacetic acid (TFA) and triisopropylsilane (TIPS) were purchased from commercial suppliers and used without further purification. CH_2Cl_2 (DCM) was distilled from calcium hydride under nitrogen. THF was distilled from sodium and benzophenone under nitrogen. Chromatography was performed using 60 Å silica gel.

Resin loading was estimated using the procedure described by Gude at al.[89] Peptide synthesis was performed manually using a rotary mixer for agitation. Peptide synthesis progress was monitored by treating small portions of resin with 95/2.5/2.5 TFA/H_2O/TIPS for 60 min, removing the solvent under a N_2 stream, redissolving the peptide in 1:1 MeCN/H_2O, and analyzing by RP-HPLC and LRMS using a linear ion trap mass spectrometer.

Analytical and semi-preparative HPLC was performed using a Waters 600 controller equipped with Waters 2487 dual wavelength detector set to 220 nm and 280 nm. Analytical HPLC was accomplished with a Higgins Analytical Inc., (Mountainview, CA, USA) CLIPEUS reversed-phase C18 column (10 mm, 250 mm x 4.6 mm, 1 mL min^{-1} flow rate). Semi-preparative HPLC was performed with a Higgins Analytical Inc., CLIPEUS reversed-phase C18 column (10 mm, 250 mm x 20 mm, 10 mL min^{-1} flow rate).

High-resolution positive ion electrospray (ESI+) mass spectra were obtained using a hybrid quadrupole-orbitrap mass spectrometer, dissolving samples in 1:1 MeOH:H_2O + 0.1% formic acid.

All mass spectra were collected in positive mode. ^{1}H and ^{13}C NMR spectra were collected on a Bruker ASCEND 300 MHz spectrophotometer. Chemical shifts (δ) for ^{1}H and ^{13}C NMR spectra run in DMSO-d_6 are reported in ppm relative to the residual solvent peaks at 2.50 ppm and 39.52 ppm, respectively. δ for ^{1}H NMR spectra run in $CDCl_3$ are reported in ppm relative to the residual solvent peak at 7.26 ppm. All peaks are relative to an internal standard (trimethylsilane, 0 ppm).

Antibacterial activity of each synthetic antibiotic was determined using a broth dilution assay in which overnight bacterial cultures are diluted to approximately $1x10^6$ CFU/mL based on the measured optical density at 600 nm (OD600).[90] A series of two-fold serial dilution in LB broth were preformed directly on a 96-well microplate which were then inoculated with equal volume of diluted bacterial culture. 96-well plates were then incubated for 24 h at 37 ºC at which point the MIC was determined by the lowest peptide concentration at which there was no visible bacterial growth was observed.

Large unilamellar vesicles (LUVs) were prepared from 1,2-dioleoyl-sn-glycero-3-phosphoglycerol sodium salt (DOPG) and 1,2-dioleoyl-sn-glycero-3-phosphocholine (DOPC) (Avanti Polar Lipids, Alabaster, Alabama) in a 1:1 molar ratio by polycarbonate membrane extrusion as previously described by Muraih et al.[23] The combined lipid concentration was 5 mM, dissolved in a HEPES buffered saline solution (pH 7.4, 20 mM HEPES, 150 mM NaCl). The molar extinction coefficient of Dap at 365 nm was determined to be $\varepsilon = 4530\ M^{-1}cm^{-1}$.[91]

Fluorescence emission spectra were acquired with a PTI QuantaMaster 400 fluorometer (Horiba) following a protocol that has been previously described for daptomycin.[66] Measurements were taken in 20 mM HEPES buffer solution containing LUVs at a concentration of 250 μM, peptide concentration of 3 μM, 150 mM NaCl at pH 7.4 and buffer was warmed to 37 °C. A

calcium chloride solution was added to give the desired final concentrations. Emission spectra were collected following a 3 min equilibration time.

4.2 Experimental Section for Chapter 2

Fmoc-D-Asn(Me)-OH (8): 4-Methylmorpholine (0.15 mL, 1.34 mmol) was added to a solution of Fmoc-Asp-O^{t}Bu (0.50 g, 1.22 mmol) in anhydrous THF (20 mL), followed by isobutyl chloroformate (0.17 mL, 1.34 mmol) at 0 ºC. The solution was stirred at 0 ºC for 10 min and methylamine in H_2O (1 mL, 3.66 mmol) was added. Reaction mixture was allowed to stir for 18 h under N_2 at room temperature. The reaction was quenched with addition of saturated aqueous NH_4Cl (30 mL) and the reaction mixture extracted with ethyl acetate (3 x 30 mL). The combined organic layer was dried over anhydrous $MgSO_4$, then evaporated under vacuum. The crude mixture was dissolved in 25% TFA/DCM and stirred for 1 h. The reaction mixture was evaporated, and the crude solid was washed with diethyl ether/hexanes. Once filtered and dried, **8** was obtained as an off-white solid and used without further purification in subsequent steps. (0.42 g, 84%). **8** is a literature compound and characterized using ^{1}H NMR: (300 MHz, DMSO-d_6): δ 7.77 (d, J = 7.2 Hz, 2H), 7.68 (bs, NH), 7.58 (d, J = 8.5 Hz, 2H), 7.42 (d, J=8.7 Hz, NH), 7.25 (m, 4H), 4.16 (m, 4H), 2.44 (m, 3H), 2.38 (m, 2H).

General Amino Acid Coupling Procedure for compounds 10-12,15: To a solution of Fmoc-D-Asp-O^{t}Bu (3 equiv.) and NMM (10 equiv.) in N,N-dimethylformamide (DMF) (10 mL) was added HCTU (5 equiv.), then the corresponding alkyl amine (1.1 equiv.). The reaction stirred at room temperature for 1 h. Upon completion the product was precipitated with water (20 mL). The

product was filtered and dried. A white solid was obtained and used without further purification in subsequent steps.

General Amino Acid Coupling Procedure for Compounds 13-14: To a solution of Fmoc-D-Asp-O^{t}Bu (1 g, 4 eqiuv.) and DIPEA (5 equiv.) in dichloromethane (DCM) (50 mL) was added BOP (4 equiv.), then the corresponding alkyl amine (1.1 equiv.). The reaction stirred at room temperature for 1 h. The product was concentrated, then redissolved in DMF (5 mL), and precipitated with water (20 mL). This process was repeated once more. Product was obtained as an off-white solid.

General Procedure for *tert*-butyl Deprotection: Crude **Fmoc-Asn(R)-O^{t}Bu** was dissolved in 25 % TFA/DCM and stirred for 3 h. The reaction mixture was evaporated, and the crude solid was washed with diethyl ether/hexanes. Once filtered and dried, the corresponding amino acid was obtained as an off-white solid and used without further purification in subsequent steps.

Fmoc-D-Asn(Et)-OH (11): ^{1}H NMR: (300 MHz, DMSO-d_6): δ 7.88 (m, 3H), 7.70 (d, J = 7.2 Hz, 2H), 7.52 (d, J= 7.2, NH), 7.38 (m, 4H), 4.29 (m, 4H), 3.07 (m, 2H), 2.57 (dd, J= 5.0, 15.1 Hz, 1H), 2.45 (m, 1H), 1.41 (m, 2H), 1.05 (t, 3H, J= 7.5 Hz). ^{13}C (75 MHz, DMSO-d_6): δ 173.6, 169.2, 156.3, 144.3, 141.2, 128.1, 127.5, 125.7, 120.6, 66.1, 51.2, 47.1, 37.5, 33.9, 15.1. HRMS (ESI+) *m*/*z*: $[M + H]^+$ calcd for $C_{21}H_{23}O_5N_2$ 383.16015; found 383.16140

Fmoc-D-Asn(Pr)-OH (11): ^{1}H NMR: (300 MHz, DMSO-d_6): δ 7.90 (m, 3H), 7.71 (d, J = 7.3 Hz, 2H), 7.47−7.27 (m, NH), 7.38 (m, 4H), 4.27 (m, 4H), 3.00 (dq, J= 6.1 Hz, 12.5 Hz, 2H), 2.61 (m, 1H), 2.45 (m, 1H), 1.41 (m, 2H), 0.826 (t, 3H, J= 5.7 Hz). ^{13}C (75 MHz, DMSO-d_6): δ 173.6, 169.4, 156.3, 144.3, 141.2, 128.1, 127.5, 125.7, 120.6, 66.2, 51.2, 47.1, 37.6, 22.8, 11.8. HRMS (ESI+) *m*/*z*: $[M + H]^+$ calcd for $C_{22}H_{25}O_5N_2$ 397.17580; found 397.17454

Fmoc-D-Asn(Bu)-OH (12): ^{1}H NMR: (300 MHz, DMSO-d_6): δ 7.90 (d, J = 7.1 Hz, 2H), 7.82 (t, J= 7.1 Hz, NH), 7.71 (d, J = 7.7 Hz, 2H), 7.53 (d, J=9.5 Hz, NH), 7.38 (m, 4H), 4.33 (m, 4H), 3.04 (dd, J= 6.5 Hz, 13.0 Hz, 2H), 2.58 (dd, J=5.8, 15.3, 1H), 2.46 (dq, J=8.3, 15.3, 2H), 1.31 (m, 4H), 0.845 (t, 3H, J=7.3 Hz). ^{13}C (75 MHz, DMSO-d_6): δ 173.6, 169.2, 156.3, 144.3, 141.2, 128.1, 127.6, 125.7, 120.6, 66.2, 51.2, 47.1, 37.5, 33.9, 15.1. HRMS (ESI+) *m*/*z*: $[M + H]^+$ calcd for $C_{23}H_{27}O_5N_2$ 411.19145; found 411.19086

Fmoc-D-Asn(Hex)-OH (13): ^{1}H NMR: (300 MHz, DMSO-d_6): δ 7.90 (d, J = 8.5 Hz, 2H), 7.84 (t, J= 9.9 Hz, NH), 7.71 (d, J = 7.4 Hz, 2H), 7.54 (d, J= 8.2 Hz, NH), 7.38 (m, 4H), 4.32 (m, 4H), 3.03 (dd, J= 5.6 Hz, 11.8 Hz, 2H), 2.62-2.43 (dq, J= 5.7, J= 13.1, 2H), 1.31 (m, 8H) 0.845 (t, 3H, J=6.9 Hz). ^{13}C (75 MHz, DMSO-d_6): δ 173.6, 169.3, 156.3, 144.3, 141.2. 128.1, 127.5, 125.7, 120.6, 66.2, 51.2, 47.1, 37.5, 31.5, 29.5, 26.5, 22.5, 14.4. HRMS (ESI+) *m*/*z*: $[M + H]^+$ calcd for $C_{25}H_{31}O_5N_2$ 439.22275; found 439.22103

Fmoc-D-Asn(Oct)-OH (14): ^{1}H NMR: (300 MHz, DMSO-d_6): δ 7.84 (d, J = 7.5 Hz, 2H), 7.78 (b, NH), 7.66 (d, J = 7.5 Hz, 2H), 7.53 (d, J=7.5 Hz, NH), 7.32 (m, 4H), 4.27 (m, 4H), 2.98 (b, 2H), 2.49 (dd, J=5.8, 15.3, 1H), 2.46 (dq, J=9.4, 14.1, 2H), 1.25 (m, 4H), 0.775 (b, 3H). ^{13}C (75 MHz, DMSO-d_6): δ 173.6, 169.3353, 156.2738, 144.2247, 141.1699, 128.1125, 127.5391, 125.7054, 120.5656, 66.2118, 51.2326, 47.0705, 37.5494, 31.7155, 29.5076, 29.1922, 29.1203, 26.846, 22.5395, 14.3822. HRMS (ESI+) *m*/*z*: $[M + H]^+$ calcd for $C_{27}H_{35}O_5N_2$ 467.25405; found 467.25458

Fmoc-D-Asn(Pip)-OH (15): ^{1}H NMR: (300 MHz, DMSO-d_6): δ 7.89 (d, J = 7.6 Hz, 2H), 7.70 (d, J = 7.4 Hz, 2H), 7.38 (m, 4H), 7.36 (bs, NH), 4.34 (m, 4H), 3.38 (m, 4H), 2.73 (m, 2H), 1.48 (m, 6H).

General Procedures for Fmoc SPPS of Dap Analogues: The SPPS synthesis was performed manually 2'-Cl-TrtCl polystyrene resin (theoretical substitution = 1.5 mmol/g, 66.6 mg, 0.1 mmol, 1 equiv. in the synthesis of Dap analogues). The resin was then transferred to a disposable peptide cartridge and rinsed with DCM, followed by loading with Fmoc-Gly-OH (4.0 equiv.) and DIPEA (8.0 equiv.) in DCM (10.0 mL) for 24 h. The resin was capped with 17:2:1 DCM:MeOH:DIPEA (3 × 10 min), and the loading efficiency was determined to be 0.694 mmol g^{-1} in the synthesis of Dap alkyl analogues and 0.459 mmol g^{-1} in the synthesis of Dap-Asn(OH) analogues.

General Deprotection and Peptide Coupling Procedure for Dap-D-Asn(Me)2: The resin was swollen in DMF (30 min) then Fmoc-deprotected with 2-methylpiperidine (2-MP)/DMF (20%; 2 × 10 min). After washing the resin with DMF (3 × 5 min), a solution of Fmoc-L-Thr-OH (4 equiv.), hydroxybenzotriazole (HOBt, 4 equiv.) and diisopropylcarbodiimide (DIC, 4 equiv.) in DMF (4 mL) was added to the resin. After rotary agitation for 3 h at room temperature, the cartridge was drained and was washed with DMF (3 × 5 min). All subsequent Fmoc deprotections and couplings, with the exclusion of the ester bond and the cyclization, were performed in this way.

General Deprotection and Peptide Coupling Procedure for Dap-D-Asn(R)2: For the peptides containing compounds **9**-**15**, the resin was swollen in DMF (30 min) and then Fmoc-deprotected with 4-methylpiperidine (4-MP)/DMF (10%; 2 × 5 min). After washing the resin with DMF (3 × 5 min), a solution of Fmoc-L-Thr-OH (3 equiv.), hexafluorophosphate 6-chlorobenzotriazole tetramethyl uronium (HCTU, 5 equiv.) and N-methylmorpholine (NMM, 10 equiv.) in DMF (2.5 mL) was added to the resin. After rotary agitation for 10 min at room temperature, the resin containing cartridge was drained and the resin was washed with DMF (3 × 5 min). All subsequent Fmoc deprotections and couplings, with the exclusion of the ester bond and the cyclization, were performed in this way.

General Esterification Procedure: Esterification of all peptides (with exception of **Dap-D-Asn(Hex)2**) with Fmoc-Kyn(Boc)-OH involved adding a solution of amino acid (10 equiv) in dry DCM (2.5 mL) with addition of DIC (10 equiv) and the mixture was incubated for 30 min. The solution was added to peptide followed by DMAP (0.1 equiv). The rection was agitated for 18 h before the cartridge was drained and the resin was washed with DCM (3 x 5 min) then DMF (5 x 5 min). Reaction completion was tested by RP-HPLC and MS.

Esterification of Dap-D-Asn(Hex)2: Esterification used the same procedure as other **Dap-D-Asn(R)2** analogues, but dry DCM solvent was replaced with a solution of 1:1:1 NMP:DCM:DMF and 1% Triton X-100. Reaction completion was tested by RP-HPLC and MS.

General Resin Cleavage Procedure: Once Fmoc-Orn(Boc)-OH was coupled on and Fmoc-deprotected with 4MP/DMF, the peptide was cleaved from the resin by swelling in DCM (10 min) and then treating with 1% TFA/DCM (6 × 1 min) followed by 1% MeOH/DCM (6 × 1 min). A ninhydrin test was used to determine when all the peptide was removed from the resin. The peptide containing solution was then diluted with toluene and concentrated.

General Peptide Cyclization Procedure: The residue was dissolved in dry DMF (200 mL) and to this was added a solution of (7-azabenzotriazol-1-yloxy)tripyrrolidinophospho-nium hexafluorophosphate (PyAOP, 5 equiv.), 1-hydroxy-7-aza-benzotriazole (HOAt, 5 equiv.) and 2,4,6-collidine (10 equiv.) in DMF (5 mL). After stirring at room temperature for 48 h, the cyclization was determined to be complete by TLC (90:10:1 DCM:MeOH:AcOH). The cyclization solution was concentrated *in vacuo* and the residue was dissolved in EtOAc (200 mL) and then washed with $NaHSO_4$ (1 M, 2 × 200 mL), saturated aqueous $NaHCO_3$ (2 × 200 mL) and brine (2×200 mL). After drying the organic layer with $MgSO_4$, the crude peptide was filtered and concentrated *in vacuo.*

General Global Deprotection Procedure: The crude peptide was cooled in an ice-water bath and suspended in TFA:TIPS:H_2O (95:2.5:2.5). Cooling was removed immediately after the addition and the resulting solution was stirred for 1.5 h at room temperature. The solution was then concentrated with a stream of dry N_2. The deprotected peptide was precipitated from the oily residue through the addition of cold diethyl ether. The solid was washed with diethyl ether 3 times before being dissolved in 3:2 H2O:MeCN. Pure peptides were isolated from this solution by semi preparative HPLC in H_2O and MeCN over 60 min. Dap-containing fractions were combined, concentrated i*n vacuo* and lyophilized from Milli-Q H2O to give **Dap-Asn(R)2** peptides as an off-white powder.

Dap-D-Asn(Me)2: Purity of the peptide was verified by analytical RP-HPLC (t_r = 31.6 min, linear gradient of 90:10 to 10:90 H_2O/MeCN + 0.1% TFA over 60 min). HRMS (ESI+) *m*/*z*: $[M + 2H]^{2+}$ calcd for $C_{73}H_{105}O_{26}N_{17}$ 817.87028; found 817.87279

Dap-D-Asn(Et)2: Purity of the peptide was verified by analytical RP-HPLC (t_r = 33.8 min, linear gradient of 90:10 to 10:90 H_2O/MeCN + 0.1% TFA over 60 min). HRMS (ESI+) *m*/*z*: $[M + H]^{+}$ calcd for $C_{74}H_{107}O_{26}N_{17}$ 1649.75677; found 1649.75521

Dap-D-Asn(Pr)2: Purity of the peptide was verified by analytical RP-HPLC (t_r = 36.1 min, linear gradient of 90:10 to 10:90 H_2O/MeCN + 0.1% TFA over 60 min). HRMS (ESI+) *m*/*z*: $[M + H]^{2+}$ calcd for $C_{75}H_{109}O_{26}N_{17}$ 831.88593; found 831.88506

Dap-D-Asn(Bu)2: Purity of the peptide was verified by analytical RP-HPLC (t_r = 35.2 min, linear gradient of 90:10 to 10:90 H_2O/MeCN + 0.1% TFA over 60 min). HRMS (ESI+) *m*/*z*: $[M + H]^{+}$ calcd for $C_{76}H_{111}O_{26}N_{17}$ 1677.78807; found 1677.78698

Dap-D-Asn(Pip)2: Purity of the peptide was verified by analytical RP-HPLC (t_r = 35.6 min, linear gradient of 90:10 to 10:90 H_2O/MeCN + 0.1% TFA over 60 min). HRMS (ESI+) *m*/*z*: $[M + H]^+$ calcd for $C_{77}H_{113}O_{26}N_{17}$ 1689.78807; found 1689.78766

Dap-D-Asn(Hex)2: Purity of the peptide was verified by analytical RP-HPLC (t_r = 38.1 min, linear gradient of 90:10 to 10:90 H_2O/MeCN + 0.1% TFA over 60 min). HRMS (ESI+) *m*/*z*: $[M + H]^+$ calcd for $C_{78}H_{115}O_{26}N_{17}$ 1705.81937; found 1705.81194

Dap-D-Asn(Oct)2: Purity of the peptide was verified by analytical RP-HPLC (t_r = 42.1 min, linear gradient of 90:10 to 10:90 H_2O/MeCN + 0.1% TFA over 60 min). HRMS (ESI+) *m*/*z*: $[M + H]^{2+}$ calcd for $C_{80}H_{119}O_{26}N_{17}$ 866.92506; found 866.92653

4.3 Experimental Section for Chapter 3

Fmoc-Asp(O^{t}Bu)-OAllyl (17): Fmoc-Asp(O*t*-Bu)-OH (**16**) (3.0 g, 7.51 mmol) and DIPEA (2.57 mL, 15.02 mmol) and allyl bromide (8.3 mL, 11.62 mmol) were stirred in acetonitrile (15 mL) and heated under reflux at 40 ºC for 3 h. The resulting solution was allowed to cool, then into the flask was poured ethyl acetate (200 mL). The solution was washed with brine (3 x 200 mL) and the organic layer was collected and dried over $MgSO_4$, then concentrated *in vacuo,* to afford compound **17** as an off-orange oil and used without further purification in subsequent steps. (2.7 g, 90%). **17** is a literature compound and characterized using ^{1}H NMR: (300 MHz, DMSO-d_6): δ 7.88 (d, J = 7.2 Hz, 2H), 7.86 (b, NH), 7.70 (d, J = 6.4 Hz, 2H), 7.38 (m, 4H), 5.89 (m, 1H), 5.31 (d, J = 17.8 Hz, 1H), 5.20 (d, J = 10.2 Hz, 1H), 4.59 (d, J = 4.9 Hz, 2H), 4.47 (m, 1H), 4.34 (d, J = 6.8 Hz, 2H), 4.24 (t, J = 6.5 Hz, 1H), 2.69 (m, 1H), 1.39 (s, 9H).

Fmoc-Asn(OTrt)-OAllyl (19): Compound **17** was subjected to 25% TFA/DCM (20 mL) for 4 h at room temperature. The solution was evaporated *in vacuo* with toluene (3 x 10 mL) and redissolved in ethyl acetate (150 mL). The solution was washed with subsequent additions of 1 M $NaHSO_4$ (2 x 200 mL) and brine (2 x 200 mL) and the organic layer was collected and dried over $MgSO_4$, then concentrated *in vacuo,* to afford compound **18**, which was used without further purification. 4-Methylmorpholine (0.72 mL, 5.57 mmol) was added to a solution of **18** (2.0 g, 5.06 mmol) in anhydrous THF (20 mL), followed by isobutyl chloroformate (0.62 mL, 5.57 mmol) at 0 ºC. The solution was stirred at 0 ºC for 15 min and O-tritylhydroxylamine (1.39 g, 5.06 mmol) was added. Reaction mixture was allowed to stir at room temperature for 18 h under argon. The reaction was quenched by saturated aqueous NH_4Cl (30 mL) and the reaction mixture was extracted with ethyl acetate (3 x 30 mL). The combined organic layer was dried over anhydrous $MgSO_4$ and evaporated *in vacuo*. The crude product was purified using column chromatography (30% ethyl acetate in hexanes) to afford compound **19** (2.4 g, 75%) over two steps as an off-white solid. **19** is a literature compound and characterized using ^{1}H NMR: (300 MHz, DMSO-d_6): δ 7.90 (d, J = 7.5 Hz, 2H), 7.70 (d, J = 7.3 Hz, 2H), 7.38 (m, 4H), 7.35 (m, NH), 7.32 (b, 15H), 5.83 (m, 1H), 5.26 (dd, J = 1.2, 17.5 Hz, 1H), 5.17 (d, J= 10.5 , 1H), 4.50 (d, J = 4.9 Hz, 2H), 4.28 (m, 4H), 2.29 (m, 2H).

Fmoc-Asn(OTrt)-OH (20): N-ethylaniline (1.62 mL, 12.9 mmol) was added into a solution of **19** (2.4 g, 3.82 mmol) in anhydrous THF (20 mL) under argon. $Pd(PPh_3)_4$ (350 mg, 0.43 mmol) was added, and the reaction mixture was stirred for 3 h under argon at room temperature. The reaction was quenched using 0.1 M HCl (15 mL) and the reaction mixture extracted with ethyl acetate (3 x 30 mL). The combined organic layer was dried over anhydrous $MgSO_4$, then evaporated under vacuum. The crude product was precipitated in diethyl ether to afford compound **20** (1.8 g, 77%).

20 is a literature compound and characterized using ^{1}H NMR: (300 MHz, DMSO-d_6): δ 7.90 (d, J = 7.4 Hz, 2H), 7.73 (d, J = 7.3 Hz, 2H), 7.38 (m, 4H), 7.33 (m, 15H), 4.27 (m, 4H), 2.34 (m, 1H), 2.24 (m, 1H).

N-(2,4-dimethoxybenzyloxy)phthalimide (30): To a solution of 2,4-dimethoxybenzyl alcohol (2.7 g, 1 equiv.) in chloroform (120 mL) under argon were added N-hydroxyphthalimide (3.5 g, 1.3 equiv.) and triphenylphosphine (5.7 g, 1.3 equiv.). Diethylazodicarboxylate (3.5 ml, 1 equiv.) was added and the solution stirred overnight at room temperature. The solvent was evaporated *in vacuo* and the residue purified by flash chromatography on silica using dichloromethane as eluant, yielding **30.** (4.9 g, 98%): ^{1}H NMR ($CDCl_3$): 7.78 (m, 2H), 7.72 (m, 2H), 7.30 (d, 1H, J= 8.2 Hz), 6.43 (m, 2H), 5.21 (s, 2H), 3.79 (s, 3H), 3.72 (s, 3H).

O-2,4-dimethoxybenzylhydroxylamine (31): 30 (4.5 g, 14 mmol) and hydrazine hydrate (10 ml) in ethanol (95 %, 100 ml) was heated under reflux for 15 minutes and then allowed to cool. The mixture was filtered and the residue washed with ethanol. The filtrate was evaporated to dryness in vacuo to give **31.** (2.1 g, 79%) as a colourless oil: ^{1}H NMR ($CDCl_3$): 7.27 (d, 1H, J= 9.1 Hz), 6.49 (m, 2H), 5.30 (bs, 2H), 4.70 (s, 2H), 3.85 (s, 3H), 3.83 (s, 3H).

Fmoc-Asn(ODMB)-OAllyl (32): Compound **31** was first prepared as a colourless oil as previously described by Barlaam et al.[87] To a solution of **18** (200 mg, 0.50 mmol) in DMF (2 mL) was successively added HOBt (88 mg, 0.65 mmol), 2,4-dimethoxybenzyl hydroxylamine (**31**) (135 mg, 0.74 mmol), and dimethylaminopropylethylcarbodiimide hydrochloride (143 mg, 0.74 mmol). The mixture was stirred at room temperature for 18 hours. The mixture was diluted with ethyl actetate and washed with water, saturated $NaHCO_3$, brine, then dried over $MgSO_4$ and evaporated *in vacuo*. The residue was redissolved in DMF and compound

32 was precipitated from solution and filtered. This compound was used in subsequent steps without further purification.

Fmoc-Asn(ODMB)-OH (33): N-ethylaniline (0.2 mL, 0.87 mmol) was added into a solution of Fmoc-Asn(OTrt)-OAllyl (**32**) (162 mg, 0.29 mmol) in anhydrous THF (2 mL) under argon. $Pd(PPh_3)_4$ (70 mg, 0.03 mmol) was added, and the reaction mixture was stirred for 3 h under argon at room temperature. The reaction was quenched using 0.1 M HCl (15 mL) and the reaction mixture extracted with ethyl acetate (3 x 30 mL). The combined organic layer was dried over anhydrous $MgSO_4$, then evaporated under vacuum. The crude product was subject to flash chromatography in 28/70/2 ethyl acetate/hexanes/AcOH yielding compound **33** (0.123 mg, 82%). NMR: (300 MHz, DMSO-d_6): δ 7.86 (d, J= 7.4 Hz, 2H), 7.70 (d, J= 5.8 Hz, 2H), 7.45 (m, 4H), 7.30 (m, NH), 6.53 (m, 2H), 6.35 (m, J= 7.0 Hz, 1H), 5-01-4.90 (m, 2H), 4.10-4.65 (m, 1H), 4.46 (m, 2H), 4.31 (m, J=5.7 Hz, 1H), 3.87 (m, 6H), 3.40-2.77 (m, 2H). ^{13}C (75 MHz, DMSO-d_6): δ 173.3, 166.7, 161.5, 159.3, 144.3, 141.2, 132.5, 128.1, 127.6, 125.7, 120.5, 116.5, 104.9, 98.7, 79.6, 71.9, 66.2, 55.9, 55.7, 50.8, 47.0. HRMS (ESI+) *m*/*z*: $[M + H]^+$ calcd for $C_{28}H_{29}O_8N_2$ 521.19184; found 521.19311

Fmoc-Asn(OH)-OH (34): 20 (500 mg, 0.84 mmol) was dissolved in 25 % TFA/DCM (10 mL) and stirred for 1 h. The reaction mixture was diluted with toluene (5 mL) and evaporated. The crude solid was then washed with diethyl ether/hexanes. Once filtered and dried, **34** was obtained as an off-white solid. (1.5 g, 65%). HR-MS was attempted to characterize this amino acid, however we believe that it undergoes a Lossen rearrangement in the instrument, avoiding detection. ^1H NMR: (300 MHz, DMSO-d_6): δ 8.00 (d, J= 7.1 Hz, NH), 7.88 (d, J= 7.4 Hz, 2H), 7.70 (m, 2H), 7.37 (m, 4H), 4.31 (m, 4H), 2.84 (m, 1H), 2.54 (m, 1H). ^{13}C NMR: (75 MHz, DMSO-d_6): δ 173.2, 172.2, 156.3, 144.3, 141.2, 128.1, 127.6, 125.7, 125.6, 120.6, 66.2, 51.0, 47.1, 36.6

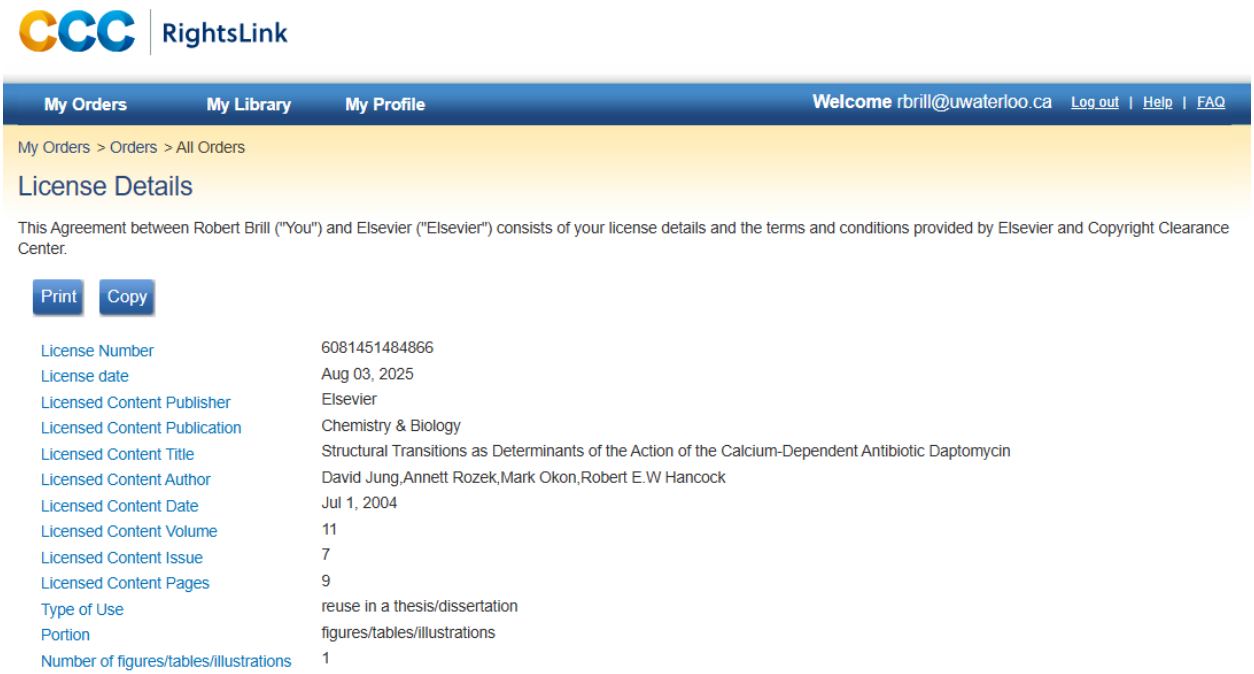
General procedures for Fmoc SPPS of Dap-Asn(OH) Analogues: The **Dap-Asn(OH)2** analogue was prepared via Fmoc SPPS as previously described, with slight variation. Coupling of amino acid **20** on peptide **25** used 4 equiv. of the appropriate Fmoc-protected amino acid and PyBOP (4 equiv.) which were dissolved in 1:1 DMF:DCM. DIPEA (8 equiv) was added into the mixture to activate the Fmoc-amino acid. The solution was added to the resin and agitated for one hour at room temperature. The resin was then washed with DMF (3 x 1 min), DCM (3 x 1 min), successively. The completion of coupling was tested using the Ninhydrin reagent, yielding peptide **26**. Peptide **23** was coupled with amino acid **34** using the PyBOP procedure described above. The **Dap-Asn(OH)7** analogue was prepared via Fmoc SPPS as previously described, with slight variation where the residue at position two was coupled as Fmoc-D-Asn(Trt)-OH using general Fmoc SPPS procedure and the sequence was continued as previously described.

Dap-D-Asn(OH)2

Purity of the peptide was verified by analytical RP-HPLC (t_r = 31.9 min, linear gradient of 90:10 to 10:90 H_2O/MeCN + 0.1% TFA over 60 min). HRMS (ESI+) *m*/*z*: $[M + 2H]^{2+}$ calcd for $C_{72}H_{103}N_{17}O_{27}$ 818.85992; found 818.8680

Letter of Copyright Permission

Permission for Figure 1.4



CCC RightsLink

My Orders | My Library | My Profile | Welcome rbrill@uwaterloo.ca | Log out | Help | FAQ

My Orders > Orders > All Orders

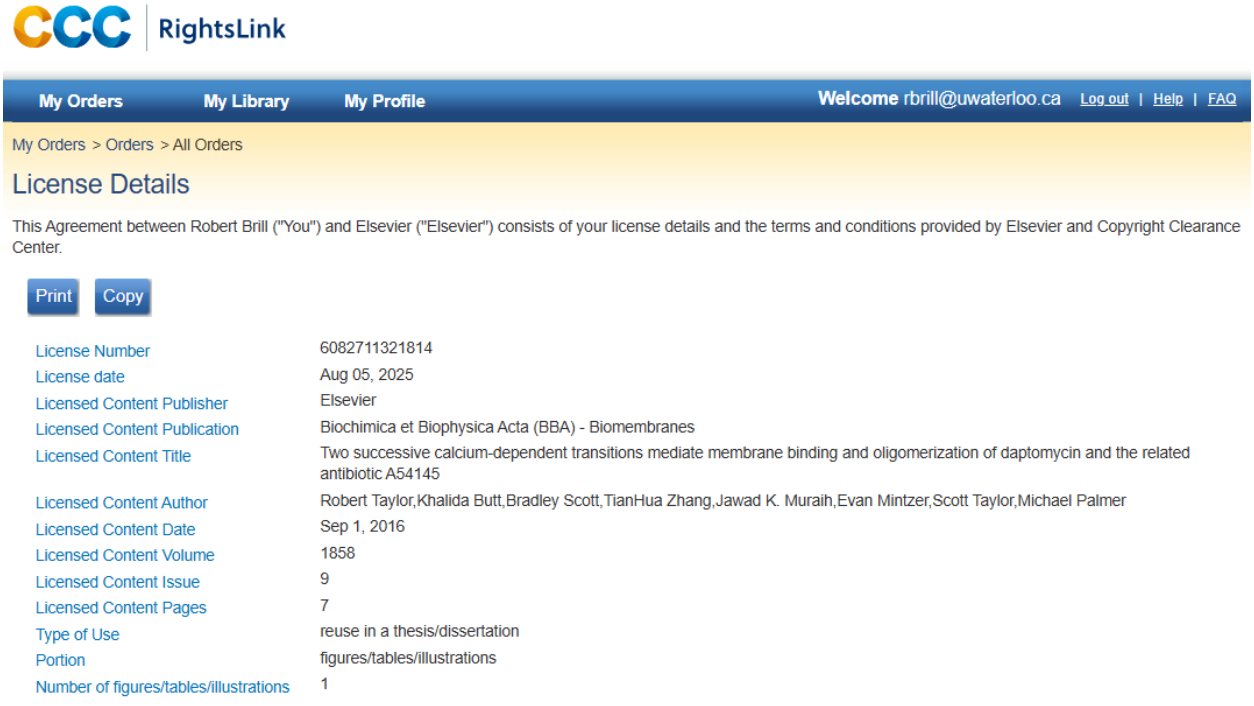
License Details

This Agreement between Robert Brill ("You") and Elsevier ("Elsevier") consists of your license details and the terms and conditions provided by Elsevier and Copyright Clearance Center.

Print Copy

License Number	6081451484866
License date	Aug 03, 2025
Licensed Content Publisher	Elsevier
Licensed Content Publication	Chemistry & Biology
Licensed Content Title	Structural Transitions as Determinants of the Action of the Calcium-Dependent Antibiotic Daptomycin
Licensed Content Author	David Jung,Annett Rozek,Mark Okon,Robert E.W Hancock
Licensed Content Date	Jul 1, 2004
Licensed Content Volume	11
Licensed Content Issue	7
Licensed Content Pages	9
Type of Use	reuse in a thesis/dissertation
Portion	figures/tables/illustrations
Number of figures/tables/illustrations	1

Permission for Figure 1.5



CCC RightsLink

My Orders | My Library | My Profile | Welcome rbrill@uwaterloo.ca | Log out | Help | FAQ

My Orders > Orders > All Orders

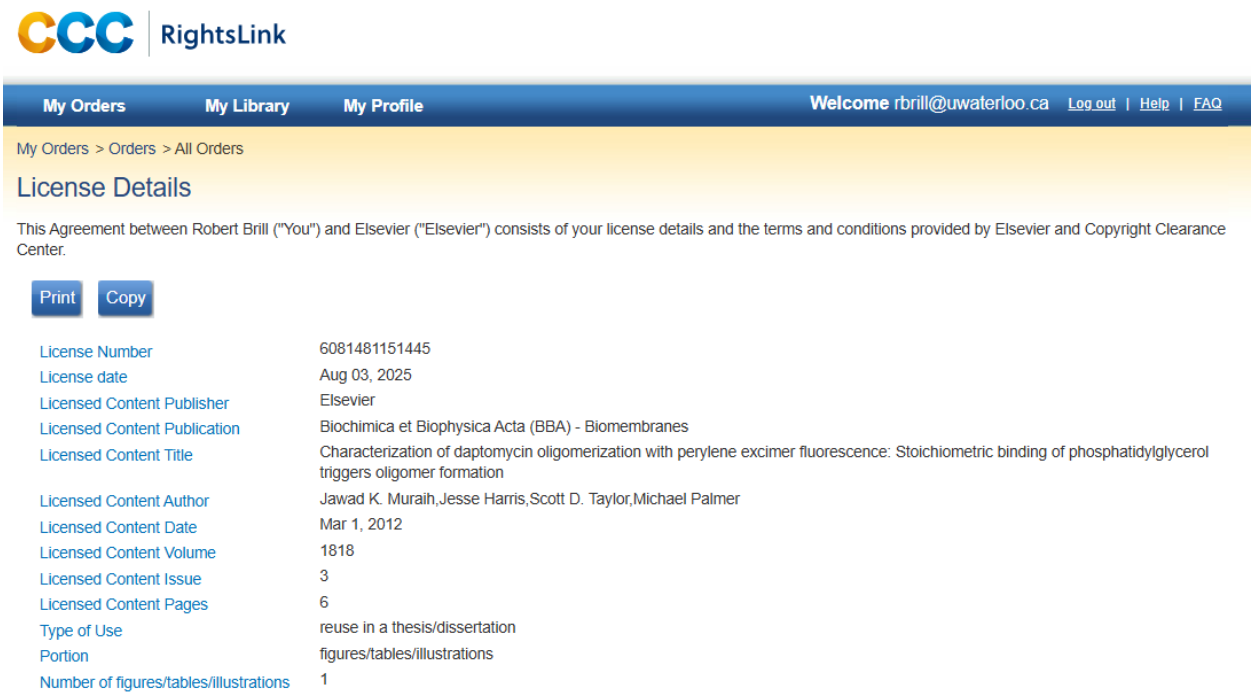
License Details

This Agreement between Robert Brill ("You") and Elsevier ("Elsevier") consists of your license details and the terms and conditions provided by Elsevier and Copyright Clearance Center.

Print Copy

License Number	6082711321814
License date	Aug 05, 2025
Licensed Content Publisher	Elsevier
Licensed Content Publication	Biochimica et Biophysica Acta (BBA) - Biomembranes
Licensed Content Title	Two successive calcium-dependent transitions mediate membrane binding and oligomerization of daptomycin and the related antibiotic A54145
Licensed Content Author	Robert Taylor,Khalida Butt,Bradley Scott,TianHua Zhang,Jawad K. Muraih,Evan Mintzer,Scott Taylor,Michael Palmer
Licensed Content Date	Sep 1, 2016
Licensed Content Volume	1858
Licensed Content Issue	9
Licensed Content Pages	7
Type of Use	reuse in a thesis/dissertation
Portion	figures/tables/illustrations
Number of figures/tables/illustrations	1

Permission for Figure 1.7



CCC RightsLink

My Orders | My Library | My Profile | Welcome rbrill@uwaterloo.ca | Log out | Help | FAQ

My Orders > Orders > All Orders

License Details

This Agreement between Robert Brill ("You") and Elsevier ("Elsevier") consists of your license details and the terms and conditions provided by Elsevier and Copyright Clearance Center.

Print Copy

License Number	6081481151445
License date	Aug 03, 2025
Licensed Content Publisher	Elsevier
Licensed Content Publication	Biochimica et Biophysica Acta (BBA) - Biomembranes
Licensed Content Title	Characterization of daptomycin oligomerization with perylene excimer fluorescence: Stoichiometric binding of phosphatidylglycerol triggers oligomer formation
Licensed Content Author	Jawad K. Muraih,Jesse Harris,Scott D. Taylor,Michael Palmer
Licensed Content Date	Mar 1, 2012
Licensed Content Volume	1818
Licensed Content Issue	3
Licensed Content Pages	6
Type of Use	reuse in a thesis/dissertation
Portion	figures/tables/illustrations
Number of figures/tables/illustrations	1

References

(1) Aminov, R. I. A Brief History of the Antibiotic Era: Lessons Learned and Challenges for the Future. *Front Microbiol*. **2010**, *1* (134). https://doi.org/10.3389/fmicb.2010.00134.

(2) Fleming, A. On the antibacterial action of cultures of a penicillium, with special reference to their use in the isolation of B. influenzae. 1929. *Bull World Health Organ*. **2001,** 79 (8) https://*doi.org/10.1093/cid/2.1.129*

(3) Lee Ventola, C. The Antibiotic Resistance Crisis Part 1: Causes and Threats. *P&T* **2015**; 40 (4). 277–283. https://doi.org/10.1186/s12889-021-11163-3

(4) Salam, M. A.; Al-Amin, M. Y.; Salam, M. T.; Pawar, J. S.; Akhter, N.; Rabaan, A. A.; Alqumber, M. A. A. Antimicrobial Resistance: A Growing Serious Threat for Global Public Health. *Healthcare*. **2023**, 11 (13), 1946 https://doi.org/10.3390/healthcare11131946.

(5) Becerra, S. C.; Roy, D. C.; Sanchez, C. J.; Christy, R. J.; Burmeister, D. M. An Optimized Staining Technique for the Detection of Gram Positive and Gram Negative Bacteria within Tissue. *BMC Res Notes* **2016**, *9* (1). https://doi.org/10.1186/s13104-016-1902-0.

(6) Loyola-Cruz, M. Á.; Gonzalez-Avila, L. U.; Martínez-Trejo, A.; Saldaña-Padilla, A.; Hernández-Cortez, C.; Bello-López, J. M.; Castro-Escarpulli, G. ESKAPE and Beyond: The Burden of Coinfections in the COVID-19 Pandemic. *Pathogens*. **2023,** 12 (5) 743. https://doi.org/10.3390/pathogens12050743.

(7) Santajit, S.; Indrawattana, N. Mechanisms of Antimicrobial Resistance in ESKAPE Pathogens. *BioMed Research International*. **2016**, 7 (2), 53-67. https://doi.org/10.1155/2016/2475067.

(8) Steed, M. E.; Rybak, M. J. Ceftaroline: A New Cephalosporin with Activity against Resistant Gram-Positive Pathogens. *Pharmacotherapy*. **2010,** 2 (25), 375–389. https://doi.org/10.1592/phco.30.4.375.

(9) Arias, C. A.; Murray, B. E. The Rise of the Enterococcus: Beyond Vancomycin Resistance. *Nature Reviews Microbiology*. **2012**, 10 (4), 266–278. https://doi.org/10.1038/nrmicro2761.

(10) Shariati, A.; Dadashi, M.; Moghadam, M. T.; van Belkum, A.; Yaslianifard, S.; Darban-Sarokhalil, D. Global Prevalence and Distribution of Vancomycin Resistant, Vancomycin Intermediate and Heterogeneously Vancomycin Intermediate

Staphylococcus Aureus Clinical Isolates: A Systematic Review and Meta-Analysis. *Sci Rep* **2020**, *10* (1). https://doi.org/10.1038/s41598-020-69058-z.

(11) Rossolini, G. M.; Arena, F.; Pecile, P.; Pollini, S. Update on the Antibiotic Resistance Crisis. *Current Opinion in Pharmacology*. **2014**. 56–60. https://doi.org/10.1016/j.coph.2014.09.006.

(12) Debono, M.; Barnhart, M.; Carrell, C. B.; Hoffmann, J. A.; Occolowitz, J. L.; Abbott, B. J.; Fukuda, D. S.; Hamill, R. L.; Biemann, K.; Herlihy, W. C. A21978C, a complex of new acidic peptide antibiotics: isolation, chemistry, and mass spectral structure elucidation. *J Antibiot.* **1987**. 40 (6). https://doi.org10.7164/antibiotics.40.761.

(13) Wood, T. M.; Martin, N. I. The Calcium-Dependent Lipopeptide Antibiotics: Structure, Mechanism, & Medicinal Chemistry. *MedChemComm*. Royal Society of Chemistry **2019** 10 (5), 634–646. https://doi.org/10.1039/c9md00126c.

(14) Huang, H. W. DAPTOMYCIN, Its Membrane-Active Mechanism vs. That of Other Antimicrobial Peptides. *Biochimica et Biophysica Acta - Biomembranes*. **2020,** 1862 (10), 18-33. https://doi.org/10.1016/j.bbamem.2020.183395.

(15) Fowler, V. G.; Boucher, H. W.; Corey, G. R.; Abrutyn, E.; Karchmer, A. W.; Rupp, M. E.; Levine, D. P.; Chambers, H. F.; Tally, F. P.; Vigliani, G. A.; Cabell, C. H.; Link, A. S.; Demeyer, I.; Filler, S. G.; Zervos, M.; Cook, P.; Parsonnet, J.; Bernstein, J. M.; Forrest, G. N.; Fätkenheuer, G.; Gareca, M.; Rehm, S. J.; Reinhardt Brodt, H.; Tice, A.; Cosgrove, S. E. *Daptomycin versus Standard Therapy for Bacteremia and Endocarditis Caused by Staphylococcus Aureus*; **2006**, 355 (7), 653-65.

(16) Canepari, P.; Boaretti, M.; Del Mar Lleo, M.; Satta, G. Lipoteichoic Acid as a New Target for Activity of Antibiotics: Mode of Action of Daptomycin (LY146032). *Antimicrob Agents Chemother* **1990**, *34* (6), 1220–1226. https://doi.org/10.1128/AAC.34.6.1220.

(17) Eliopoulos, G. M.; Willey, S.; Reiszner, E.; Spitzer, P. G.; Caputo, G.; Moellering, R. C. *In Vitro and In Vivo Activity of LY 146032, a New Cyclic Lipopeptide Antibiotic*; **1986**, 30(4):532-5. https://journals.asm.org/journal/aac.

(18) Jung, D.; Rozek, A.; Okon, M.; Hancock, R. E. W. Structural Transitions as Determinants of the Action of the Calcium-Dependent Antibiotic Daptomycin. *Chem Biol* **2004**, *11 (7)*, 949–957. https://doi.org/10.1016/j.

(19) Moreira, R.; Taylor, S. D. A54145 Factor D Is Not Less Susceptible to Inhibition by Lung Surfactant than Daptomycin. *ACS Infect Dis* **2022**, *8* (9), 1935–1947. https://doi.org/10.1021/acsinfecdis.2c00313.

(20) Teo JQ, Cai Y, Lim TP, Tan TT, Kwa AL. Carbapenem Resistance in Gram-Negative Bacteria: The Not-So-Little Problem in the Little Red Dot. *Microorganisms*. **2016** 16 (1). doi: 10.3390/microorganisms4010013.

(21) Silverman, J. A.; Mortin, L. I.; G VanPraagh, A. D.; Li, T.; Alder, J.; Ave, H. *Inhibition of Daptomycin by Pulmonary Surfactant: In Vitro Modeling and Clinical Impact*; **2004**, 191(12):2149-52. https://academic.oup.com/jid/article/191/12/2149/842668.

(22) Grein, F.; Müller, A.; Scherer, K. M.; Liu, X.; Ludwig, K. C.; Klöckner, A.; Strach, M.; Sahl, H. G.; Kubitscheck, U.; Schneider, T. Ca2+-Daptomycin Targets Cell Wall Biosynthesis by Forming a Tripartite Complex with Undecaprenyl-Coupled Intermediates and Membrane Lipids. *Nat Commun* **2020**, *11* (1). https://doi.org/10.1038/s41467-020-15257-1.

(23) Muraih, J. K.; Pearson, A.; Silverman, J.; Palmer, M. Oligomerization of Daptomycin on Membranes. *Biochim Biophys Acta Biomembr* **2011**, *1808* (4), 1154–1160. https://doi.org/10.1016/j.bbamem.2011.01.001.

(24) Taylor, R.; Butt, K.; Scott, B.; Zhang, T.; Muraih, J. K.; Mintzer, E.; Taylor, S.; Palmer, M. Two Successive Calcium-Dependent Transitions Mediate Membrane Binding and Oligomerization of Daptomycin and the Related Antibiotic A54145. *Biochim Biophys Acta Biomembr* **2016**, *1858* (9), 1999–2005. https://doi.org/10.1016/j.bbamem.2016.05.020.

(25) Allen, N. E.; Hobbs, J. N.; Alborn, W. E. *Inhibition of Peptidoglycan Biosynthesis in Gram-Positive Bacteria by LY146032*. *Antimicrob Agents Chemother*. **1987,** 31(7):1093-9. https://doi.org/10.1128/AAC.31.7.1093.

(26) Silverman, J. A.; Perlmutter, N. G.; Shapiro, H. M. Correlation of Daptomycin Bactericidal Activity and Membrane Depolarization in Staphylococcus Aureus. *Antimicrob Agents Chemother* **2003**, *47* (8), 2538–2544. https://doi.org/10.1128/AAC.47.8.2538-2544.2003.

(27) Zhang, T.; Muraih, J. K.; MacCormick, B.; Silverman, J.; Palmer, M. Daptomycin Forms Cation- and Size-Selective Pores in Model Membranes. *Biochim Biophys Acta Biomembr* **2014**, *1838* (10), 2425–2430. https://doi.org/10.1016/j.bbamem.2014.05.014.

(28) Seydlová, G.; Sokol, A.; Lišková, P.; Konopásek, I.; Fišer, R. Daptomycin Pore Formation and Stoichiometry Depend on Membrane Potential of Target Membrane. *Antimicrob Agents Chemother* **2019**, *63* (1). https://doi.org/10.1128/AAC.01589-18.

(29) Zuttion, F.; Colom, A.; Matile, S.; Farago, D.; Pompeo, F.; Kokavecz, J.; Galinier, A.; Sturgis, J.; Casuso, I. High-Speed Atomic Force Microscopy Highlights New Molecular Mechanism of Daptomycin Action. *Nat Commun* **2020**, *11* (1). https://doi.org/10.1038/s41467-020-19710-z.

(30) Silverman, J. A.; Perlmutter, N. G.; Shapiro, H. M. Correlation of Daptomycin Bactericidal Activity and Membrane Depolarization in Staphylococcus Aureus. *Antimicrob Agents Chemother* **2003**, *47* (8), 2538–2544. https://doi.org/10.1128/AAC.47.8.2538-2544.2003.

(31) Muraih, J. K.; Harris, J.; Taylor, S. D.; Palmer, M. Characterization of Daptomycin Oligomerization with Perylene Excimer Fluorescence: Stoichiometric Binding of Phosphatidylglycerol Triggers Oligomer Formation. *Biochim Biophys Acta Biomembr* **2012**, *1818* (3), 673–678. https://doi.org/10.1016/j.bbamem.2011.10.027.

(32) Taylor, R.; Beriashvili, D.; Taylor, S.; Palmer, M. Daptomycin Pore Formation Is Restricted by Lipid Acyl Chain Composition. *ACS Infect Dis* **2017**, *3* (11), 797–801. https://doi.org/10.1021/acsinfecdis.7b00138.

(33) Kreutzberger, M. A.; Pokorny, A.; Almeida, P. F. Daptomycin-Phosphatidylglycerol Domains in Lipid Membranes. *Langmuir* **2017**, *33* (47), 13669–13679. https://doi.org/10.1021/acs.langmuir.7b01841.

(34) Hobbs, J. K.; Miller, K.; O'Neill, A. J.; Chopra, I. Consequences of Daptomycin-Mediated Membrane Damage in Staphylococcus Aureus. *Journal of Antimicrobial Chemotherapy* **2008**, *62* (5), 1003–1008. https://doi.org/10.1093/jac/dkn321.

(35) Müller, A.; Wenzel, M.; Strahl, H.; Grein, F.; Saaki, T. N. V.; Kohl, B.; Siersma, T.; Bandow, J. E.; Sahl, H. G.; Schneider, T.; Hamoen, L. W. Daptomycin Inhibits Cell Envelope Synthesis by Interfering with Fluid Membrane Microdomains. *Proc Natl Acad Sci U S A* **2016**, *113* (45), E7077–E7086. https://doi.org/10.1073/pnas.1611173113.

(36) Howe, A.; Sofou, S. Daptomycin-Induced Lipid Phases on Model Lipid Bilayers: Effect of Lipid Type and of Lipid Leaflet Order on Membrane Permeability. *Journal of Physical Chemistry B* **2021**, *125* (22), 5775–5785. https://doi.org/10.1021/acs.jpcb.1c02047.

(37) Lee, M. T.; Yang, P. Y.; Charron, N. E.; Hsieh, M. H.; Chang, Y. Y.; Huang, H. W. Comparison of the Effects of Daptomycin on Bacterial and Model Membranes. *Biochemistry* **2018**, *57* (38), 5629–5639. https://doi.org/10.1021/acs.biochem.8b00818.

(38) Gray, D. A.; Wenzel, M. More than a Pore: A Current Perspective on the in Vivo Mode of Action of the Lipopeptide Antibiotic Daptomycin. *Antibiotics*. 2020. 9(1), 17. https://doi.org/10.3390/antibiotics9010017.

(39) Tran, T. T.; Munita, J. M.; Arias, C. A. Mechanisms of Drug Resistance: Daptomycin Resistance. *Ann N Y Acad Sci* **2015**, *1354* (1), 32–53. https://doi.org/10.1111/nyas.12948.

(40) Nguyen, A. H.; Hood, K. S.; Mileykovskaya, E.; Miller, W. R.; Tran, T. T. Bacterial Cell Membranes and Their Role in Daptomycin Resistance: A Review. *Frontiers in Molecular Biosciences*. **2022,** 14 (9). https://doi.org/10.3389/fmolb.2022.1035574.

(41) Mishra, N. N.; Bayer, A. S. Correlation of Cell Membrane Lipid Profiles with Daptomycin Resistance in Methicillin-Resistant Staphylococcus Aureus. *Antimicrob Agents Chemother* **2013**, *57* (2), 1082–1085. https://doi.org/10.1128/AAC.02182-12.

(42) Rashid, R.; Cazenave-Gassiot, A.; Gao, I. H.; Nair, Z. J.; Kumar, J. K.; Gao, L.; Kline, K. A.; Wenk, M. R. Comprehensive Analysis of Phospholipids and Glycolipids in the Opportunistic Pathogen Enterococcus Faecalis. *PLoS One* **2017**, *12* (4). https://doi.org/10.1371/journal.pone.0175886.

(43) Yang, S. J.; Nast, C. C.; Mishra, N. N.; Yeaman, M. R.; Fey, P. D.; Bayer, A. S. Cell Wall Thickening Is Not a Universal Accompaniment of the Daptomycin Nonsusceptibility Phenotype in Staphylococcus Aureus: Evidence for Multiple Resistance Mechanisms. *Antimicrob Agents Chemother* **2010**, *54* (8), 3079–3085. https://doi.org/10.1128/AAC.00122-10.

(44) Ernst, C. M.; Slavetinsky, C. M.; Kuhn, C. J.; Hauser, S. N.; Nega, J. N.; Mishra, M. N.; Gekeler, N. N.; Bayer, C. S.; Peschel, A. S. Gain-of-Function RESEARCH ARTICLE Molecular Biology and Physiology Crossm. *mbio.asm.org* **2018**, *9*, 1659–1677. https://doi.org/10.1128/mBio.

(45) Tran, T. T.; Panesso, D.; Mishra, N. N.; Mileykovskaya, E.; Guan, Z.; Munita, J. M.; Reyes, J.; Diaz, L.; Weinstock, G. M.; Murray, B. E.; Shamoo, Y.; Dowhan, W.; Bayer, A. S.; Arias, C. A. Daptomycin-Resistant Enterococcus Faecalis Diverts the Antibiotic Molecule from the Division Septum and Remodels Cell Membrane Phospholipids. *mBio* **2013**, *4* (4). https://doi.org/10.1128/mBio.00281-13.

(46) Arias, C. A.; Panesso, D.; McGrath, D. M.; Qin, X.; Mojica, M. F.; Miller, C.; Diaz, L.; Tran, T. T.; Rincon, S.; Barbu, E. M.; Reyes, J.; Roh, J. H.; Lobos, E.; Sodergren, E.; Pasqualini, R.; Arap, W.; Quinn, J. P.; Shamoo, Y.; Murray, B. E.; Weinstock, G. M. Genetic Basis for In Vivo Daptomycin Resistance in Enterococci. *New England*

Journal of Medicine **2011**, *365* (10), 892–900. https://doi.org/10.1056/nejmoa1011138.

(47) Peleg, A. Y.; Miyakis, S.; Ward, D. V.; Earl, A. M.; Rubio, A.; Cameron, D. R.; Pillai, S.; Moellering, R. C.; Eliopoulos, G. M. Whole Genome Characterization of the Mechanisms of Daptomycin Resistance in Clinical and Laboratory Derived Isolates of Staphylococcus Aureus. *PLoS One* **2012**, *7* (1). https://doi.org/10.1371/journal.pone.0028316.

(48) Jiang, J. H.; Bhuiyan, M. S.; Shen, H. H.; Cameron, D. R.; Rupasinghe, T. W. T.; Wu, C. M.; Le Brun, A. P.; Kostoulias, X.; Domene, C.; Fulcher, A. J.; McConville, M. J.; Howden, B. P.; Lieschke, G. J.; Peleg, A. Y. Antibiotic Resistance and Host Immune Evasion in Staphylococcus Aureus Mediated by a Metabolic Adaptation. *Proc Natl Acad Sci U S A* **2019**, *116* (9), 3722–3727. https://doi.org/10.1073/pnas.1812066116.

(49) Davlieva, M.; Zhang, W.; Arias, C. A.; Shamoo, Y. Biochemical Characterization of Cardiolipin Synthase Mutations Associated with Daptomycin Resistance in Enterococci. *Antimicrob Agents Chemother* **2013**, *57* (1), 289–296. https://doi.org/10.1128/AAC.01743-12.

(50) Su, X.; Dowhan, W. Regulation of Cardiolipin Synthase Levels in Saccharomyces Cerevisiae. *Yeast* **2006**, *23* (4), 279–291. https://doi.org/10.1002/yea.1352.

(51) Peleg, A. Y.; Miyakis, S.; Ward, D. V.; Earl, A. M.; Rubio, A.; Cameron, D. R.; Pillai, S.; Moellering, R. C.; Eliopoulos, G. M. Whole Genome Characterization of the Mechanisms of Daptomycin Resistance in Clinical and Laboratory Derived Isolates of Staphylococcus Aureus. *PLoS One* **2012**, *7* (1). https://doi.org/10.1371/journal.pone.0028316.

(52) Hachmann, A. B.; Angert, E. R.; Helmann, J. D. Genetic Analysis of Factors Affecting Susceptibility of Bacillus Subtilis to Daptomycinvt. *Antimicrob Agents Chemother* **2009**, *53* (4), 1598–1609. https://doi.org/10.1128/AAC.01329-08.

(53) Hachmann, A. B.; Sevim, E.; Gaballa, A.; Popham, D. L.; Antelmann, H.; Helmann, J. D. Reduction in Membrane Phosphatidylglycerol Content Leads to Daptomycin Resistance in Bacillus Subtilis. *Antimicrob Agents Chemother* **2011**, *55* (9), 4326–4337. https://doi.org/10.1128/AAC.01819-10.

(54) Jordan, S.; Junker, A.; Helmann, J. D.; Mascher, T. Regulation of LiaRS-Dependent Gene Expression in Bacillus Subtilis: Identification of Inhibitor Proteins, Regulator Binding Sites, and Target Genes of a Conserved Cell Envelope Stress-Sensing Two-

Component System. *J Bacteriol* **2006**, *188* (14), 5153–5166. https://doi.org/10.1128/JB.00310-06.

(55) Schrecke, K.; Jordan, S.; Mascher, T. Stoichiometry and Perturbation Studies of the LiaFSR System of Bacillus Subtilis. *Mol Microbiol* **2013**, *87* (4), 769–788. https://doi.org/10.1111/mmi.12130.

(56) Khan, A.; Davlieva, M.; Panesso, D.; Rincon, S.; Miller, W. R.; Diaz, L.; Reyes, J.; Cruz, M. R.; Pemberton, O.; Nguyen, A. H.; Siegel, S. D.; Planet, P. J.; Narechania, A.; Latorre, M.; Rios, R.; Singh, K. V; Ton-That, H.; Garsin, D. A.; Tran, T. T.; Shamoo, Y.; Arias, C. A. Antimicrobial Sensing Coupled with Cell Membrane Remodeling Mediates Antibiotic Resistance and Virulence in Enterococcus Faecalis. **2019,** 116 (52), 26925-26932. https://doi.org/10.1073/pnas.1916037116/-/DCSupplemental.

(57) Miller, W. R.; Tran, T. T.; Diaz, L.; Rios, R.; Khan, A.; Reyes, J.; Prater, A. G.; Panesso, D.; Shamoo, Y.; Arias, C. A. LiaR-Independent Pathways to Daptomycin Resistance in Enterococcus Faecalis Reveal a Multilayer Defense against Cell Envelope Antibiotics. *Mol Microbiol* **2019**, *111* (3), 811–824. https://doi.org/10.1111/mmi.14193.

(58) Munita, J. M.; Tran, T. T.; Diaz, L.; Panesso, D.; Reyes, J.; Murray, B. E.; Ariasa, C. A. A Liaf Codon Deletion Abolishes Daptomycin Bactericidal Activity against Vancomycin-Resistant Enterococcus Faecalis. *Antimicrob Agents Chemother* **2013**, *57* (6), 2831–2833. https://doi.org/10.1128/AAC.00021-13.

(59) Lam, H. Y.; Zhang, Y.; Liu, H.; Xu, J.; Wong, C. T. T.; Xu, C.; Li, X. Total Synthesis of Daptomycin by Cyclization via a Chemoselective Serine Ligation. *J Am Chem Soc* **2013**, *135* (16), 6272–6279. https://doi.org/10.1021/ja4012468.

(60) Chow, H. Y.; Po, K. H. L.; Jin, K.; Qiao, G.; Sun, Z.; Ma, W.; Ye, X.; Zhou, N.; Chen, S.; Li, X. Establishing the Structure-Activity Relationship of Daptomycin. *ACS Med Chem Lett* **2020**, *11* (7), 1442–1449. https://doi.org/10.1021/acsmedchemlett.0c00175.

(61) Lohani, C. R.; Taylor, R.; Palmer, M.; Taylor, S. D. Solid-Phase Total Synthesis of Daptomycin and Analogs. *Org Lett* **2015**, *17* (3), 748–751. https://doi.org/10.1021/acs.orglett.5b00043.

(62) Moreira, R.; Wolfe, J.; Taylor, S. D. A High-Yielding Solid-Phase Total Synthesis of Daptomycin Using a Fmoc SPPS Stable Kynurenine Synthon. *Org Biomol Chem* **2021**, *19* (14), 3144–3153. https://doi.org/10.1039/d0ob02504f.

(63) *Merrifield, R. B. Solid phase peptide synthesis. I. The synthesis of a tetrapeptide. J. Am. Chem. Soc.* **1963**, 85 (14), 2149– 2154 https://doi.org/: 10.1021/ja00897a025

(64) Dettin, M.; Pegoraro, S.; Rovero, P.; Bicciato, S.; Bagno, A.; Di Bello, C. SPPS of Difficult Sequences: A Comparison of Chemical Conditions, Synthetic Strategies and on-Line Monitoring. *Journal of Peptide Research* **1997**, *49* (1), 103–111. https://doi.org/10.1111/j.1399-3011.1997.tb01126.x.

(65) Grünewald, J.; Sieber, S. A.; Mahlert, C.; Linne, U.; Marahiel, M. A. Synthesis and Derivatization of Daptomycin: A Chemoenzymatic Route to Acidic Lipopeptide Antibiotics. *J Am Chem Soc* **2004**, *126* (51), 17025–17031. https://doi.org/10.1021/ja045455t.

(66) Barnawi, G.; Noden, M.; Taylor, R.; Lohani, C.; Beriashvili, D.; Palmer, M.; Taylor, S. D. An Entirely Fmoc Solid Phase Approach to the Synthesis of Daptomycin Analogs. *Peptide Science* **2019**, *111* (1). https://doi.org/10.1002/bip.23094.

(67) Scull, E. M.; Bandari, C.; Johnson, B. P.; Gardner, E. D.; Tonelli, M.; You, J.; Cichewicz, R. H.; Singh, S. Chemoenzymatic Synthesis of Daptomycin Analogs Active against Daptomycin-Resistant Strains. *Appl Microbiol Biotechnol* **2020**, *104* (18), 7853–7865. https://doi.org/10.1007/s00253-020-10790-x.

(68) Elshahawi, S. I.; Cao, H.; Shaaban, K. A.; Ponomareva, L. V.; Subramanian, T.; Farman, M. L.; Spielmann, H. P.; Phillips, G. N.; Thorson, J. S.; Singh, S. Structure and Specificity of a Permissive Bacterial C-Prenyltransferase. *Nat Chem Biol* **2017**, *13* (4), 366–368. https://doi.org/10.1038/nchembio.2285.

(69) Chow, H. Y.; Po, K. H. L.; Gao, P.; Blasco, P.; Wang, X.; Li, C.; Ye, L.; Jin, K.; Chen, K.; Chan, E. W. C.; You, X.; Yi Tsun Kao, R.; Chen, S.; Li, X. Methylation of Daptomycin Leading to the Discovery of Kynomycin, a Cyclic Lipodepsipeptide Active against Resistant Pathogens. *J Med Chem* **2020**, *63* (6), 3161–3171. https://doi.org/10.1021/acs.jmedchem.9b01957.

(70) Guan, D.; Li, J.; Chen, F.; Li, J.; Bian, X.; Yu, Y.; Feng, X.; Lan, L.; Huang, W. A Facile and Selective Derivatization Approach on Kynurenine-NH2 in Daptomycin, Leading to the Discovery of Hexakynomycin to Combat Multidrug-Resistant Gram-Positive Pathogens Especially Daptomycin-Resistant Bacteria. *Eur J Med Chem* **2023**, *259*. https://doi.org/10.1016/j.ejmech.2023.115638.

(71) Tebano, G.; Zaghi, I.; Baldasso, F.; Calgarini, C.; Capozzi, R.; Salvadori, C.; Cricca, M.; Cristini, F. Antibiotic Resistance to Molecules Commonly Prescribed for the Treatment of Antibiotic-Resistant Gram-Positive Pathogens: What Is Relevant for the Clinician? *Pathogens*. **2024**. 13(1), 88. https://doi.org/10.3390/pathogens13010088.

(72) Citarella, A.; Moi, D.; Pinzi, L.; Bonanni, D.; Rastelli, G. Hydroxamic Acid Derivatives: From Synthetic Strategies to Medicinal Chemistry Applications. *ACS Omega*. **2021**, 135 (2), 21843–21849. https://doi.org/10.1021/acsomega.1c03628.

(73) Maola, K.; Wilbs, J.; Touati, J.; Sabisz, M.; Kong, X.; Baumann, A.; Deyle, K.; Heinis, C. Engineered Peptide Macrocycles Can Inhibit Matrix Metalloproteinases with High Selectivity. *Angewandte Chemie* **2019**, *131* (34), 11927–11931. https://doi.org/10.1002/ange.201906791.

(74) Buijs, N. P.; Vlaming, H. C.; Kotsogianni, I.; Arts, M.; Willemse, J.; Duan, Y.; Alexander, F. M.; Cochrane, S. A.; Schneider, T.; Martin, N. I. A Classic Antibiotic Reimagined: Rationally Designed Bacitracin Variants Exhibit Potent Activity against Vancomycin-Resistant Pathogens. *Proc Natl Acad Sci U S A* **2024**, *121* (29). https://doi.org/10.1073/pnas.2315310121.

(75) Eliopoulos, G. M.; Thauvin,' Benjamin Gerson, C.; Moellering, R. C. *In Vitro Activity and Mechanism of Action of A21978C1, a Novel Cyclic Lipopeptide Antibiotic*; **1985,** 27(3):357-62. https://journals.asm.org/journal/aac.

(76) Ho, S. W.; Jung, D.; Calhoun, J. R.; Lear, J. D.; Okon, M.; Scott, W. R. P.; Hancock, R. E. W.; Straus, S. K. Effect of Divalent Cations on the Structure of the Antibiotic Daptomycin. *European Biophysics Journal* **2008**, *37* (4), 421–433. https://doi.org/10.1007/s00249-007-0227-2.

(77) Francesconi, O.; Gentili, M.; Bartoli, F.; Bencini, A.; Conti, L.; Giorgi, C.; Roelens, S. Phosphate Binding by a Novel Zn(II) Complex Featuring a Trans-1,2-Diaminocyclohexane Ligand. Effective Anion Recognition in Water. *Org Biomol Chem* **2015**, *13* (6), 1860–1868. https://doi.org/10.1039/c4ob02321h.

(78) Zhong, Z.; Anslyn, E. V. A Colorimetric Sensing Ensemble for Heparin. *J Am Chem Soc* **2002**, *124* (31), 9014–9015. https://doi.org/10.1021/ja020505k.

(79) Hood, C. A.; Fuentes, G.; Patel, H.; Page, K.; Menakuru, M.; Park, J. H. Fast Conventional Fmoc Solid-Phase Peptide Synthesis with HCTU. *Journal of Peptide Science* **2008**, *14* (1), 97–101. https://doi.org/10.1002/psc.921.

(80) Hojo, K.; Ichikawa, H.; Fukumori, Y.; Kawasaki, K. Development of a Method for the Solid-Phase Peptide Synthesis in Water. In *International Journal of Peptide Research and Therapeutics*; **2008**, 14(5), 373–380. https://doi.org/10.1007/s10989-008-9145-0.

(81) Mupparapu, N.; Lin, Y. H. C.; Kim, T. H.; Elshahawi, S. I. Regiospecific Synthesis of Calcium-Independent Daptomycin Antibiotics Using a Chemoenzymatic Method.

Chemistry - A European Journal **2021**, *27* (12), 4176–4182. https://doi.org/10.1002/chem.202005100.

(82) Barnawi, G.; Noden, M.; Goodyear, J.; Marlyn, J.; Schneider, O.; Beriashvili, D.; Schulz, S.; Moreira, R.; Palmer, M.; Taylor, S. D. Discovery of Highly Active Derivatives of Daptomycin by Assessing the Effect of Amino Acid Substitutions at Positions 8 and 11 on a Daptomycin Analogue. *ACS Infect Dis* **2022**, *8* (4), 778–789. https://doi.org/10.1021/acsinfecdis.1c00483.

(83) Ball, L. J.; Goult, C. M.; Donarski, J. A.; Micklefield, J.; Ramesh, V. NMR Structure Determination and Calcium Binding Effects of Lipopeptide Antibiotic Daptomycin. *Org Biomol Chem* **2004**, *2* (13), 1872–1878. https://doi.org/10.1039/b402722a.

(84) Ho, S. W.; Jung, D.; Calhoun, J. R.; Lear, J. D.; Okon, M.; Scott, W. R. P.; Hancock, R. E. W.; Straus, S. K. Effect of Divalent Cations on the Structure of the Antibiotic Daptomycin. *European Biophysics Journal* **2008**, *37* (4), 421–433. https://doi.org/10.1007/s00249-007-0227-2.

(85) Rotondi, K. S.; Gierasch, L. M. A Well-Defined Amphipathic Conformation for the Calcium-Free Cyclic Lipopeptide Antibiotic, Daptomycin, in Aqueous Solution. *Biopolymers - Peptide Science Section* **2005**, *80* (2–3), 374–385. https://doi.org/10.1002/bip.20238.

(86) Xia, Y.; To, J.; Chan, N. Y.; Hu, S.; Liew, H. T.; Balamkundu, S.; Zhang, X.; Lescar, J.; Bhattacharjya, S.; Tam, J. P.; Liu, C. F. Nγ-Hydroxyasparagine: A Multifunctional Unnatural Amino Acid That Is a Good P1 Substrate of Asparaginyl Peptide Ligases. *Angewandte Chemie - International Edition* **2021**, *60* (41), 22207–22211. https://doi.org/10.1002/anie.202108125.

(87) Barlaam, B.; Hamon, A.; Maudet, M. *New Hydroxylamines for the Synthesis of Hydroxamic Acids*; **1998,** 39 (43) 7819-8002. https://doi.org/10.1002/CHIN.199901080

(88) Thomas, M.; Alsarraf, J.; Araji, N.; Tranoy-Opalinski, I.; Renoux, B.; Papot, S. The Lossen Rearrangement from Free Hydroxamic Acids ARTICLE The Lossen Rearrangement from Free Hydroxamic Acids. *Org Biomol Chem* **2019**, *17* (22) 5420-5427. https://doi.org/10.1039/c9ob00789ji.

(89) Gude, M.; Ryf, J.; White, P. D. *An Accurate Method for the Quantitation of Fmoc-Derivatized Solid Phase Supports*; 2003.

(90) Wiegand, I.; Hilpert, K.; Hancock, R. E. W. Agar and Broth Dilution Methods to Determine the Minimal Inhibitory Concentration (MIC) of Antimicrobial Substances. *Nat Protoc* **2008**, *3* (2), 163–175. https://doi.org/10.1038/nprot.2007.521.

(91) Tsentalovich, Y. P.; Snytnikova, O. A.; Sherin, P. S.; Forbes, M. D. E. Photochemistry of Kynurenine, a Tryptophan Metabolite: Properties of the Triplet State. *Journal of Physical Chemistry A* **2005**, *109* (16), 3565–3568. https://doi.org/10.1021/jp045142k.

Appendices: Spectral Data of New Compounds

Appendix A: Chapter 2

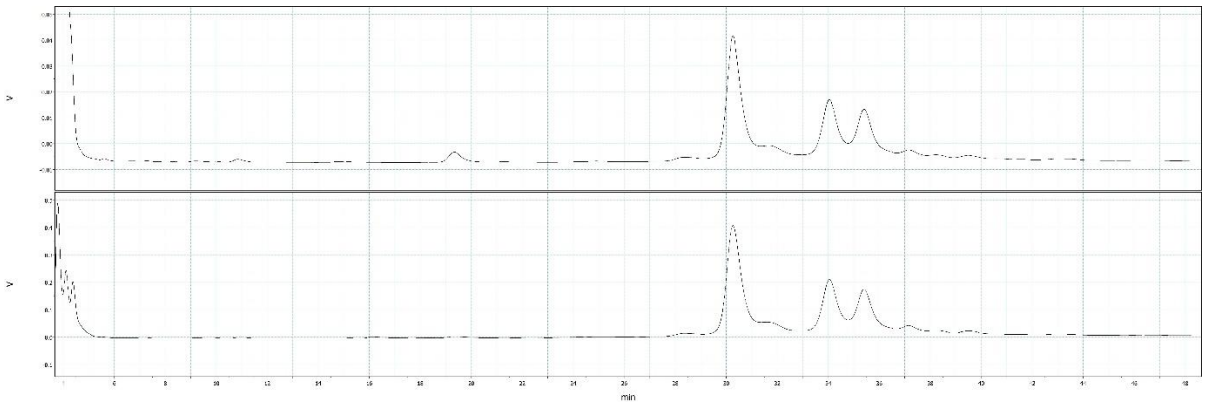


Figure A. 1. HPLC chromatogram of crude Dap-D-Asn(Me)2 after cleavage. 70-45 (H_2O/MeCN+0.1 % TFA) in 60 min. Top Panel: λ=280 nm. Bottom Panel: λ=220 nm.

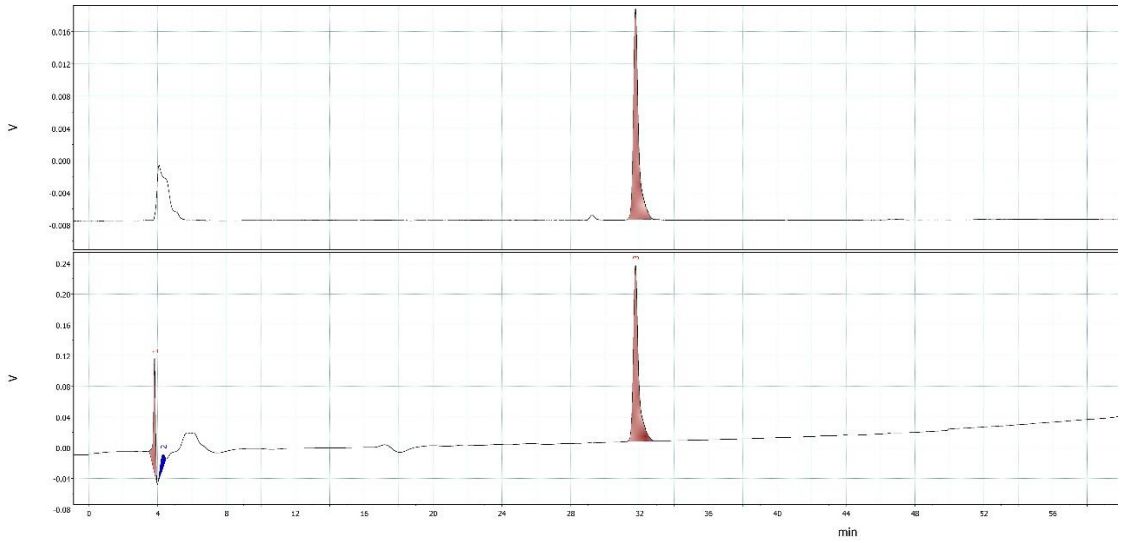
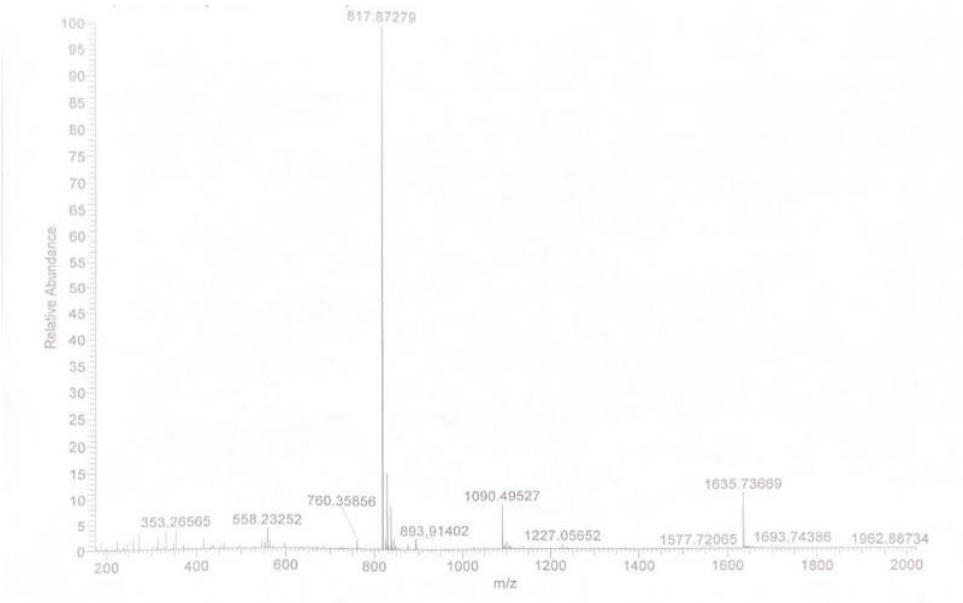


Figure A. 2. HPLC chromatogram of pure synthetic Dap-D-Asn(Me)2. Gradient: 90-10 (H_2O/MeCN+0.1 % TFA) in 60 min. Top Panel: λ=280 nm. Bottom Panel: λ=220 nm.

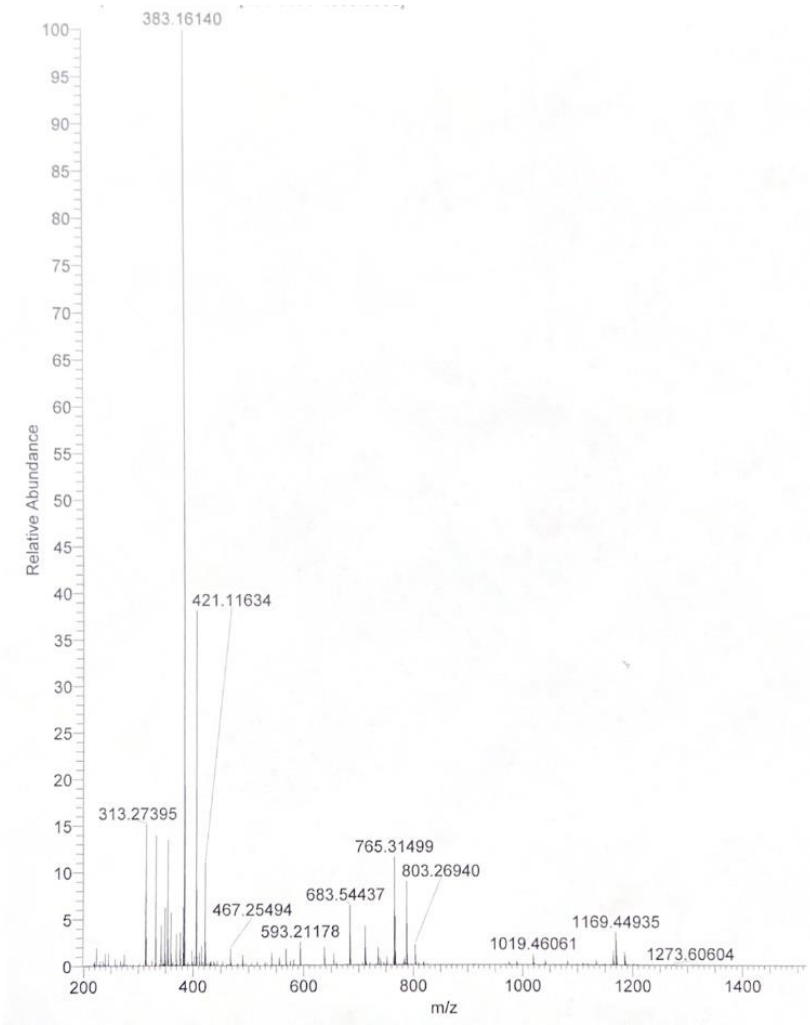


Elemental composition search on mass 817.87279

m/z= 812.87279-822.87279

m/z	Theo. Mass	Delta (ppm)	RDB equiv.	Composition
817.87279	817.87028	3.06	30.0	$C_{73}H_{105}O_{26}N_{17}$

Figure A. 3. ESI+HRMS of pure Dap-D-Asn(Me)2. $[M+H]^+$ at m/z=1635.73669 and $[M+2H]^{2+}$ at m/z=817.87279.



Elemental composition search on mass 383.16140

m/z= 378.16140-388.16140

m/z	Theo. Mass	Delta (ppm)	RDB equiv.	Composition
383.16140	383.16015	3.27	11.5	$C_{21}H_{23}O_5N_2$
	383.17138	-26.05	11.5	$C_{20}H_{23}O_4N_4$
	383.14757	36.09	12.0	$C_{20}H_{21}O_5N_3$

Figure A. 4. ESI+HRMS of pure Fmoc-D-Asn(Et)-OH. $[M+H]^+$ at m/z=383.16140 and $[M+K]^+$ at m/z=421.11634.

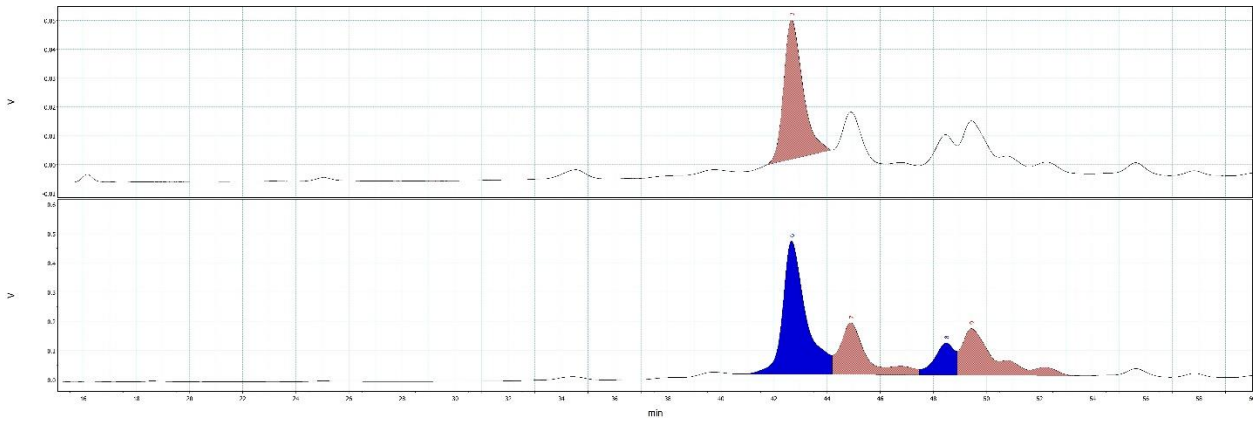


Figure A. 5. HPLC chromatogram of crude Dap-D-Asn(Et)2 after cleavage. 70-55 (H_2O/MeCN+0.1 % TFA) in 60 min (λ=220 nm)

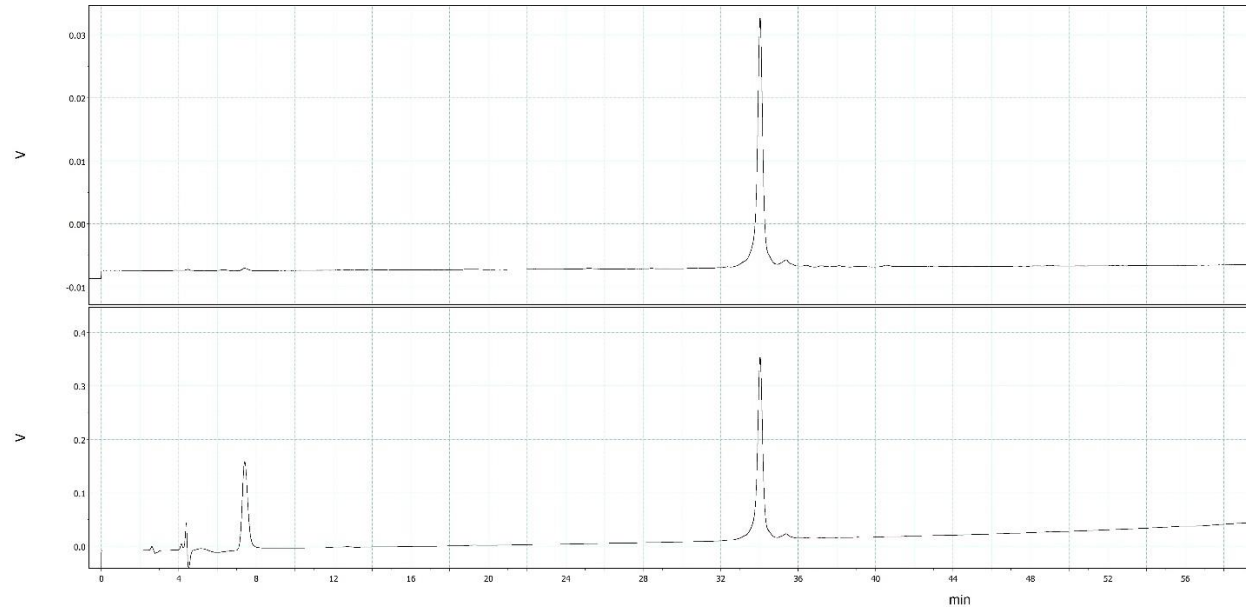
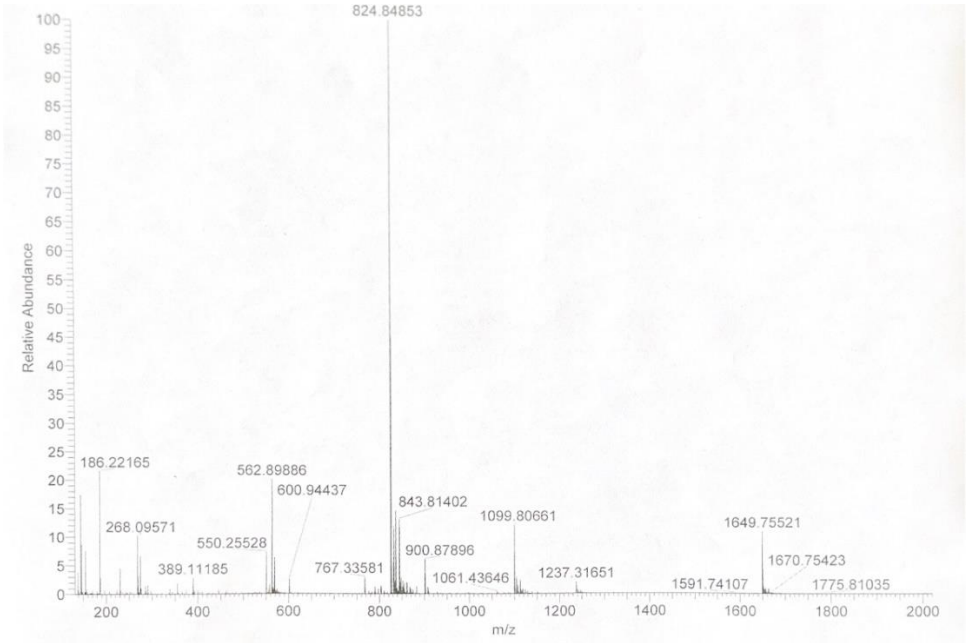


Figure A. 6. HPLC chromatogram of pure synthetic Dap-D-Asn(Et)2. Gradient: 90-10 (H_2O/MeCN+0.1 % TFA) in 60 min. Top Panel: λ=280 nm. Bottom Panel: λ=220 nm.

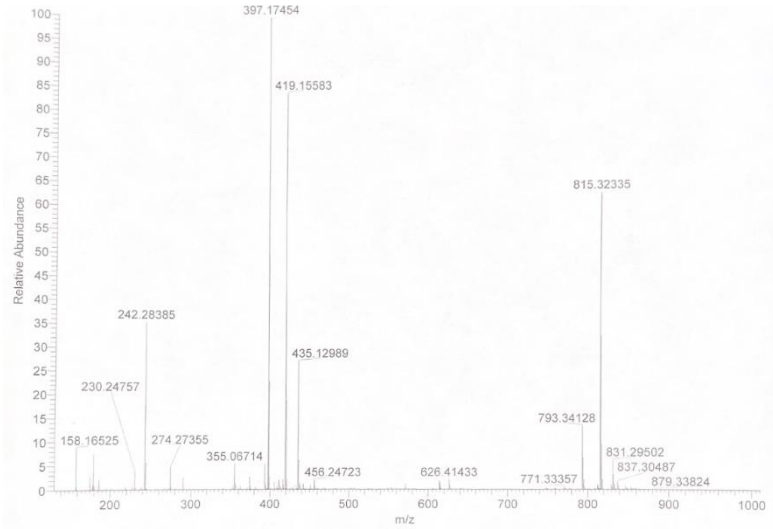


Elemental composition search on mass 1649.75521

m/z= 1644.75521-1654.75521

m/z	Theo. Mass	Delta (ppm)	RDB equiv.	Composition
1649.75521	1649.75677	-0.94	30.0	$C_{74}H_{107}O_{26}N_{17}$
	1649.74419	6.68	30.5	$C_{73}H_{105}O_{26}N_{18}$
	1649.76934	-8.57	29.5	$C_{75}H_{109}O_{26}N_{16}$

Figure A. 7. ESI+HRMS of pure Dap-D-Asn(Et)2. $[M+H]^+$ at m/z=1649.75521, $[M+Na]^+$ at m/z=1670.75423 and $[M+2H]^{2+}$ at m/z=824.84853.



Elemental composition search on mass 397.17454

m/z= 392.17454-402.17454

m/z	Theo. Mass	Delta (ppm)	RDB equiv.	Composition
397.17454	397.17580	-3.17	11.5	$C_{22}H_{25}O_5N_2$
	397.16456	25.12	11.5	$C_{23}H_{25}O_6$
	397.16322	28.50	12.0	$C_{21}H_{23}O_5N_3$

Figure A. 8. ESI+HRMS of pure Fmoc-D-Asn(Pr)-OH. $[M+H]^+$ at m/z=397.17454, $[M+Na]^+$ at m/z=419.15583 and $[M+K]^+$ at m/z=435.12989.

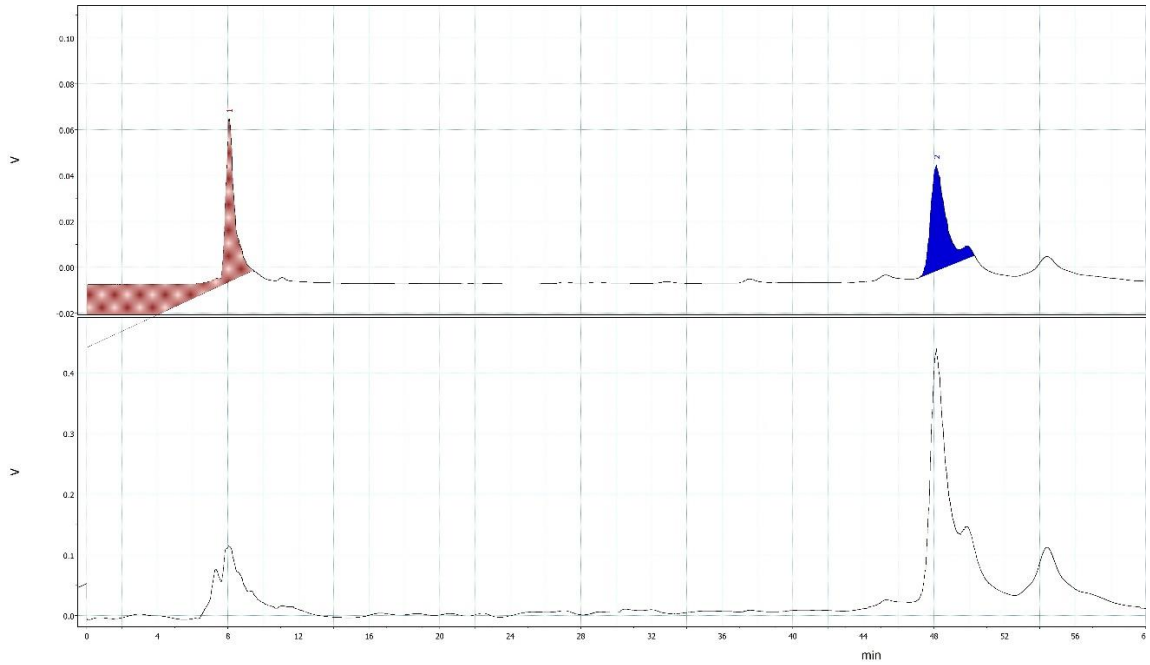


Figure A. 9. HPLC chromatogram of crude Dap-D-Asn(Pr)2 after cleavage. 65-60 (H_2O/MeCN+0.1 % TFA) in 60 min. Top Panel: λ=280 nm. Bottom Panel: λ=220 nm.

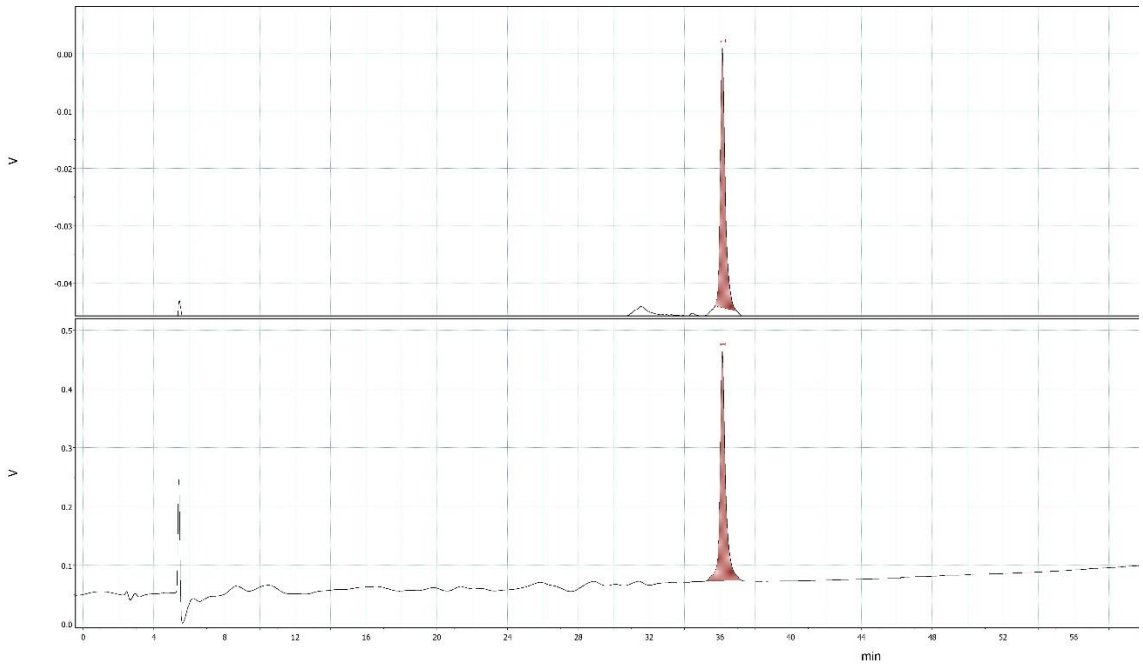
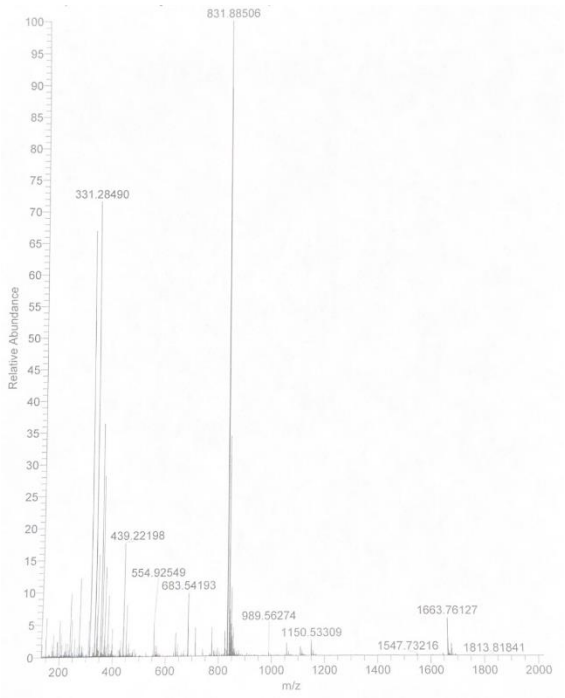


Figure A. 10. HPLC chromatogram of pure synthetic Dap-D-Asn(Pr)2. Gradient: 90-10 (H_2O/MeCN+0.1 % TFA) in 60 min. Top Panel: λ=280 nm. Bottom Panel: λ=220 nm.

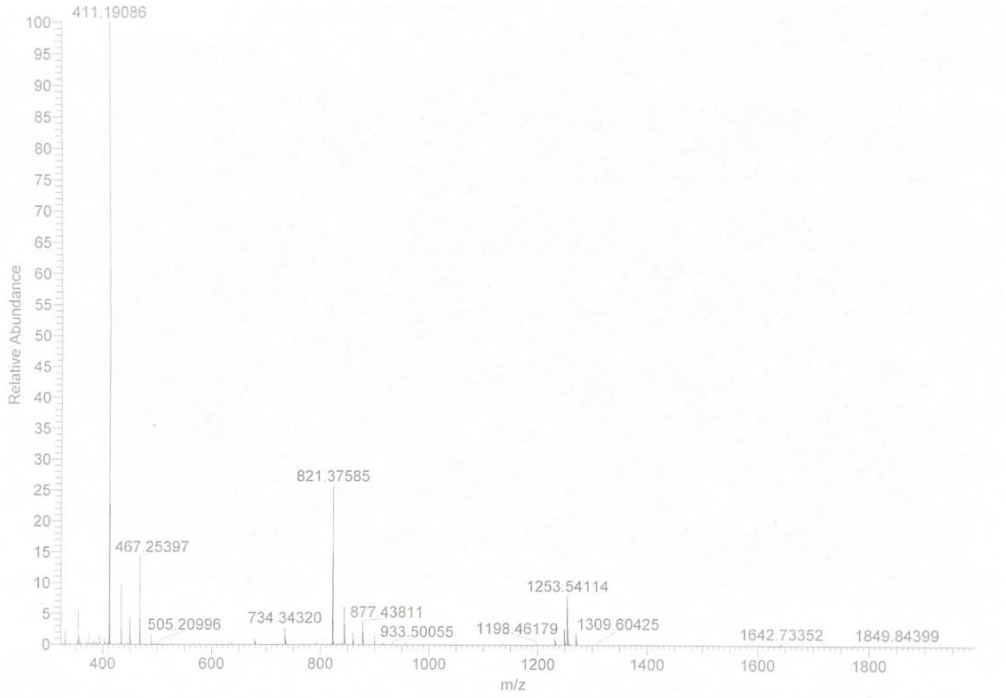


Elemental composition search on mass 831.88506

m/z= 826.88506-836.88506

m/z	Theo. Mass	Delta (mmu)	RDB equiv.	Composition
831.88506	831.88593	-0.87	30.0	$C_{75}H_{109}O_{26}N_{17}$

Figure A. 11. ESI+HRMS of pure Dap-D-Asn(Pr)2. $[M+H]^+$ at m/z=1663.76127 and $[M+2H]^{2+}$ at m/z=831.88506.



Elemental composition search on mass 411.19086

m/z= 406.19086-416.19086

m/z	Theo. Mass	Delta (ppm)	RDB equiv.	Composition
411.19086	411.19145	-1.43	11.5	$C_{23}H_{27}O_5N_2$

Figure A. 12. ESI+HRMS of pure Fmoc-D-Asn(Bu)-OH. $[M+H]^+$ at m/z=411.19086

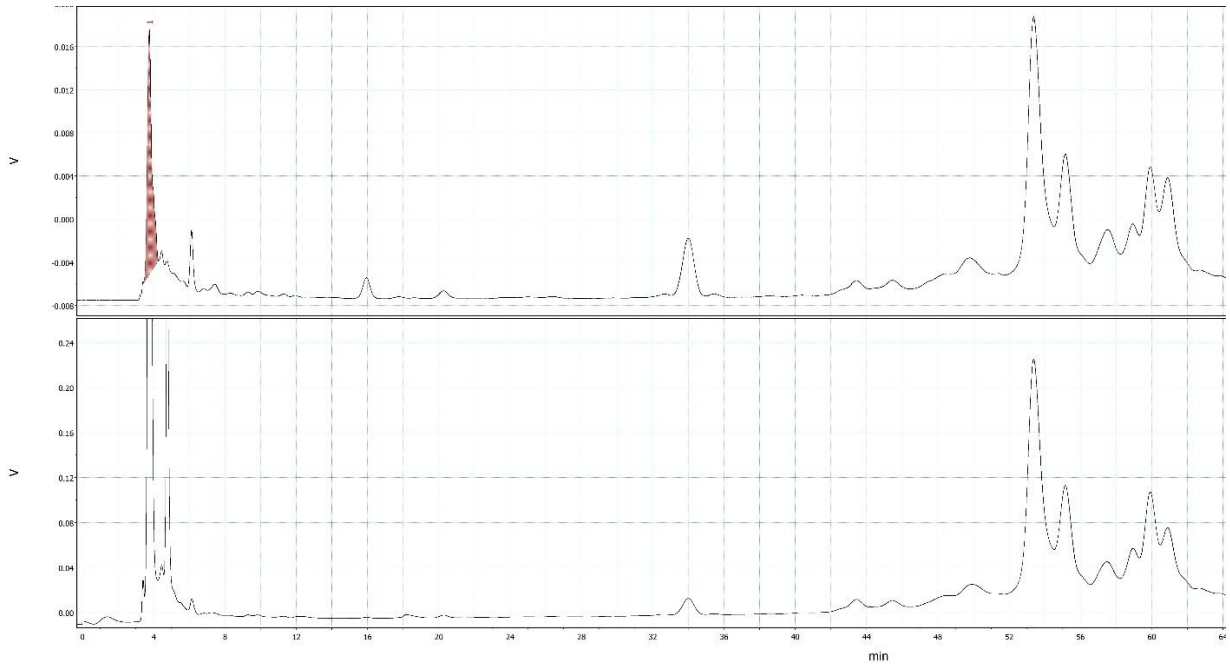


Figure A. 13. HPLC chromatogram of crude Dap-D-Asn(Bu)2 after cleavage. 70-55 (H_2O/MeCN+0.1 % TFA) in 60 min. Top Panel: λ=280 nm. Bottom Panel: λ=220 nm.

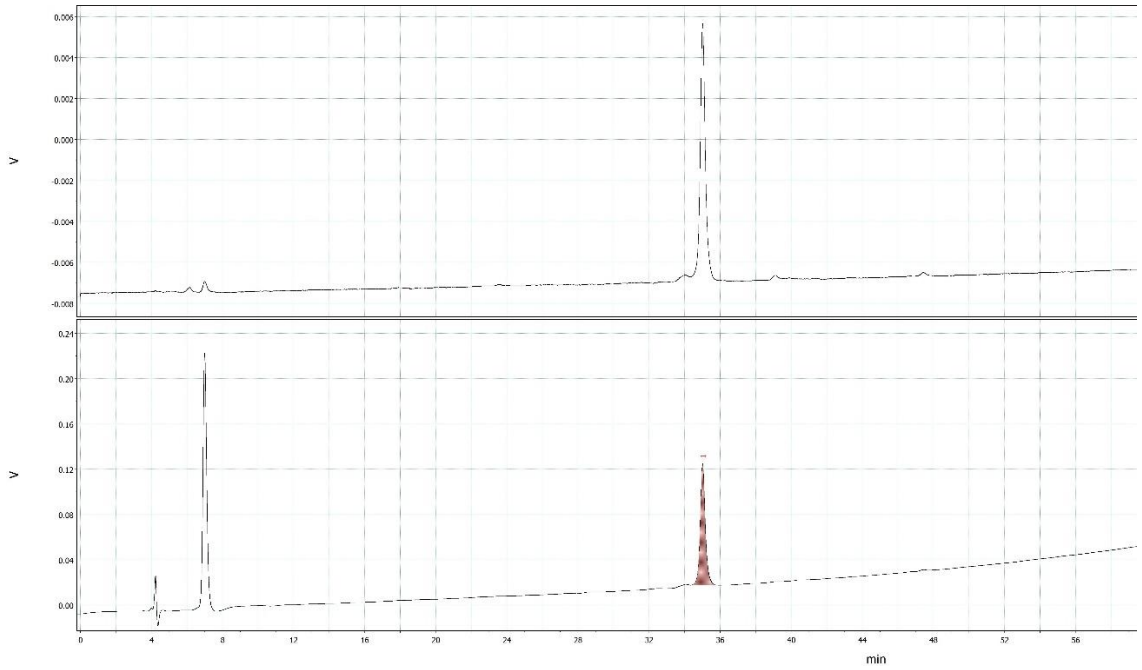
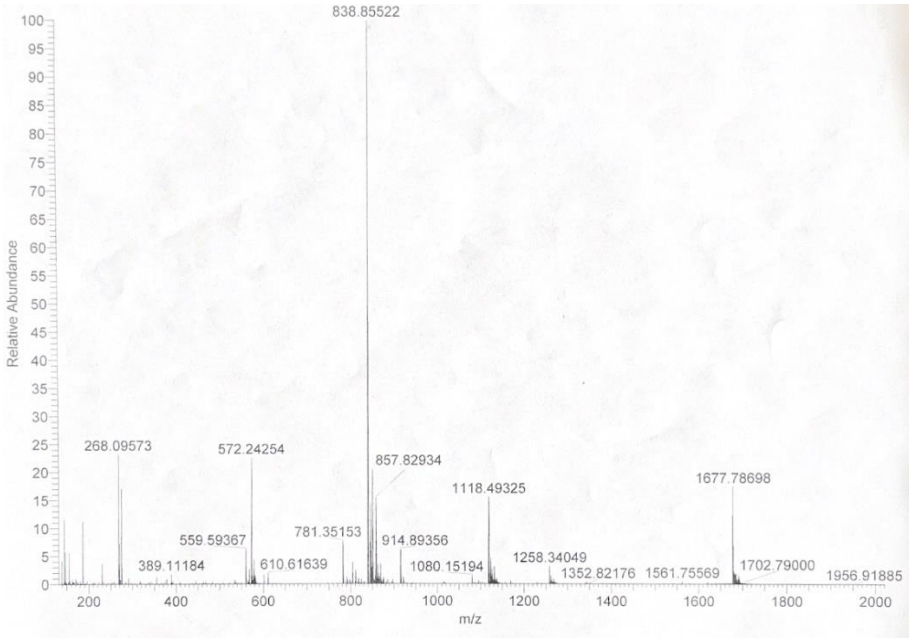


Figure A. 14. HPLC chromatogram of pure synthetic Dap-D-Asn(Bu)2. Gradient: 90-10 (H_2O/MeCN+0.1 % TFA) in 60 min. Top Panel: λ=280 nm. Bottom Panel: λ=220 nm

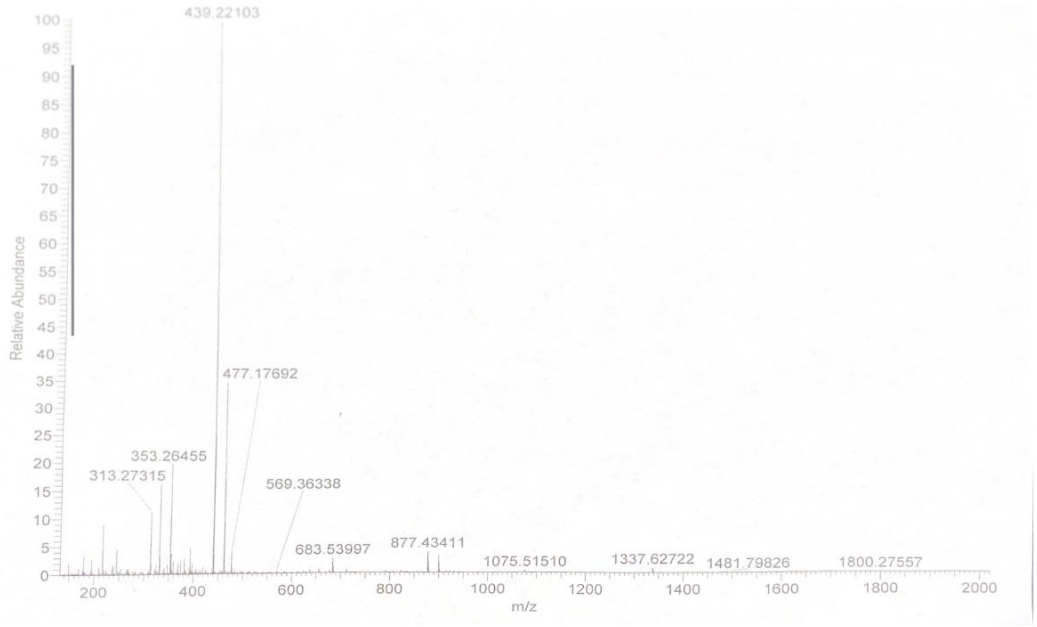


Elemental composition search on mass 1677.78698

m/z= 1672.78698-1682.78698

m/z	Theo. Mass	Delta (mmu)	RDB equiv.	Composition
1677.78698	1677.78807	-1.09	30.0	$C_{76}H_{111}O_{26}N_{17}$
	1677.77549	11.49	30.5	$C_{75}H_{109}O_{26}N_{18}$

Figure A. 15. ESI+HRMS of pure Dap-D-Asn(Bu)2. $[M+H]^+$ at m/z=1677.78698 and $[M+2H]^{2+}$ at m/z=838.85522.



Elemental composition search on mass 439.22103

m/z= 434.22103-444.22103

m/z	Theo. Mass	Delta (mmu)	RDB equiv.	Composition
439.22103	439.22275	-1.72	11.5	$C_{25}H_{31}O_5N_2$

Figure A. 16. ESI+HRMS of pure Fmoc-D-Asn(Hex)-OH. $[M+H]^+$ at m/z=439.22103, $[M+K]^+$ at m/z=477.17692

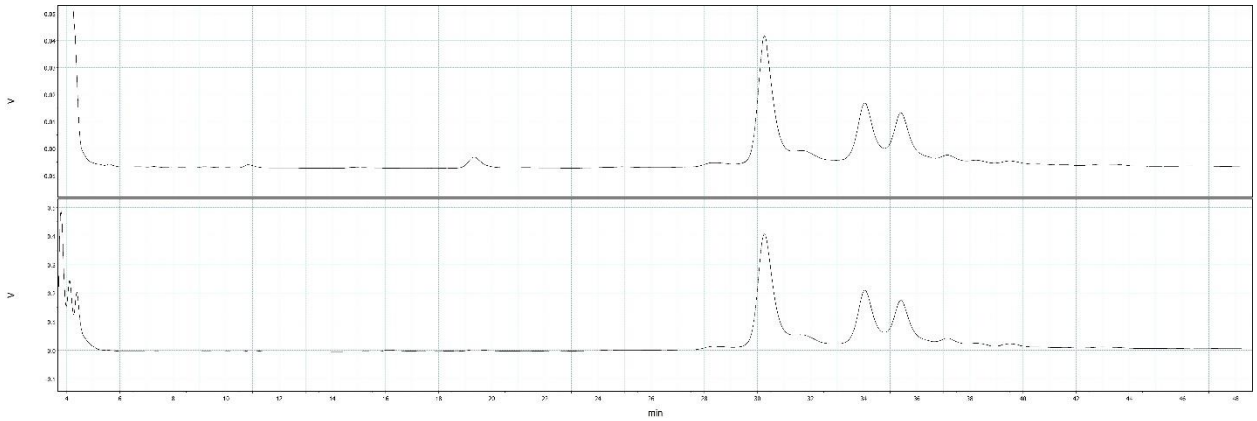


Figure A. 17. HPLC chromatogram of crude Dap-D-Asn(Hex)2 after cleavage. 65-50 (H_2O/MeCN+0.1 % TFA) in 60 min. Top Panel: λ=280 nm. Bottom Panel: λ=220 nm.

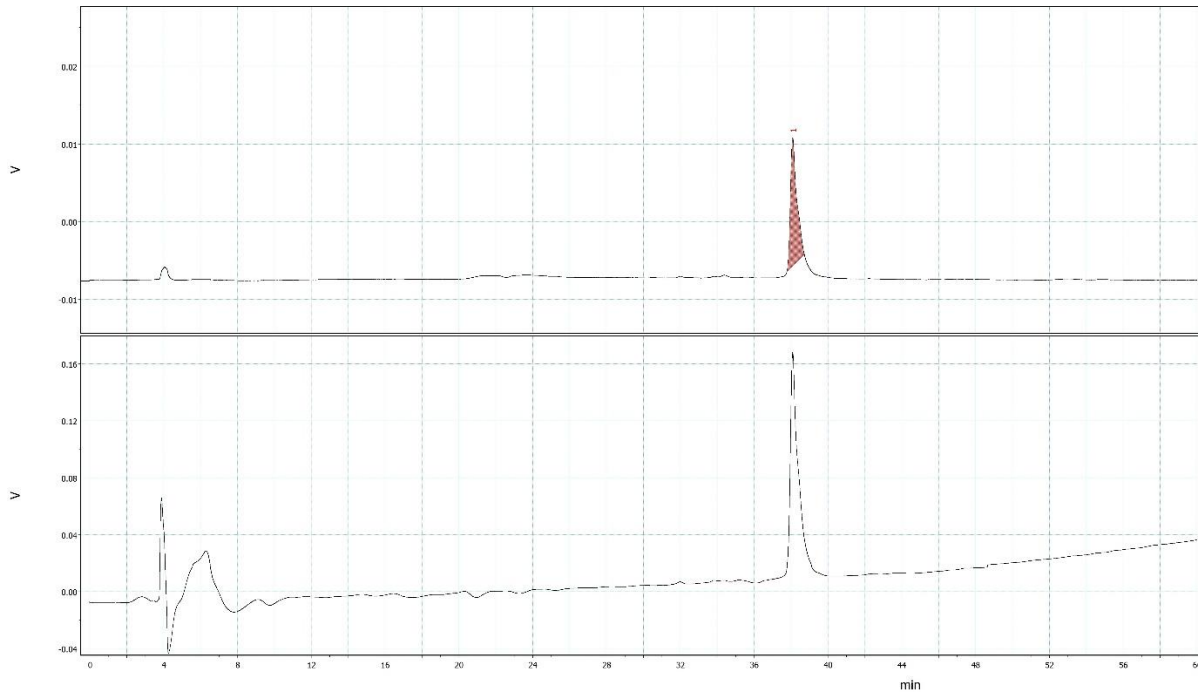
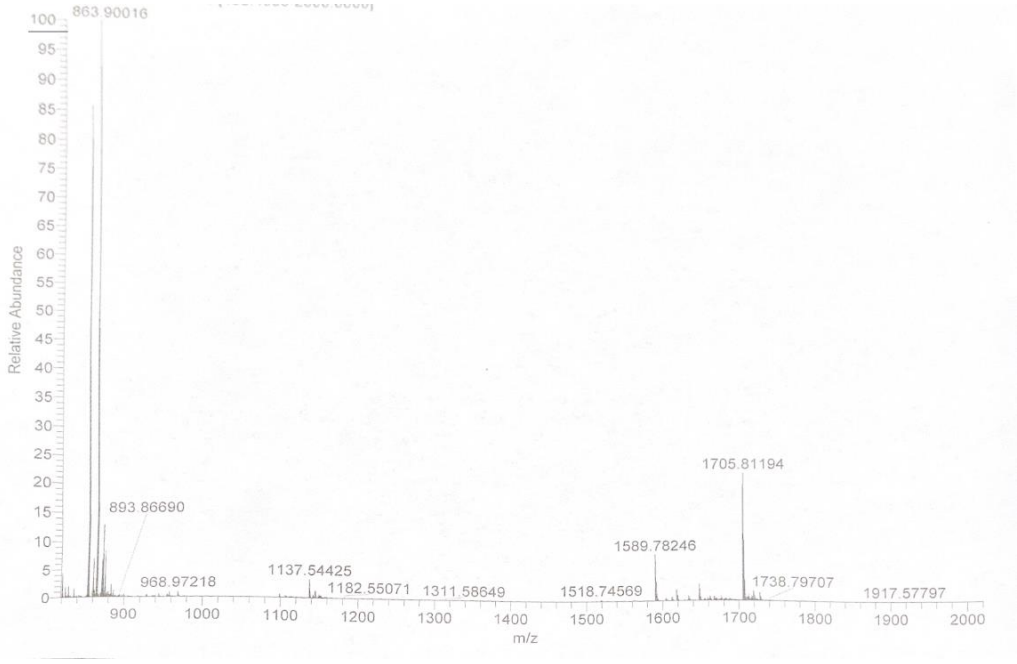


Figure A. 18. HPLC chromatogram of pure synthetic Dap-D-Asn(Hex)2 after cleavage. 90-10 (H_2O/MeCN+0.1 % TFA) in 60 min. Top Panel: λ=280 nm. Bottom Panel: λ=220 nm.

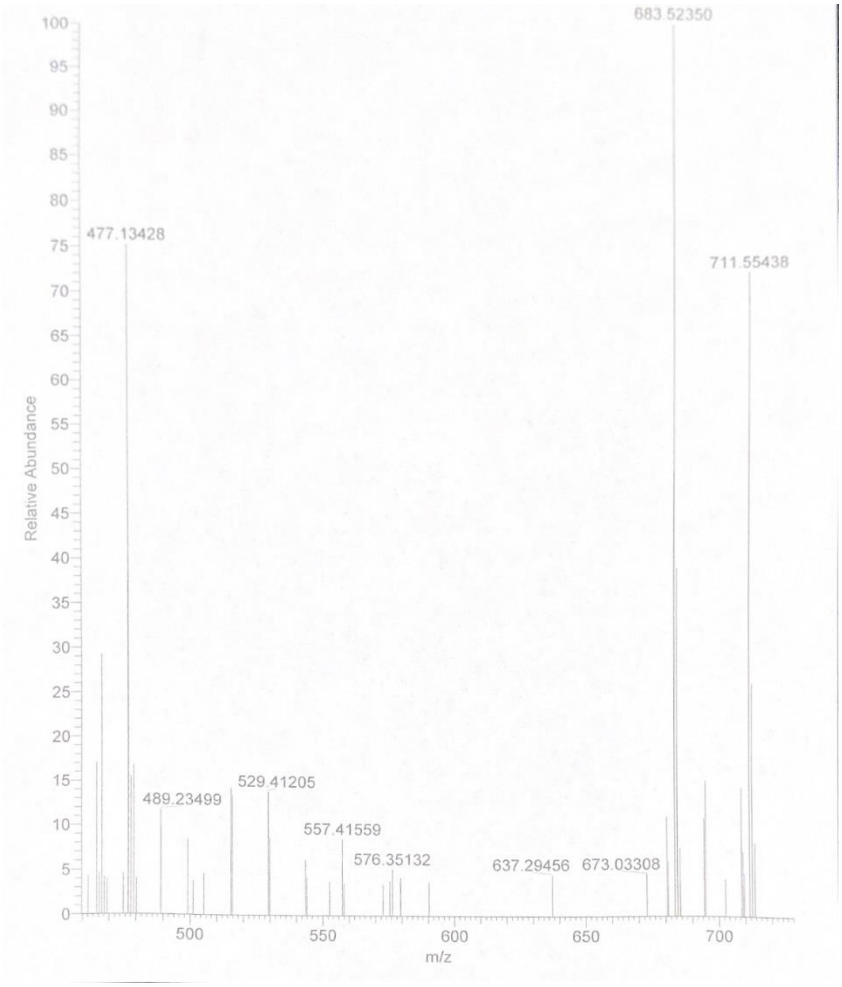


Elemental composition search on mass 1705.81194

m/z= 1700.81194-1710.81194

m/z	Theo. Mass	Delta (ppm)	RDB equiv.	Composition
1705.81194	1705.81937	-4.35	30.0	$C_{78}H_{115}O_{26}N_{17}$
	1705.79556	9.60	30.5	$C_{78}H_{113}O_{27}N_{16}$

Figure A. 19. ESI+HRMS of pure Dap-D-Asn(Hex)2. $[M+H]^+$ at m/z=1705.81194 and $[M+2H]^{2+}$ at m/z=863.90016



Elemental composition search on mass 467.25458

m/z= 462.25458-472.25458

m/z	Theo. Mass	Delta (ppm)	RDB equiv.	Composition
467.25458	467.25405	1.14	11.5	$C_{27}H_{35}O_5N_2$
	467.24147	28.05	12.0	$C_{26}H_{33}O_5N_3$

Figure A. 20. ESI+HRMS of pure Dap-D-Asn(Oct)2. $[M+H]^+$ at m/z= 467.25458

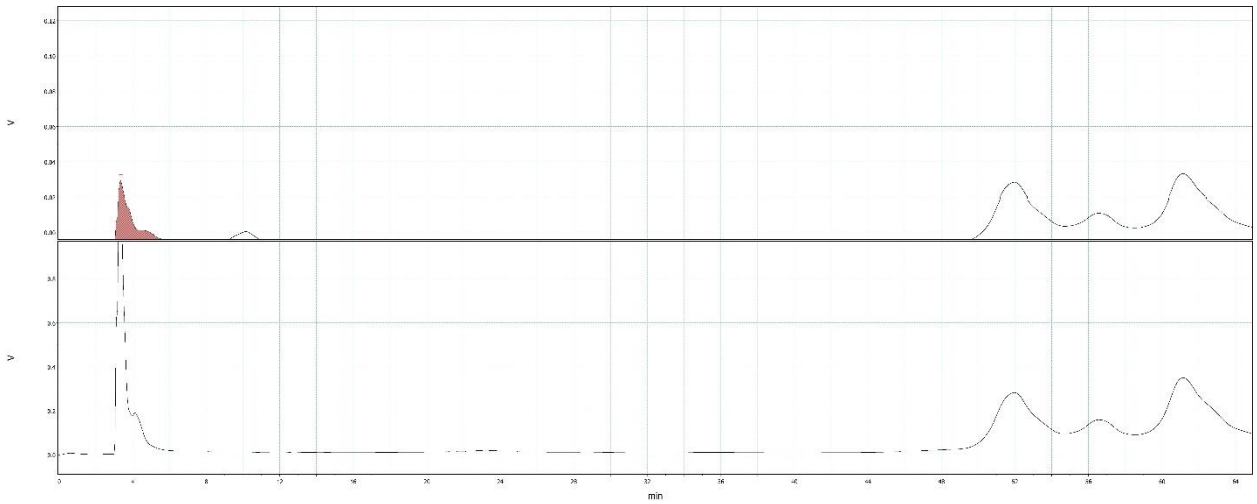


Figure A. 21. HPLC chromatogram of crude Dap-D-Asn(Oct)2 after cleavage. 75-35 (H_2O/MeCN+0.1 % TFA) in 60 min. Top Panel: λ=280 nm. Bottom Panel: λ=220 nm.

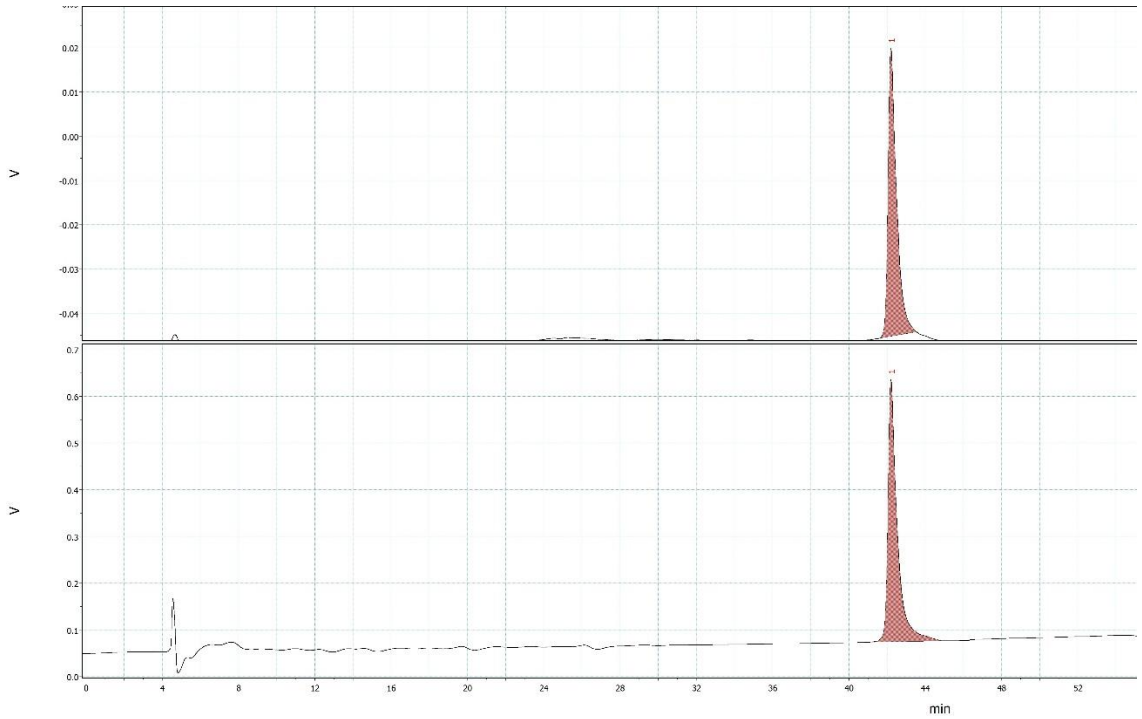
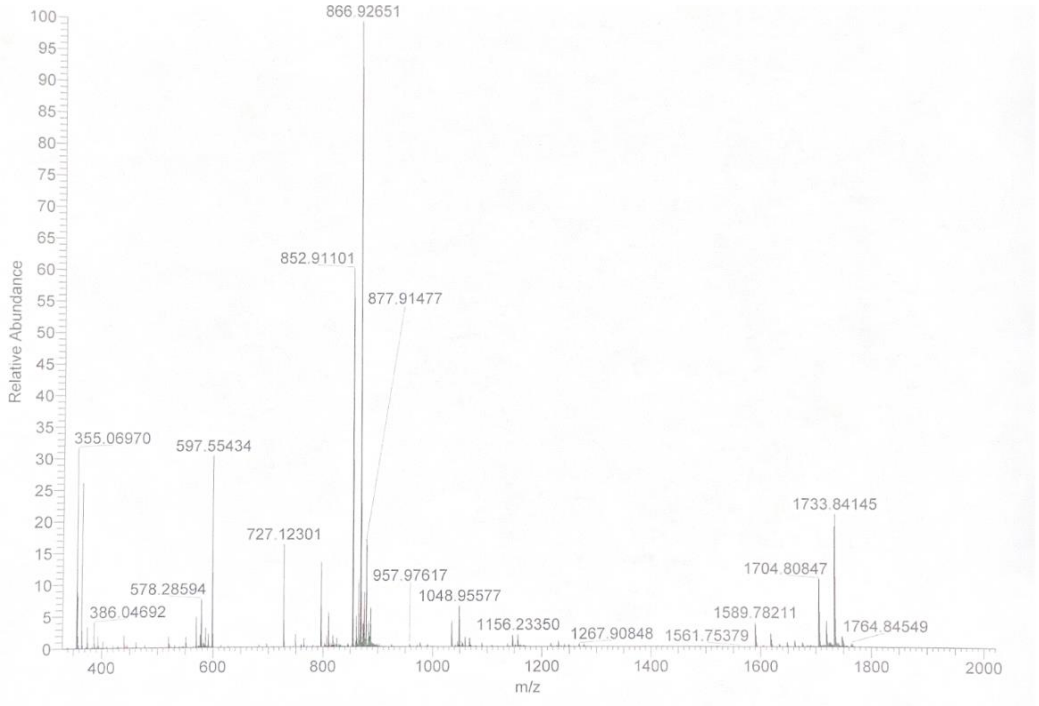


Figure A. 22. HPLC chromatogram of pure synthetic Dap-D-Asn(Oct)2. Gradient: 90-10 (H_2O/MeCN+0.1 % TFA) in 60 min (λ=220 nm)



Elemental composition search on mass 866.92653

m/z= 861.92653-871.92653

m/z	Theo. Mass	Delta (ppm)	RDB equiv.	Composition
866.92653	866.92506	1.70	30.0	$C_{80}H_{119}O_{26}N_{17}$
	866.91315	15.43	30.5	$C_{80}H_{117}O_{27}N_{16}$
	866.90687	22.68	31.0	$C_{79}H_{115}O_{27}N_{17}$

Figure A. 23. ESI+HRMS of pure Dap-D-Asn(Oct)2. $[M+H]^+$ at m/z=1733.84145, $[M+2H]^{2+}$ at m/z=866.92653 and $[M+H+Na]^{2+}$ at m/z=877.91477.

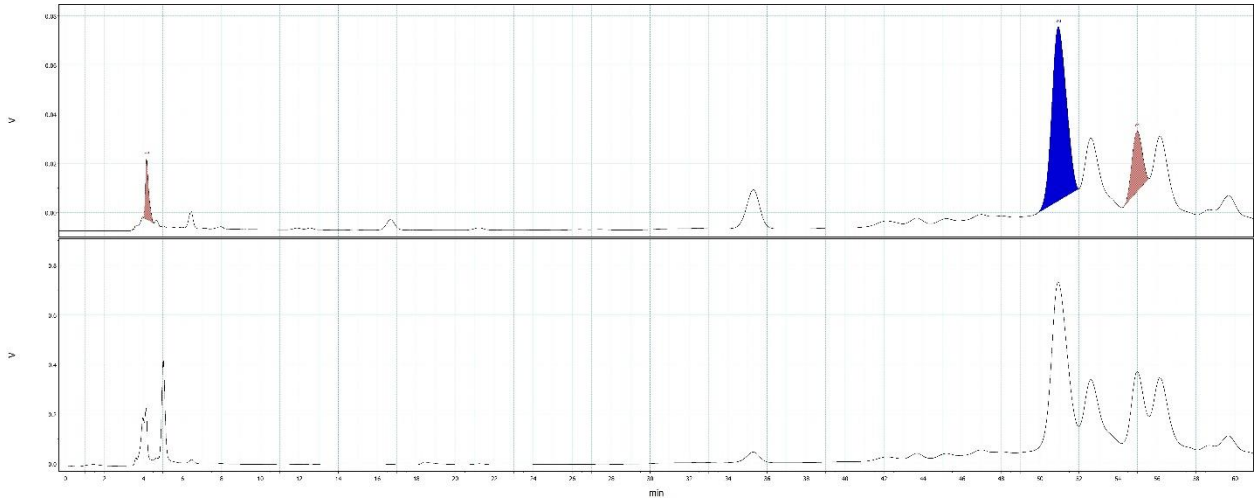


Figure A. 24. HPLC chromatogram of crude Dap-D-Asn(Pip)2 after cleavage. 70-55 (H_2O/MeCN+0.1 % TFA) in 60 min. Top Panel: λ=280 nm. Bottom Panel: λ=220 nm.

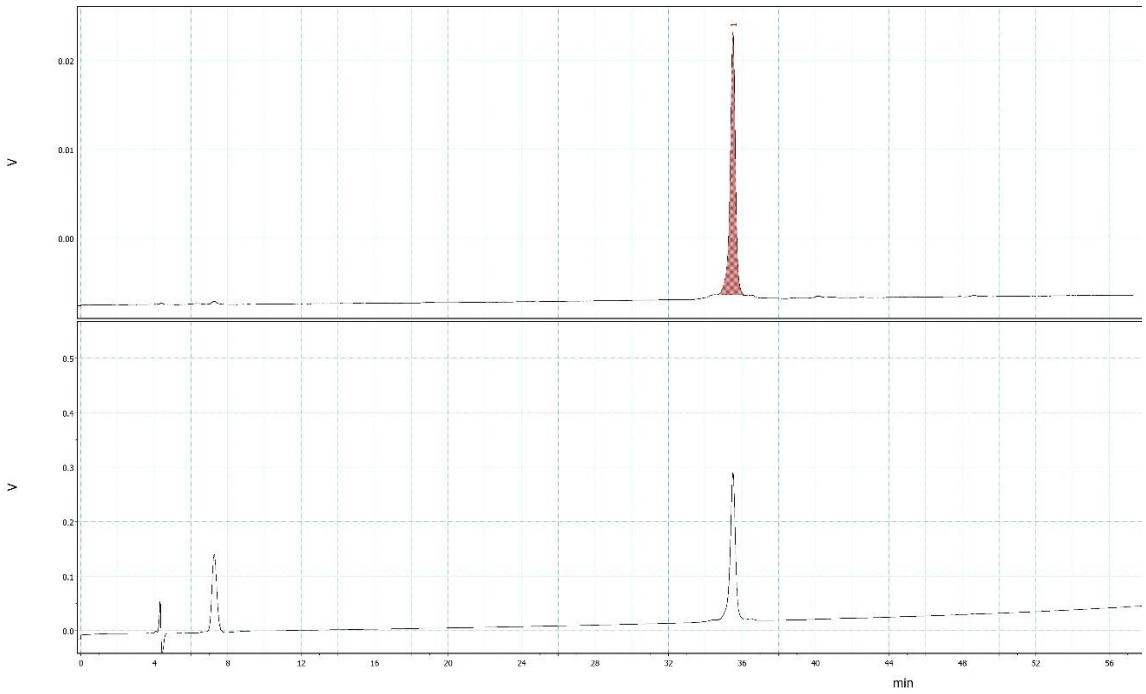
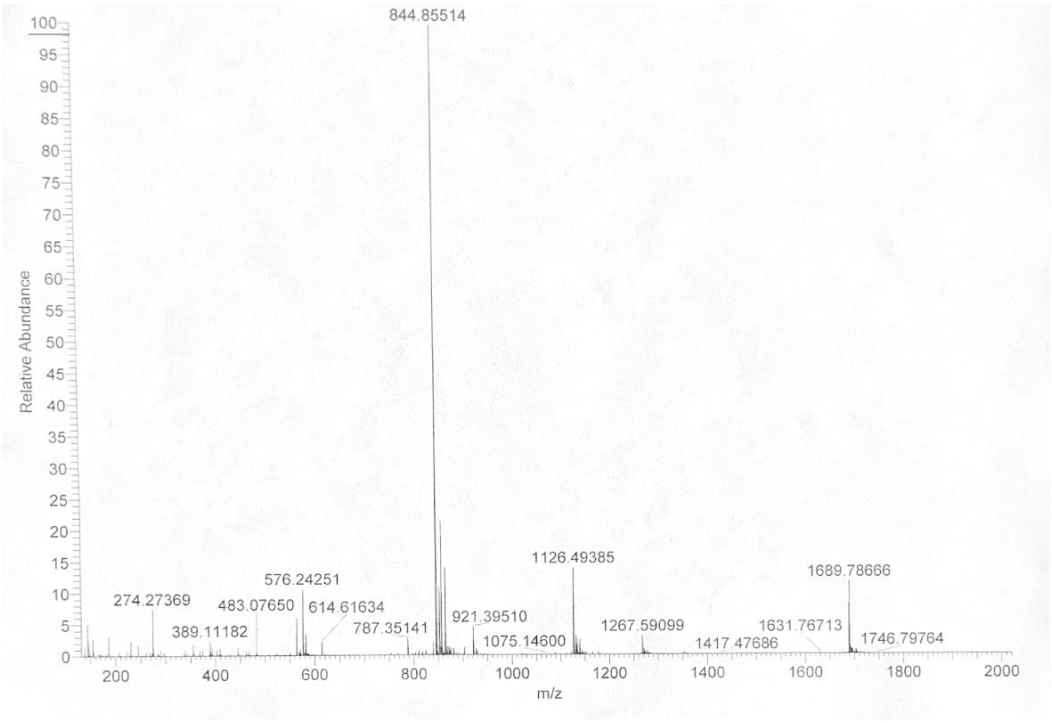


Figure A. 25. HPLC chromatogram of pure synthetic Dap-D-Asn(Pip)2. Gradient: 90-10 (H_2O/MeCN+0.1 % TFA) in 60 min. Top Panel: λ=280 nm. Bottom Panel: λ=220 nm.



Elemental composition search on mass 1689.78766

m/z= 1684.78766-1694.78766

m/z	Theo. Mass	Delta (mmu)	RDB equiv.	Composition
1689.78766	1689.78807	-0.41	31.0	$C_{77}H_{111}O_{26}N_{17}$
	1689.77549	12.17	31.5	$C_{76}H_{109}O_{26}N_{18}$
	1689.76426	23.40	31.5	$C_{77}H_{109}O_{27}N_{16}$
	1689.75168	35.98	32.0	$C_{76}H_{107}O_{27}N_{17}$
	1690.74693	-959.27	32.0	$C_{75}H_{106}O_{27}N_{18}$
	1690.75951	-971.85	31.5	$C_{76}H_{108}O_{27}N_{17}$
	1690.77208	-984.42	31.0	$C_{77}H_{110}O_{27}N_{16}$
	1690.78332	-995.66	31.0	$C_{76}H_{110}O_{26}N_{18}$
	1688.78024	1007.42	31.5	$C_{77}H_{110}O_{26}N_{17}$
	1688.76767	1019.99	32.0	$C_{76}H_{108}O_{26}N_{18}$

Figure A. 26. ESI+HRMS of pure Dap-D-Asn(Pip)2. $[M+H]^+$ at m/z=1689.78666 and $[M+2H]^{2+}$ at m/z=844.85514

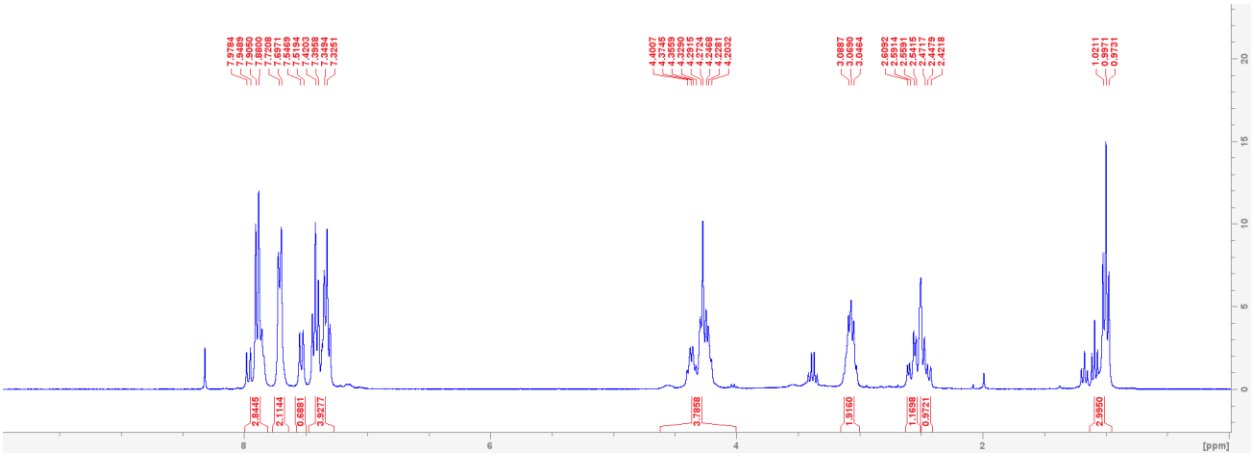


Figure A. 27. ^{1}H-NMR spectrum of Fmoc-Asn(Et)-OH (300 MHz, DMSO-d_6) at 298 K

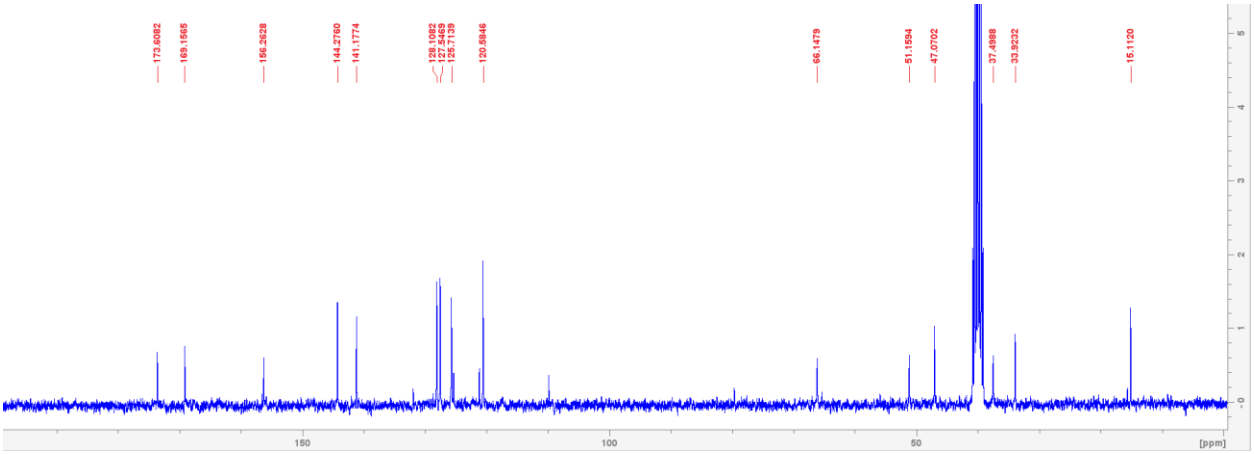


Figure A. 28. ^{13}C-NMR spectrum of Fmoc-Asn(Et)-OH (75 MHz, DMSO-d_6) at 298 K

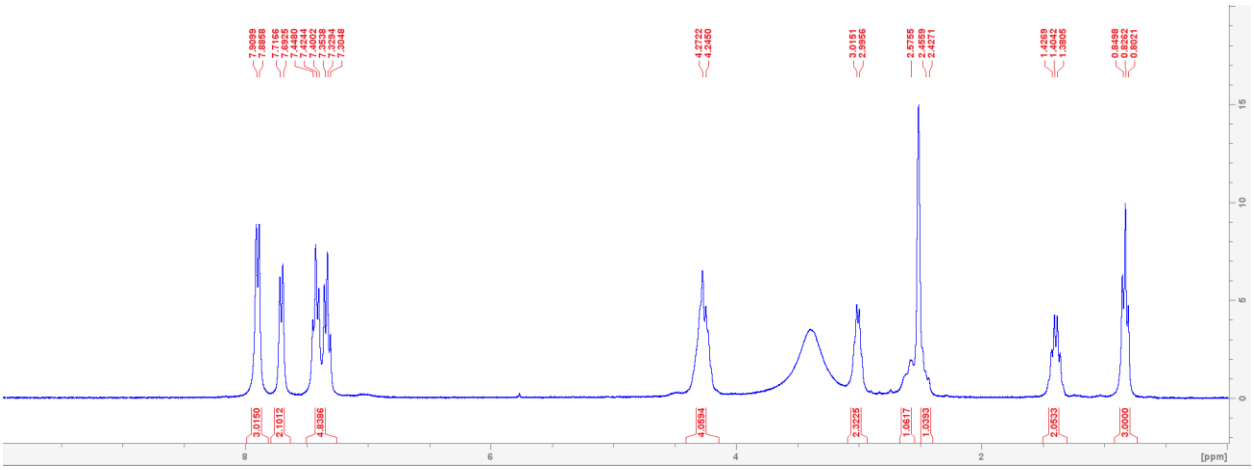


Figure A. 29 ^{1}H-NMR spectrum of Fmoc-Asn(Pr)-OH (300 MHz, DMSO-d_6) at 298 K

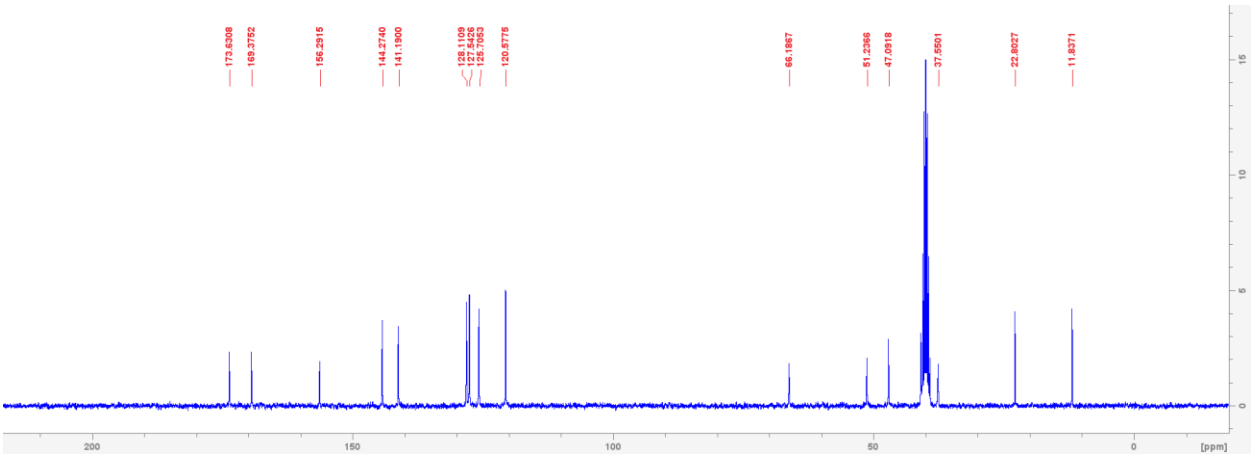


Figure A. 30. ^{13}C-NMR spectrum of Fmoc-Asn(Pr)-OH (75 MHz, DMSO-d_6) at 298 K

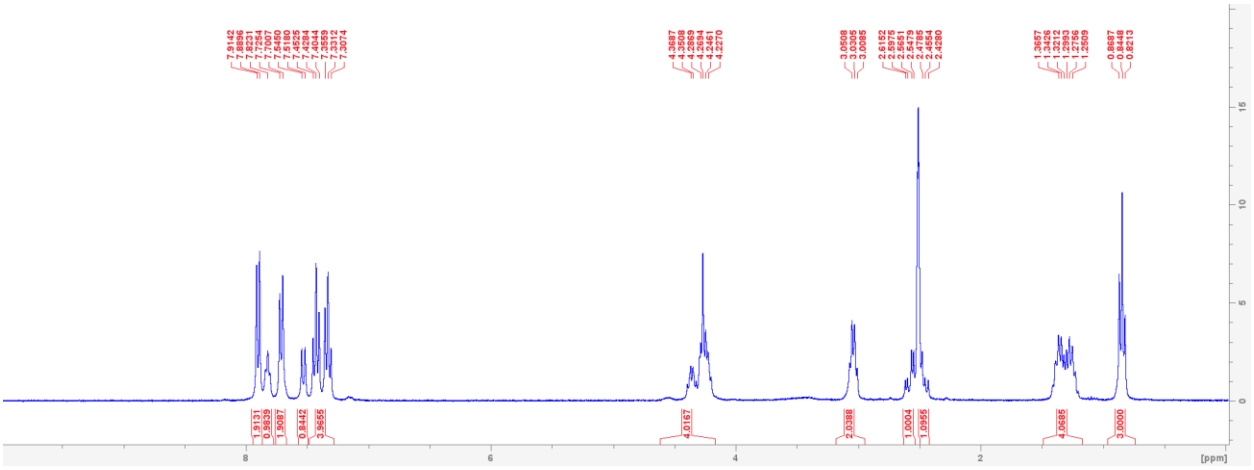


Figure A. 31 ^{1}H-NMR spectrum of Fmoc-Asn(Bu)-OH (300 MHz, DMSO-d_6) at 298 K

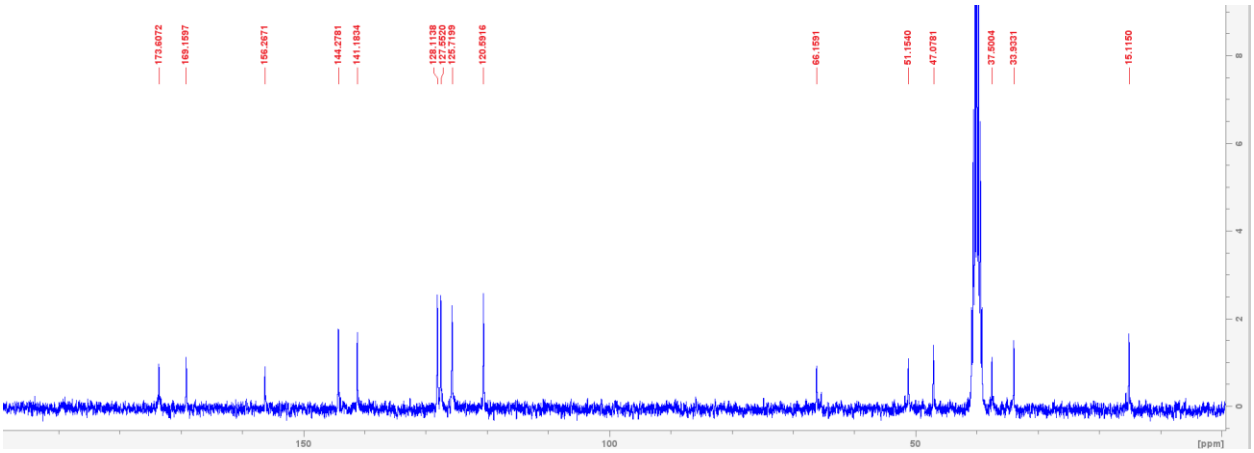


Figure A. 32. ^{13}C-NMR spectrum of Fmoc-Asn(Bu)-OH (75 MHz, DMSO-d_6) at 298 K

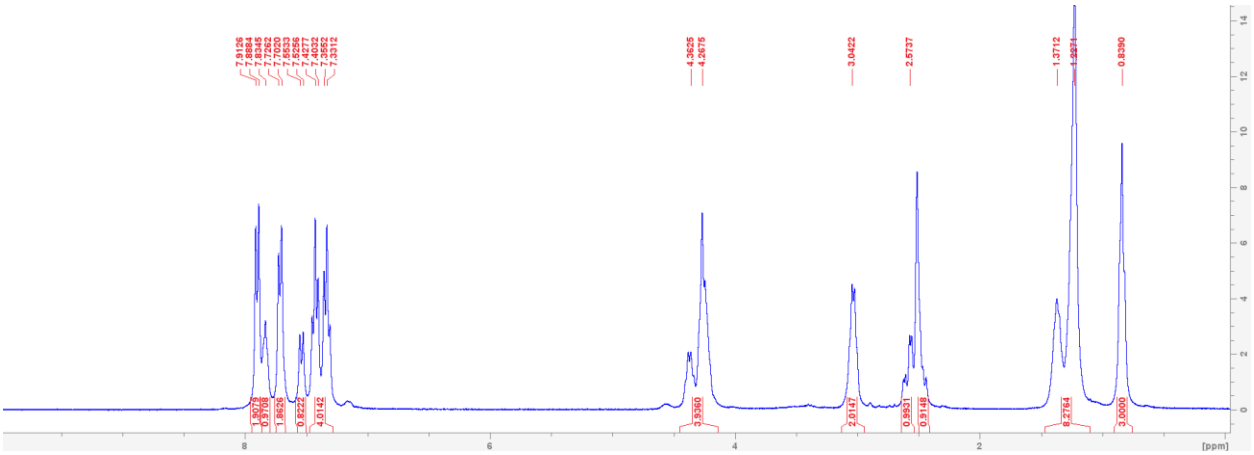


Figure A. 33. ^{1}H-NMR spectrum of Fmoc-Asn(Hex)-OH (300 MHz, DMSO-d_6) at 298 K

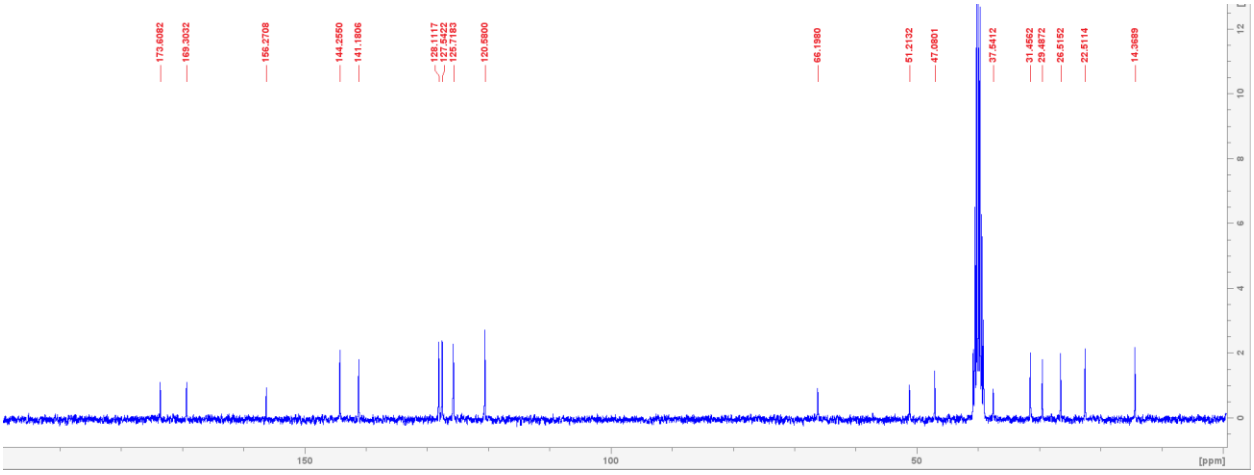


Figure A. 34. ^{13}C-NMR spectrum of Fmoc-Asn(Hex)-OH (75 MHz, DMSO-d_6) at 298 K

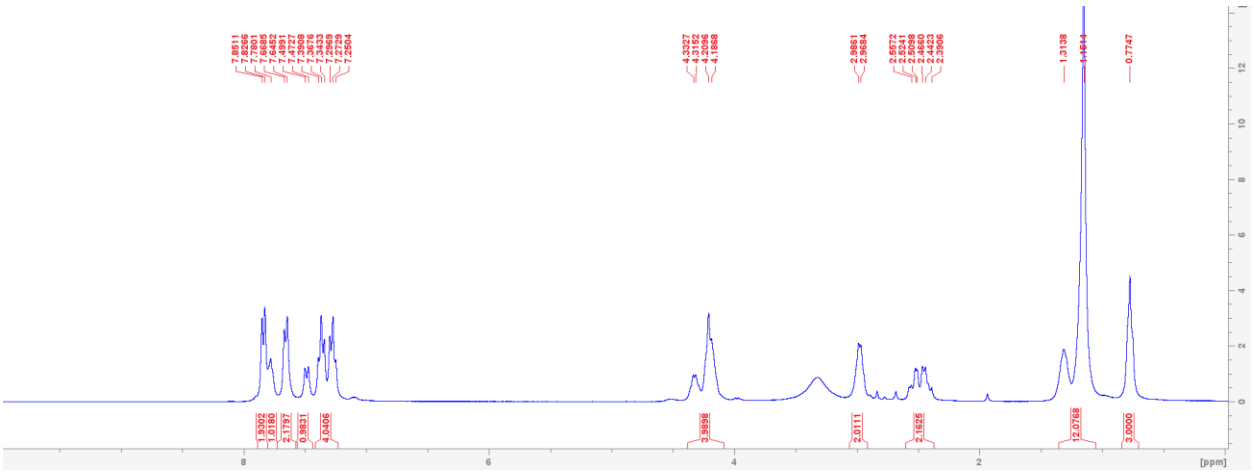


Figure A. 35. ^{1}H-NMR spectrum of Fmoc-Asn(Oct)-OH (300 MHz, DMSO-d_6) at 298 K

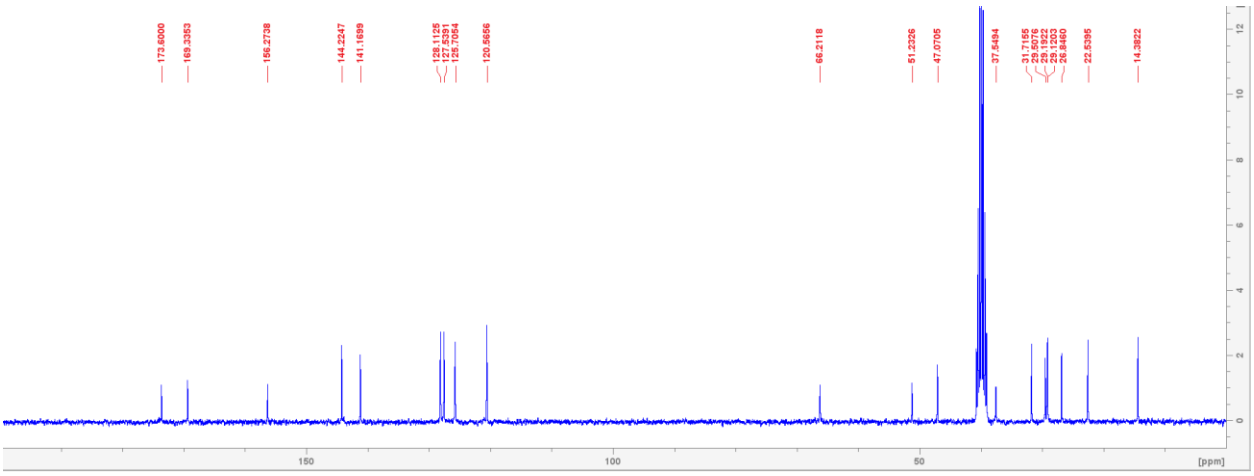


Figure A. 36. ^{13}C-NMR spectrum of Fmoc-Asn(Oct)-OH (75 MHz, DMSO-d_6) at 298 K

Appendix B: Chapter 3

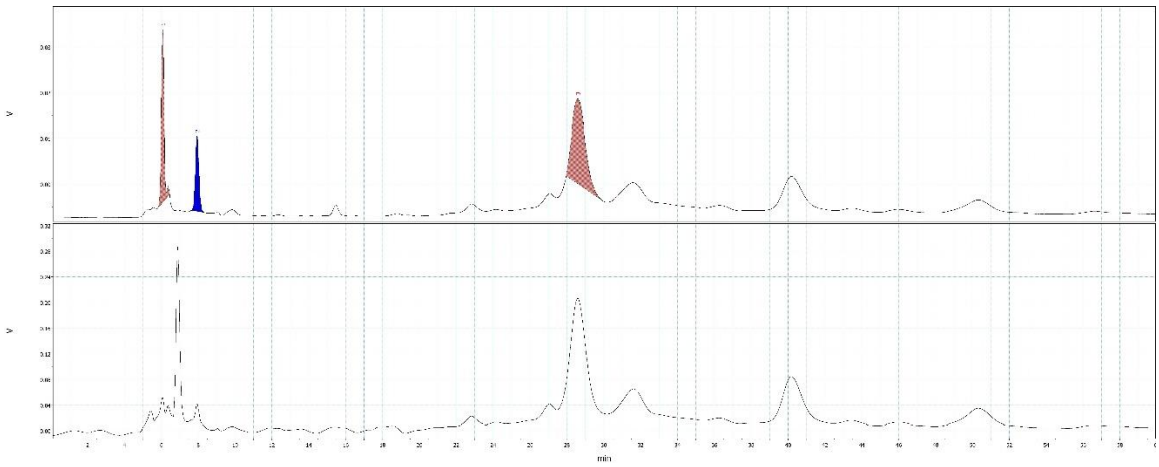


Figure B. 1. HPLC chromatogram of crude Dap-D-Asn(OH)2 after cleavage. 65-50 (H_2O/MeCN+0.1 % TFA) in 60 min. Top Panel: λ=280 nm. Bottom Panel: λ=220 nm.

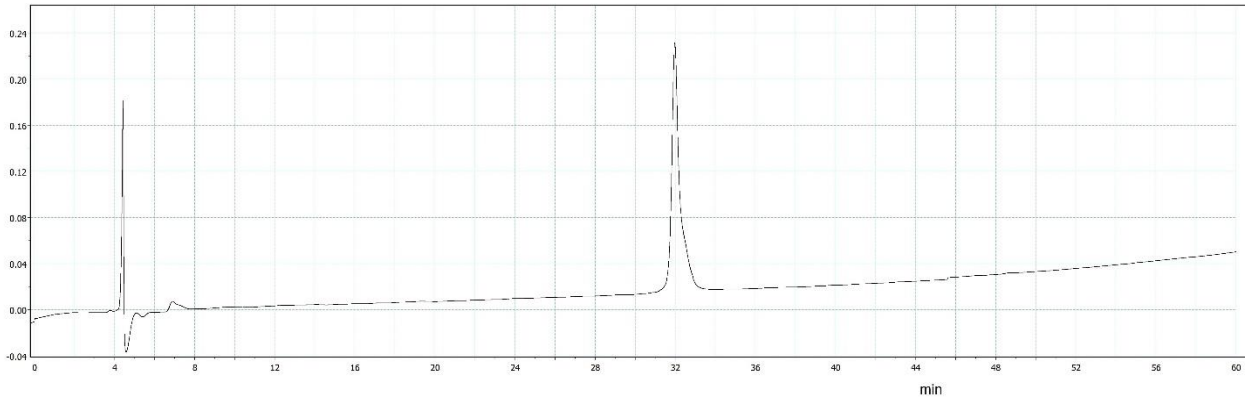
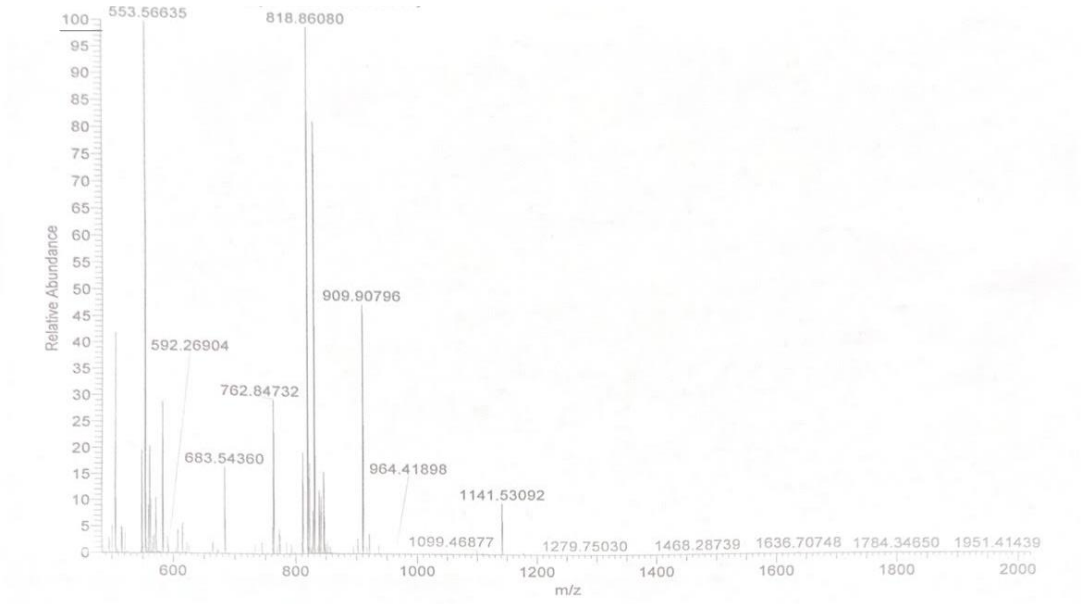


Figure B. 2 HPLC chromatogram of pure synthetic Dap-D-Asn(OH)2. Gradient: 90-10 (H_2O/MeCN+0.1 % TFA) in 60 min. Top Panel: λ=280 nm. Bottom Panel: λ=220 nm.



Elemental composition search on mass 818.86080

m/z= 813.86080-823.86080

m/z	Theo. Mass	Delta (ppm)	RDB equiv.	Composition
818.86080	818.85992	1.08	30.0	$C_{72}H_{103}O_{27}N_{17}$

Figure B. 3. ESI+HRMS of pure Dap-D-Asn(OH)2. $[M+H]^+$ at m/z=1636.70748 and $[M+2H]^{2+}$ at m/z=818.86080.

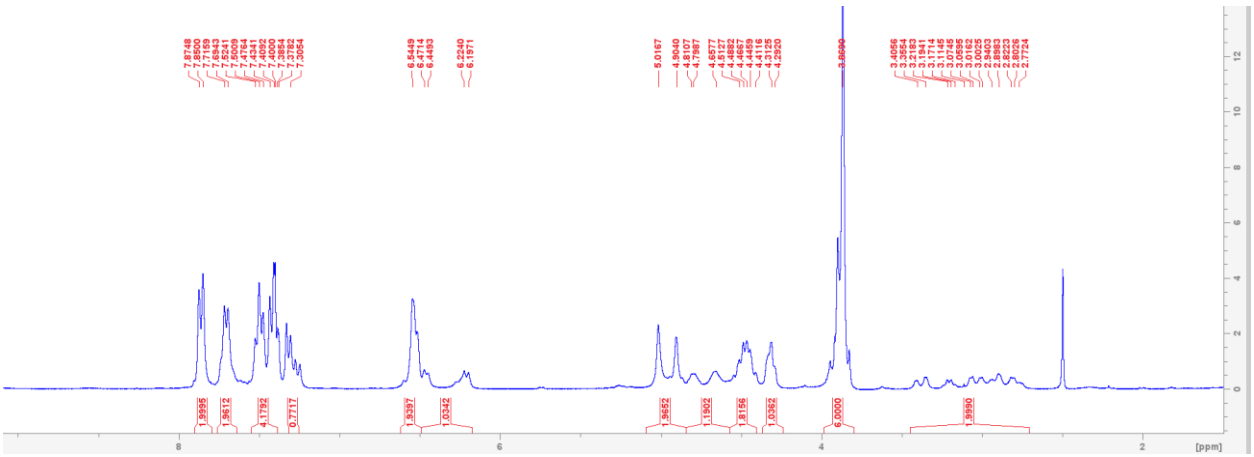


Figure B. 4. ^{1}H-NMR spectrum of Fmoc-Asn(DMB)-OH (300 MHz, DMSO-d_6) at 298 K

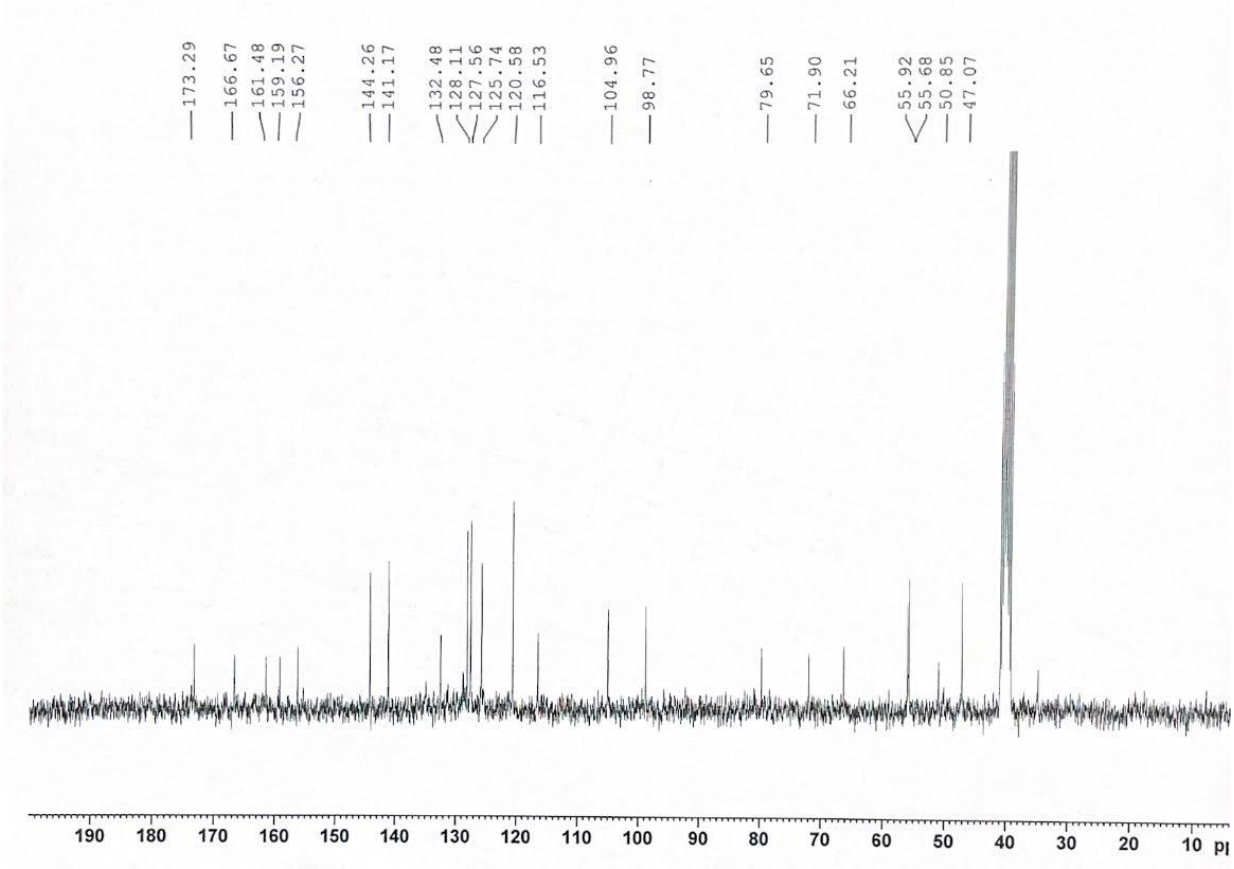


Figure B. 5. ^{13}C-NMR spectrum of Fmoc-Asn(DMB)-OH (75 MHz, DMSO-d_6) at 298 K



Elemental composition search on mass 521.19311

m/z= 516.19311-526.19311

m/z	Theo. Mass	Delta (ppm)	RDB equiv.	Composition
521.19311	521.19184	2.43	15.5	$C_{28}H_{29}O_8N_2$

Figure B. 6. ESI+HRMS of pure Dap-D-Asn(DMB)-OH. $[M+H]^+$ at m/z= 521.19311 and $[M+Na]^+$ at m/z=543.17645

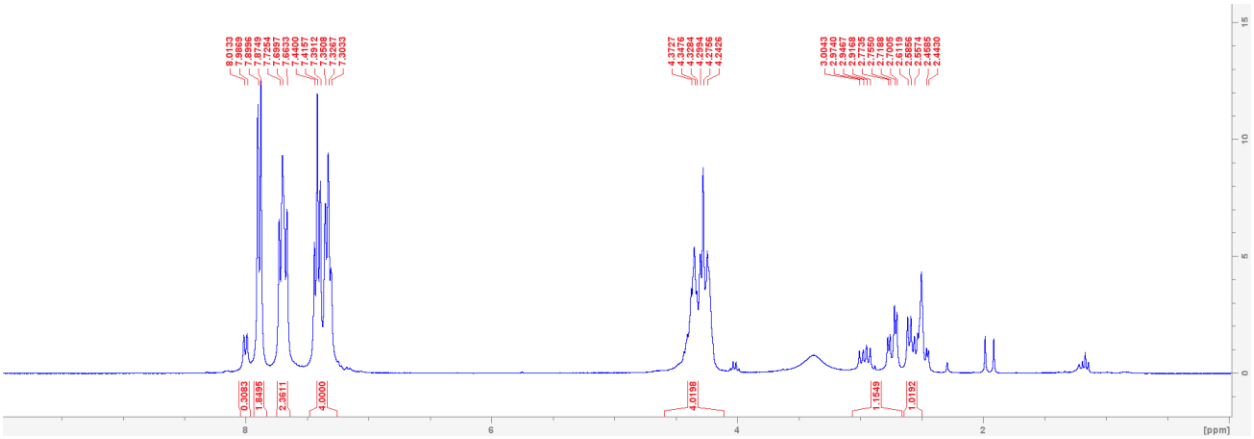


Figure B. 7. ^{1}H-NMR spectrum of Fmoc-Asn(OH)-OH (300 MHz, DMSO-d_6) at 298 K

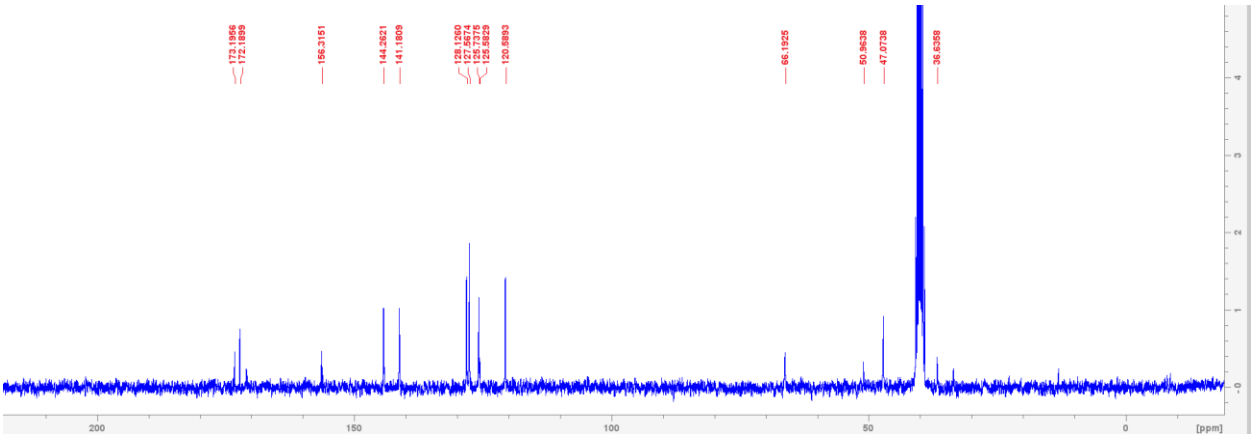


Figure B. 8. ^{13}C-NMR spectrum of Fmoc-Asn(OH)-OH (75 MHz, DMSO-d_6) at 298 K